Constraints on Physics Beyond the Standard Model and Its Observable Effects

Thesis by

Jennifer Kile

In Partial Fulfillment of the Requirements

for the Degree of

Doctor of Philosophy

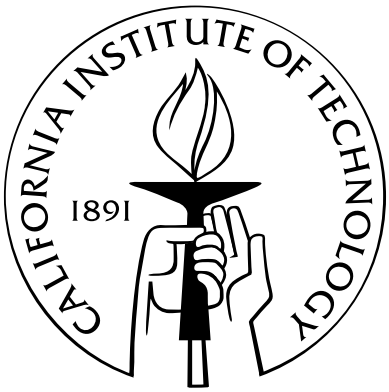

California Institute of Technology

Pasadena, California

2007

(Defended 22 May 2007)

For Max and Werner, who were always there, and for Dave, Martin, and Fletch, who never let me down.

Acknowledgements

First, I would like to thank Profs. Mark Wise and Michael Ramsey-Musolf for their extensive guidance, many helpful comments, insight, and support during the last six years. I would also like to thank the other members of my thesis committee, Profs. John Schwarz and Robert McKeown, for their willingness to examine this thesis.

Next, I would like to thank Dr. Michael Graesser, who was certainly the brains and main driving force behind the first project that I worked on here at Caltech, which here is described in Chapter 4.

I would also like to thank Peng Wang, my officemate and collaborator, who put up with a huge number of dumb questions from me throughout the last several years, and to Rebecca Erwin, who endured fewer, but nonetheless equally dumb, questions.

Next, I thank Julian von Wimmersperg for keeping me sane during the production of this thesis, frequent technical advice, and being willing to critique my writings and talks at length (and I mean *at length*). Also, I would like to thank my housemate, Hareem Maune, for occasionally making sure that I remembered to eat, and Lotty Ackerman, for the substantial amount of chocolate that she provided.

Also thanks to the other graduate students on the fourth floor of Lauritsen Lab, who didn't seem to mind my walking into their offices and talking about completely random things: Mike Salem, Moira Gresham, Donal O'Connell, Ketan Vyas, Alejandro Jenkins, Paul Cook, and Jie Yang.

I would also like to thank the many people, in addition to those already named above, who contributed helpful comments about the works described in this thesis. They include N. Bell, V. Cirigliano, M. Gorshteyn, P. Langacker, B. Nelson, P. Vogel, V. Barger, T. Han, K. Akama, C. Burgess, C. Csaki, M. Giovannini, C. Grojean, M.

Luty, M. Perelstein, and J. Vinet. Also I would like to thank J. Erler for his helpful information on using the GAPP code.

And, finally, the works in this thesis were supported by U.S. Department of Energy contracts FG02-05ER41361, DE-FG03-ER40701, FG02-05ER41361, DE-FG03-ER40701, and DE-FG-0392-ER40701, as well as National Science Foundation awards PHY-0071856 and PHY-0555674.

Abstract

In this work, we describe three analyses, all of which involve physics beyond the Standard Model. The first two discussed here are closely related; they use effective operator analyses to constrain the contributions of physics beyond the SM to observable processes. The third project involves the investigations of a particular extra-dimensions model which addresses the cosmological constant problem.

The first project which we will discuss uses the scale of neutrino mass to place model-independent constraints on the coefficients of the chirality-changing terms in the muon decay Lagrangian. We list all of the dimension-six effective operators which contribute to muon decay and Dirac mass for the neutrino. We then calculate the one-loop contributions that each of these operators makes to neutrino mass. Taking a generic element of the neutrino mass matrix to be of order ~ 1 eV, we derive limits on the contributions of these operators to the muon Michel parameters which are approximately four orders of magnitude more stringent than the current experimental results, and well below near-future experimental sensitivity. We also find two chirality-changing operators, which, due to their flavor structure, are unconstrained by neutrino mass yet contribute to muon decay. However, as these two operators differ from those constrained by neutrino mass only by their flavor indices, we naively expect their contributions to also be small; if their effects instead turn out to be observable, this may be an indication of beyond-the-Standard-Model physics with an interesting flavor structure.

In the second analysis, we again perform an effective operator analysis, this time applied to Higgs production at a linear collider. Here we include all dimension-six operators containing fermions which contribute to Higgs production. We again

include operators that contain right-handed Dirac neutrinos. We obtain limits on these operators from electroweak precision observables, the scale of neutrino mass, and limits on neutrino magnetic moments, and use these limits to constrain the contributions of these operators to the Higgs production cross-section. Although we find that all operators containing right-handed neutrinos contribute negligibly to Higgs production, we do find three operators containing only SM fields which could have observable contributions at an e^+e^- linear collider.

Lastly, we discuss the characteristics of a particular extra-dimensions model originally proposed by Carroll and Guica [54]. This model has two extra dimensions compactified into a sphere, a bulk magnetic field, and a bulk cosmological constant. In this model, the cosmological constant seen by a four-dimensional observer can be set to zero by fine-tuning the bulk magnetic field against the bulk cosmological constant. If branes with a tension are added at each of the poles of the two-sphere, solutions with zero four-dimensional cosmological constant are still possible, but the compactified dimensions must acquire a deficit angle which depends on the brane tension. However, the brane tension does not affect the fine-tuning relationship between the bulk cosmological constant and the bulk magnetic field. This feature led to the hope that, after this fine-tuning, the model might self-tune, keeping the four-dimensional cosmological constant zero regardless of what happens to the brane tension by adjusting the deficit angle. We speculated that this self-tuning property would imply a massless scalar mode in the perturbed Einstein's equations; as there exist very stringent limits on scalar-tensor theories of gravity, a massless scalar mode would make this model incompatible with observation. We conducted a search for such modes, and found none which satisfied the boundary conditions. This finding led us to speculate that this model does not, in fact, have a self-tuning property.

Contents

List of Figures

Chapter 1

Introduction

The Standard Model (SM) has demonstrated remarkable success in explaining particle interactions at energies up to a few hundred GeV. The experimental value for the anomalous magnetic moment of the muon agrees with the SM prediction to seven significant figures [1]. Fits to the LEP and SLD Z pole data [2] show that the current experimental data is well-described by the the Minimal Standard Model. And, of course, no non-SM particles have yet been discovered.

However, despite this success, few physicists believe that the SM is valid up to arbitrarily high energies; the SM contains 19 free parameters (not including neutrino masses and mixing angles!) which currently must be put in by hand, does not explain why fermions seem to come in three flavors or predict their masses, and requires the existence of a Higgs boson with a mass not too far from the weak scale, even though radiative corrections would be expected to push its mass up to the Planck scale. Additionally, as the SM does not address the issue of neutrino mass at all, does not explain the matter-antimatter asymmetry in the universe, and fails miserably to explain the cosmological constant, we now have conclusive evidence of physics beyond the SM.

To address some of these issues which the SM leaves unresolved, many ideas have been proposed for physics beyond the SM. These include supersymmetry (for an introductory review, see [3]), models of extra dimensions (see reviews [4, 5, 6]), models with with extra gauge bosons [7], technicolor [8], and many other ideas. Currently, the favored explanation for the scale of neutrino mass is the see-saw model [9, 10, 11, 12],

and the cosmological constant problem is a subject of intense study. (For some very recent reviews on the cosmological constant, see [13, 14, 15].)

While the value of studying particular new physics scenarios is evident, the richness of possibilities for physics beyond the Standard Model indicates that model-independent analyses are also worthwhile. In this work, we will use both approaches. First, in Chapters 2 and 3 we will use general operator analyses to obtain model-independent constraints on the contributions of new physics to two processes—muon decay and Higgs production. (Interestingly, both of these processes can, in principle, receive contributions from new physics which also gives rise to the (not-yet-understood) phenomenon of neutrino mass.) Then, in Chapter 4, we will study a particular extra-dimensions model which attempts to address the cosmological constant problem. We discuss the motivation for each of these analyses below.

1.1 Neutrino Mass and Muon Decay

Although the first direct evidence for neutrino mass came in the 1960s [16] with the observation of an unexpectedly low ν_e flux coming from the sun, it wasn't until the last two decades that the case for nonzero ν mass became compelling. For recent reviews, see [1], [17], and [18]. Fig. 1.1 (taken from [1]) gives a visual summary of the current knowledge of neutrino oscillation parameters taken from experiments.

Two mass regions in Fig. 1.1 are of particular interest. These roughly correspond to the regions explored by the "solar" (oscillations of ν_e or $\bar{\nu_e}$ into ν's of other flavors) and "atmospheric" (oscillations of ν_μ) experiments. The former is dominated by the most recent results of Super-Kamiokande (Super-K) [19] and the Sudbury Neutrino Observatory (SNO) [20], which look for disappearance of solar ν_e, and KamLAND [21], a reactor experiment which looks for disappearance of $\bar{\nu_e}$. Combining the results of the three experiments [19] gives the region marked "Super-K+SNO+KamLAND 95%" in Fig. 1.1, which indicates Δm^2 close to $8 \times 10^{-5}\,\mathrm{eV}^2$ and the Large Mixing Angle solution for $\tan^2\theta_\odot$. Observations of neutral-current ν interactions by SNO [22] are consistent with solar models, favoring oscillations of ν_e to other active flavors.

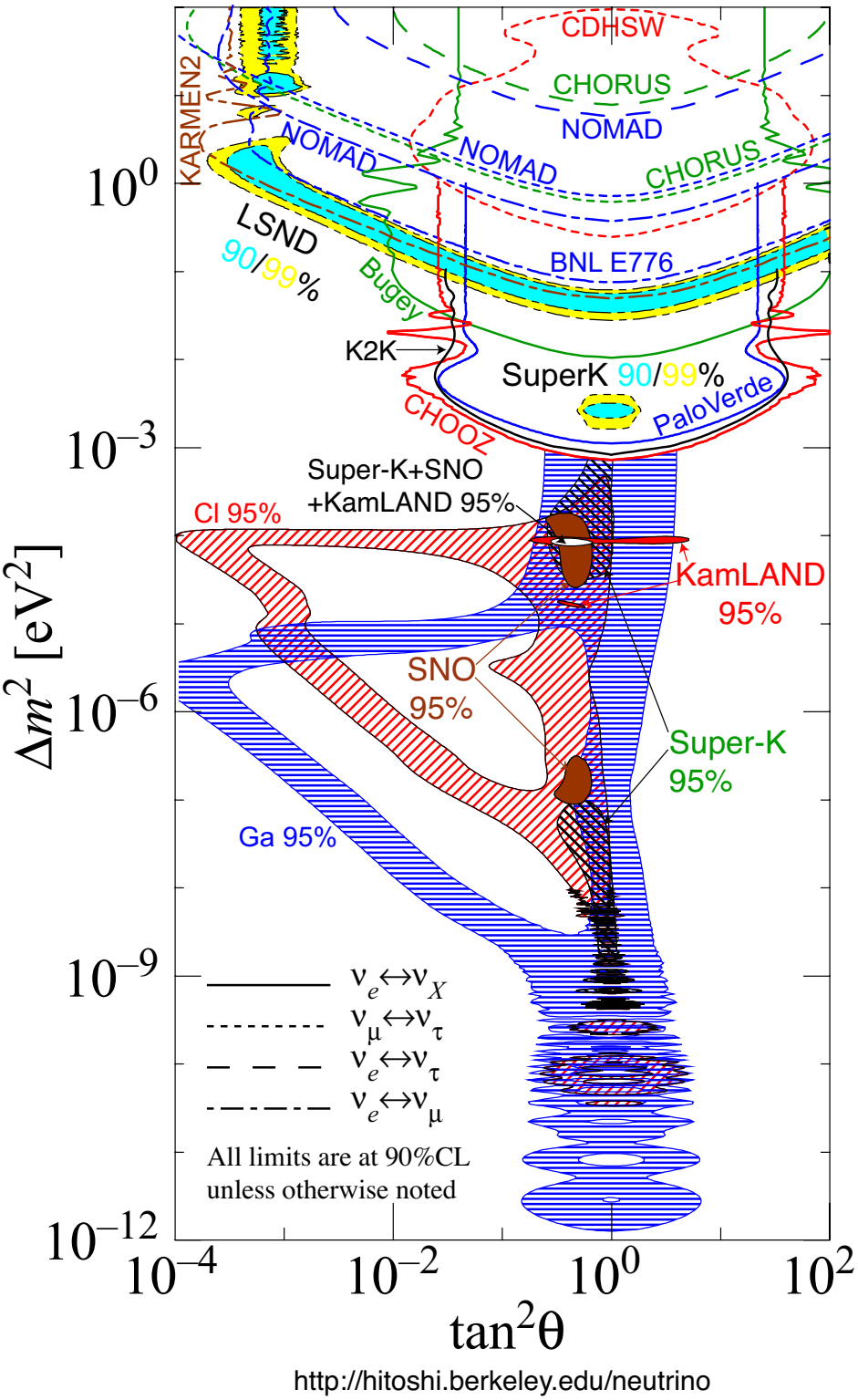

Figure 1.1: The current experimental status of ν oscillation parameters, taken from [1].

Tha atmospheric neutrino data, however, are dominated by Super-K. They report in [23] a deficit of ν_μ events dependent upon zenith angle and energy, with no corresponding deficit in ν_e events. They thus report $\sin^2 2\theta_{atm} > 0.92$ and $1.5 \times 10^{-3} < \Delta m^2 < 3.4 \times 10^{-3}\,\mathrm{eV}^2$ at 90% CL. They also report [24] a dependence upon L/E (where L is the ν flight distance and E is its energy) in their muon disappearance results, which yields similar results. Finally, they see [25] a ν_τ appearance at the 2.4σ level and find that their results are completely compatible with full $\nu_\mu - \nu_\tau$ mixing.

Also shown in Fig. 1.1 is the region favored by the LSND experiment [26, 27, 28, 29], whose results favored $\bar{\nu_\mu}$ to $\bar{\nu_e}$ oscillations with $\Delta m^2 \sim 1\,\mathrm{eV}^2$. Assuming three neutrino flavors, neutrino mass results must satisfy the simple relation

$$\Delta m^2_{12} + \Delta m^2_{23} = \Delta m^2_{13} \tag{1.1}$$

where $\Delta m^2_{ij} = m^2_i - m^2_j$. This relation cannot be satisfied by the Δm^2_{ij}s implied by the solar, atmospheric, and LSND experiments. Thus, the LSND results were considered possible evidence for a sterile neutrino ν_s. However, the very recent results of MiniBooNE [30] do not support the LSND results and there is currently no compelling evidence for a sterile ν.

While constraints from neutrino oscillations give us information about the squared mass differences Δm^2_{ij} between different mass eigenstates, they tell us nothing about the overall scale of neutrino mass. Results from tritium β decay [31, 32] give a limit of < 2 eV [1] on the sum

$$\sum_i |U_{ei}|^2 m^2_{\nu_i} \tag{1.2}$$

where U is the neutrino mixing matrix.

Limits also exist on the sum of the neutrino masses from cosmology. Constraints from WMAP and the Sloan Digital Sky Survey [33] give a limit of

$$\sum m_\nu < .42\,\mathrm{eV} \text{ at } 95\%,\ \mathrm{CL} \tag{1.3}$$

assuming three flavors of neutrinos.

It is these last two results which will be the most relevant to our work in Chapters 2 and 3. However, the presence of neutrino oscillations (and therefore nonzero neutrino mass) imply that the SM Lagrangian is not complete. If neutrinos are purely Dirac particles, the Lagrangian will receive terms of the form

$$\delta\mathcal{L} = -m_\nu^{ij}\bar{\nu_R}^i\nu_L^j + h.c. \tag{1.4}$$

where i and j are flavor indices. Thus, we must necessarily add a right-handed neutrino ν_R to the SM. However, if neutrinos are instead purely Majorana particles and receive a mass term of the form

$$\delta\mathcal{L} = -\frac{1}{2}m_\nu^{ij}\bar{\nu_R}^i\nu_R^{cj} + h.c. \tag{1.5}$$

then we find that nature allows lepton number violation. Therefore, when considering extensions to the SM, we should allow the Lagrangian to contain terms which contain right-handed Dirac neutrinos or to contain terms which violate lepton number, or both. In this work, for simplicity, we will assume that neutrinos are purely Dirac particles.

Given that neutrino mass is a window onto physics beyond the SM, it makes sense to consider the possibility that the current knowledge of neutrino mass could already be used to place constraints on new physics and its possible manifestations in observable processes. The first such process which we consider is muon decay. One can write the effective muon decay Lagrangian in the form

$$\mathcal{L}^{\mu-\text{decay}} = -\frac{4G_\mu}{\sqrt{2}}\sum_{\gamma,\,\epsilon,\,\mu} g_{\epsilon\mu}^\gamma\ \bar{e}_\epsilon\Gamma^\gamma\nu\bar{\nu}\Gamma_\gamma\mu_\mu \tag{1.6}$$

where Γ^γ runs over all possible Lorentz structures (1, γ^μ and $\sigma^{\mu\nu}/\sqrt{2}$) and ϵ and μ are the electron and muon chiralities. In the SM, $g_{LL}^V = 1$ and all others are zero. It is easy to see from Eq. 1.6, however, that the sum also includes terms that differ from those given by the $V-A$ structure of the SM and, in particular, includes

terms which contain right-handed neutrinos, such as the case $\gamma = V$, ϵ or $\mu = R$. Thus, it is not hard to imagine that if neutrino mass compels us to include in the Lagrangian effective operators which contain right-handed neutrinos, that some of these operators could contribute to $\mathcal{L}^{\mu-\text{decay}}$. A key point of the analysis which we present in Chapter 2 is that some of these operators will contribute to neutrino mass, and, thus, can be constrained by current limits on m_ν. (More specifically, one can note that dimension-six operators that contribute to m_ν without insertions of tiny neutrino Yukawa couplings will contain a single ν_R field. This implies that the terms in $\mathcal{L}^{\mu-\text{decay}}$ which can be constrained by limits on m_ν will contain one right-handed ν and one left-handed ν, and, thus, $\epsilon \neq \mu$.)

These coefficients $g^\gamma_{\epsilon\mu}$ can be translated into effects on the muon decay spectrum, which can be written as

$$\begin{aligned}\frac{d^2\Gamma}{dx\, d\cos\theta} &= \frac{m_\mu}{4\pi^2} W_{e\mu}^4 G_\mu^2 \sqrt{x^2 - x_0^2} \\ &\quad \times \left[F_{IS}(x) \pm P_\mu \cos\theta\, F_{AS}(x)\right] \\ &\quad \times \left[1 + \vec{\zeta}\cdot\vec{P}_e(x,\theta)\right]\end{aligned} \tag{1.7}$$

where $W_{e\mu} = (m_\mu^2 + m_e^2)/2m_\mu$ is the maximum e energy, $x = E_e/W_{e\mu}$, $x_0 = m_e/W_{e\mu}$, and $\vec{P}_\mu$ and $\vec{P}_e$ are the μ and e polarizations. $\vec{\zeta}$ is a vector dependent on the experimental configuration. The isotropic and anisotropic components of the decay spectrum, $F_{IS}(x)$ and $F_{AS}(x)$, can be written in terms of four of the Michel parameters (MPs) ρ, η, ξ, and δ [34, 35]:

$$F_{IS} = x(1-x) + \frac{2}{9}\rho(4x^2 - 3x - x_0^2) + \eta x_0(1-x) \tag{1.8}$$

$$F_{AS} = \frac{1}{3}\xi\sqrt{x^2 - x_0^2}\left[1 - x + \frac{2}{3}\delta\left(4x - 3 + \left(\sqrt{1 - x_0^2} - 1\right)\right)\right]. \tag{1.9}$$

In the SM these parameters take the values $\rho = \delta = \frac{3}{4}$, $\eta = 0$, and $\xi = 1$.

For our purposes, ρ will be particularly useful. It can be expressed in terms of the

$g^{\gamma}_{\epsilon\mu}$s as

$$\rho = \frac{3}{4} - \left(\frac{3}{4} \left| g^{V}_{LR} \right|^2 + \frac{3}{2} \left| g^{T}_{LR} \right|^2 + \frac{3}{4} \mathrm{Re} \left(g^{S}_{LR} g^{T*}_{LR} \right) + (L \leftrightarrow R) \right). \tag{1.10}$$

It should be noted that the $g^{S,V,T}_{LR,RL}$ all correspond to terms in Eq. 1.6 which contain right-handed neutrinos. Recently, ρ (and δ) has been measured by the TWIST Collaboration [36, 37], who hope to eventually improve their precision to the few $\times 10^{-4}$ level.

In Chapter 2, we set out investigate whether the scale of neutrino mass can be used to place limits on some of the $g^{\gamma}_{\epsilon\mu}$. We enumerate the dimension-six operators which can contribute to a Dirac mass of the neutrino or to muon decay, and then use current upper bounds on neutrino mass to derive constraints on contributions of these operators to chirality-changing (i.e, $\epsilon \neq \mu$) terms in the muon decay Lagrangian. We obtain model-independent constraints considerably stronger than the current experimental bounds and, finally, discuss the implications for currently ongoing experiments to measure the muon decay parameters. The content of Chapter 2 is largely borrowed from the work of Erwin et al. [38].

In the analysis of Chapter 2 (and later in Chapter 3), we will assume a scale of 1 eV for an upper limit on a generic entry of the neutrino mass matrix, and, for simplicity, we will assume that neutrinos are purely Dirac particles. For a similar study of muon decay where neutrinos are allowed to have Majorana mass terms, see [39]. It should be noted that our limits from neutrino mass on the effects of physics beyond the SM given in those chapters will improve if the upper bounds on the neutrino mass scale become more stringent in future measurements.

One can also ask what ramifications our results can have for certain models. A class of models for which the Michel parameters have particular relevance is Left-Right-Symmetric Models (LRSM). For a treatment of the interplay of muon decay and LRSM, we direct the reader to [40].

1.2 Fermionic Operators and Higgs Production

Continuing with our work with effective operators, we move from muon decay to Higgs production at an e^+e^- Linear Collider. Unlike muon decay, all that is known about the properties of the Higgs boson is theoretical or through indirect experimental evidence. Direct searches [41] have ruled out the ranges of the Higgs boson mass $m_H < 114.4$ at the 95% confidence level. Fits to m_H by the LEP Electroweak Working Group have yielded the range shown in Fig. 1.2 (from [42]); they obtain a 95% CL upper limit of 186 GeV, which rises to 219 GeV when the direct search results are included.

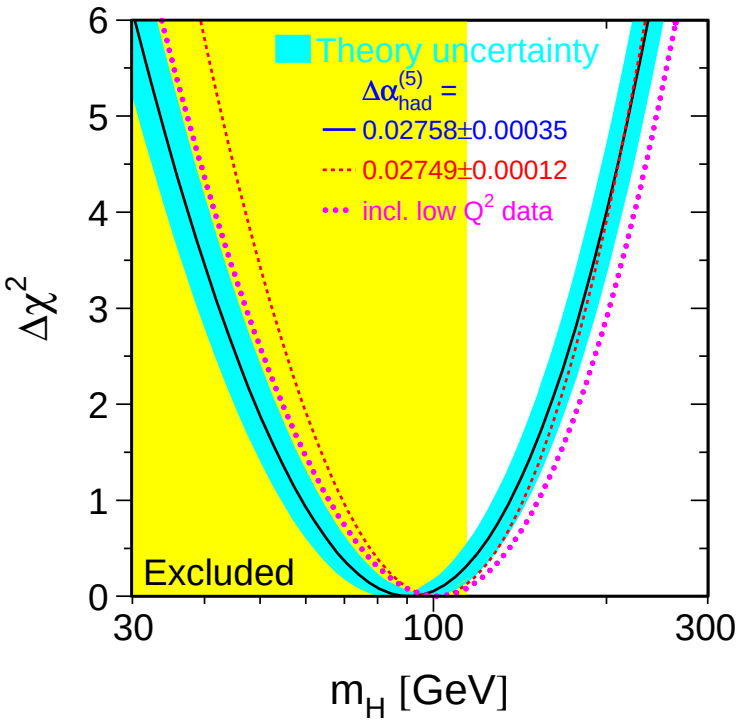

Figure 1.2: χ^2 plotted as a function of M_H, taken from [42]. The yellow band shows the region excluded by the direct searches at 95% CL.

Given the range of m_H compatible with the SM, it (or something like it) is expected to be discovered at the LHC. Assuming that such a Higgslike particle is, in fact, discovered, a linear collider will be necessary to measure its properties to determine if it really is an SM Higgs boson. Especially important are measurements of the

particle's mass, spin, and couplings to other particles. (For a short review, see [43].) Is the new particle a scalar? Are its couplings to the $W^{\pm}$ and Z particles compatible with it being the source of electroweak symmetry breaking? Are its couplings to fermions proportional to their masses? For an excellent discussion of Higgs physics at a future LC, we direct the reader to [44].

Here, we will concentrate on the observable most relevant to our work in Chapter 3, the Higgs Boson production cross-section. As the production cross-section is also important for measurements of the Higgs branching fractions [45], we will discuss their relevance as well.

A precise measurement of the Higgs production cross-section is critical for distinguishing an SM Higgs boson from scalars predicted by other models, such as supersymmetry. For example, the production cross-section for the lightest MSSM Higgs will differ from that of the SM Higgs. (For a calculation of the cross-sections for the MSSM Higgses with radiative corrections included, see [46].) In addition, [47] describes in detail how partial width and branching ratio measurements at a linear collider could be used to distinguish an SM Higgs boson from an MSSM Higgs. This would be particularly important for values of $\tan\beta$ and M_A where it is possible that only one of the MSSM scalars would be observable at the LHC.

The branching fractions of a Higgslike scalar can also be useful in distinguishing the SM from extra-dimensions scenarios. The authors of [48] find that an SM Higgs boson can be distinguished from the Randall-Sundrum scalar radion by precise measurements of its branching fractions, particularly to gg; for a particularly light radion, gg can actually be the primary decay mode, whereas a Higgs of the same mass would decay primarily to $\bar{b}b$. The authors of [49] and [50] consider how Higgs-radion mixing could affect the properties of a Higgs boson; they find that the branching ratios, particularly $H \to gg$, could differ substantially from the SM expectation. [50] additionally find that the HZZ coupling would differ from the SM scenario, leading to changes in the overall Higgs production cross-section.

There are multiple reasons why it is important to understand how much physics at a high energy scale Λ could affect the measurements of the Higgs boson properties.

First and foremost, if it turns out that the possible effects of new physics are large enough to substantially change either the expected Higgs mass range or its production or decay mechanisms, search strategies may have to be changed accordingly. Secondly, given the importance of determining the Higgs production cross-section, we would like to know whether an observed deviation from the SM expectation favors particular models, or if unknown new physics at energy scale Λ could make the interpretation of such a deviation ambiguous.

In Chapter 3, we describe the use of a general operator analysis to constrain the effects of physics beyond the SM on Higgs production at a linear collider. We restrict ourselves to dimension-six operators which contain fermions and Higgs fields (for similar analyses considering other operators, see [51, 52]), including three operators which we borrow from the muon decay analysis. We then use precision electroweak data and limits on neutrino mass to place limits on the contributions of these operators to Higgs production at a linear collider, and find operators that could have observable effects on the Higgs production cross-section. Chapter 3 borrows heavily from the work of Kile and Ramsey-Musolf [53].

1.3 Extra Dimensions and the Cosmological Constant

After the discussion of these two model-independent analyses, in Chapter 4 we investigate the characteristics of a specific model of extra dimensions which was originally proposed in [54]. This model was proposed to possibly shed new light on the cosmological constant problem, the observation of a cosmological constant more than 120 orders of magnitude smaller than the naive SM expectation of M_P^4.

Other models of extra dimensions have been proposed to address the cosmological constant problem [55, 56, 57, 58, 59]. In models with extra dimensions, the cosmological constant seen by a four-dimensional observer can receive contributions from both brane and bulk terms. Thus, in order to make the cosmological constant small, these

models introduce an unpleasant fine-tuning between different terms which contribute to the cosmological constant. The model presented in [54] also required such a fine-tuning; however, it appeared possible in this model that, once this fine-tuning took place, the volume of the extra dimensions would adjust itself so that the cosmological constant would remain zero, independent of the brane tension.

We expected that this self-tuning property would imply a massless mode in the perturbed Einstein's equations, and searched for such modes. The presence of such a mode would cause this model to be strongly disfavored, as tests of the equivalence principle [60, 61] place tight constraints on scalar-tensor theories of gravity. We found no such modes and speculated that this model did not, in fact, have a self-tuning property. Chapter 4 is taken from Graesser, Kile, and Wang [62].

Chapter 2

Muon Decay Parameters From Neutrino Mass

In this chapter, we discuss the first of our two model-independent analyses: using current limits on the scale of neutrino mass (~ 1 eV) to constrain the effects of new physics on muon decay. We specifically consider operators which can contribute to the chirality-changing terms in the muon decay Lagrangian, and we only consider the case of Dirac neutrinos. The contents of this chapter are, aside from small cosmetic changes, taken from [38].

2.1 Introduction

Precision studies of muon decay continue to play an important role in testing the Standard Model (SM) and searching for physics beyond it. In the gauge sector of the SM, the Fermi constant G_μ that characterizes the strength of the low-energy, four-lepton μ-decay operator is determined from the μ lifetime and gives one of the three most precisely known inputs into the theory. Analyses of the spectral shape, angular distribution, and polarization of the decay electrons (or positrons) probe for contributions from operators that deviate from the $(V-A)\otimes(V-A)$ structure of the SM decay operator. In the absence of time-reversal (T) violating interactions, there exist seven independent parameters—the so-called Michel parameters [34, 35, 63]—that characterize the final state charged leptons: two (ρ, η) that describe the spatially isotropic component of the lepton spectrum; two (ξ, δ) that characterize the spatially

anisotropic distribution; and three additional quantities (ξ', ξ'', η'') that are needed to describe the lepton's transverse and longitudinal polarization[1]. Two additional parameters (α'/A, β'/A) characterize a T-odd correlation between the final state lepton spin and momenta with the muon polarization: $\hat{S}_e \cdot \hat{k}_e \times \hat{S}_\mu$.

Recently, new experimental efforts have been devoted to more precise determinations of these parameters. The TWIST Collaboration has measured ρ and δ at TRIUMF [36, 37], improving the uncertainty over previously reported values by factors of ~ 2.5 and ~ 3, respectively. An experiment to measure the transverse positron polarization has been carried out at the Paul Scherrer Institute (PSI), leading to similar improvements in sensitivity over the results of earlier measurements [64]. A new determination of $P_\mu \xi$ with a similar degree of improved precision is expected from the TWIST Collaboration, and one anticipates additional reductions in the uncertainties in ρ and δ [65].

At present, there exists no evidence for deviations from SM predictions for the Michel parameters (MPs). It is interesting, nevertheless, to ask what constraints these new measurements can provide on possible contributions from physics beyond the SM. It has been conventional to characterize these contributions in terms of a set of ten four-fermion operators

$$\mathcal{L}^{\mu-\text{decay}} = -\frac{4G_\mu}{\sqrt{2}} \sum_{\gamma,\,\epsilon,\,\mu} g^\gamma_{\epsilon\mu}\ \bar{e}_\epsilon \Gamma^\gamma \nu \bar{\nu} \Gamma_\gamma \mu_\mu \tag{2.1}$$

where the sum runs over Dirac matrices $\Gamma^\gamma = 1$ (S), γ^α (V), and $\sigma^{\alpha\beta}/\sqrt{2}$ (T), and the subscripts μ and ϵ denote the chirality (R, L) of the muon and final state lepton, respectively[2]. In the SM, one has $g^V_{LL} = 1$ and all other $g^\gamma_{\epsilon\mu} = 0$. A recent, global analysis by Gagliardi, Tribble, and Williams [67] give the present experimental bounds on the $g^\gamma_{\epsilon\mu}$ that include the impact of the latest TRIUMF and PSI measurements.

Theoretically, the $g^\gamma_{\epsilon\mu}$ can be generated in different scenarios for physics beyond the

[1]The parameters η and η'' are alternately written in terms of the independent parameters α/A and β/A.

[2]The normalization of the tensor terms corresponds to the convention adopted in [66]. We do not specify the neutrino flavors in Eq. (2.1) since the μ-decay experiments do not observe the final state neutrinos.

SM. The most commonly cited illustration is the minimal left-right symmetric model that gives rise to non-zero g_{RR}^V, g_{RL}^V, and g_{LR}^V. From a model-independent standpoint, the authors of [68] recently observed that the operators in Eq. (2.1), having different chiralities for the muon and final state charged lepton, will also contribute to the neutrino mass matrix m_ν^{AB} through radiative corrections. Consequently, one expects that the present upper bounds on m_ν should imply bounds on the magnitudes of the $g_{\epsilon\mu}^\gamma$. The authors of [68] argued that the most stringent limits arise from two-loop contributions because the one-loop contributions are suppressed by three powers of the tiny, charged lepton Yukawa couplings. The two-loop constraints are nonetheless stronger than the present bounds given in [67] and could become even more so with the advent of future terrestrial and cosmological probes of the neutrino mass scale.

In this chapter, we present the results of a follow-up analysis of m_ν constraints on the μ-decay parameters, motivated by the observations of [68] and the new experimental developments in the field. Our study follows the approach of [69],[70], and [71], used recently in deriving model-independent naturalness bounds on neutrino magnetic moments implied by the scale of m_ν. We concentrate on the case of Dirac neutrinos, deferring a detailed consideration of Majorana neutrinos to a separate analysis. Although there exists a long-standing theoretical prejudice favoring the see-saw mechanism with light, Majorana neutrinos as an explanation of the small scale of m_ν, we see several reasons for studying the Dirac and Majorana cases separately:

(i) From the standpoint of string phenomenology, obtaining models with neutrino self-couplings and a type I see-saw mechanism appears to be quite difficult. Recently, the authors of [72] performed a systematic study of 175 viable ways of embedding the Standard Model gauge group in the $E_8 \times E_8$ heterotic string with Z_3 orbifold compactification and found that only two of the twenty classes of such inequivalent models admitted neutrino self-couplings. The natural scale of m_ν in these two classes lies many orders of magnitude below the scale implied by neutrino oscillation data. Interactions leading to Dirac masses occur more abundantly in such constructions. On the other hand, a subsequent study of a specific

$Z_3 \times Z_3$ orbifold string construction [73] indicated the plausibility of obtaining a type II see-saw mechanism, wherein left-handed lepton-number-violating neutrino self-couplings arise from interactions with scalar $\mathrm{SU}(2)_L$ triplet fields. Either way, however, the appearance of Majorana mass terms is not at all a generic feature of string constructions, leaving the Dirac case as a logical possibility.

(ii) Experimentally, there exists no conclusive evidence for or against the presence of light Majorana neutrinos. New searches for neutrinoless double β-decay ($0\nu\beta\beta$) could provide conclusive proof that the light neutrinos are Majorana, provided the neutrino mass spectrum has the "inverted" rather than "normal" hierarchy (for recent reviews, see, e.g., [74] and [75]). If, on the other hand, future long-baseline oscillation experiments establish the existence of the inverted hierarchy and/or ordinary β-decay measurements indicate a mass consistent with the inverted hierarchy, a null result from the $0\nu\beta\beta$ searches would imply that neutrinos are Dirac particles[3]. Either way, the investment of substantial experimental resources in these difficult measurements indicates that determining the charge conjugation properties of the neutrino is both a central question for neutrino physics as well as one that is not settled. Until it is, considering the implications of Dirac neutrinos remains a valid enterprise.

(iii) The phenomenological analyses of Dirac and Majorana masses for other neutrino properties and interactions are quite distinct. As illustrated by the recent analyses of neutrino magnetic moments in [69], [70], and [71], the characteristics of the operator basis and renormalization can be sufficiently different and complex for the two cases that separate studies of each are warranted. Moreover, the parameterization of the μ-decay Michel spectrum in the presence of Majorana neutrinos may require modification from the standard form, as indicated by the recent work of [76]. Rather than lose the reader in the details of differences in both the Michel parameterization and operator renormalization for Dirac and Majorana neutrinos, we prefer to concentrate on the Dirac case in the present

[3]We thank S. J. Freedman for useful discussions on this point.

study and consider the Majorana case in a separate paper.

Having this focus in mind, we work with an effective theory that is valid below a scale Λ lying above the weak scale $v \approx 246$ GeV and that contains $\mathrm{SU}(2)_L \times \mathrm{U}(1)_Y$-invariant operators built from Standard Model fields plus right-handed (RH) Dirac neutrinos. We consider all relevant operators up to dimension $n = 6$ that could be generated by physics above the scale Λ. For simplicity, we restrict our attention to two generations of lepton doublets and RH neutrinos. Extending the analysis to include a third generation increases the number of relevant operators but does not change the substantive conclusions. While the spirit of our work is similar to that of [68], the specifics of our analysis and conclusions differ in several respects:

i) The effective theory that we adopt allows us to compute contributions to m_ν from scales lying between the weak scale v and the scale of new physics Λ. In contrast, the authors of [68] used a Fierz transformed version of $\mathcal{L}^{\mu-\mathrm{decay}}$ in Eq. (2.1), which is not invariant under the SM gauge group and, therefore, should be used to analyze only contributions below the weak scale.

ii) We show that for the two-flavor case the operators in $\mathcal{L}^{\mu-\mathrm{decay}}$ proportional to $g_{LR}^{S,T}$ and $g_{RL}^{S,T}$ arise from twelve independent dimension $n = 6$ gauge-invariant four-fermion operators, while those containing g_{LR}^{V} and g_{RL}^{V} are generated by four independent $n = 6$ operators that contain two fermions and two Higgs scalars.

iii) While the operators that contribute to μ-decay have dimension $n = 6$ or higher, the lowest dimension neutrino mass operator occurs at $n = 4$. The authors of [68] used dimensional regularization (DR) to estimate the mixing between the $n = 6$ μ-decay and neutrino mass operators[4] but did not consider matching with the $n = 4$ operator at the scale Λ that cannot be determined with DR. We derive order-of-magnitude expectations for the $n = 6$ operator coefficients

[4]Since the computation of [68] did not employ gauge invariant operators, we consider the results to give at best reasonable estimates of constraints implied by two-loop mixing.

implied by this matching, which depends only linearly on the lepton Yukawa couplings and which gives the dominant constraints for $\Lambda \gg v$.

iv) For Λ not too different from v, constraints associated with mixing among the $n = 6$ operators can, in principle, be comparable to expectations arising from contributions to the $n = 4$ mass operator. We carry out a complete, one-loop analysis of this mixing and show that only the neutrino magnetic moment and two-fermion/two-Higgs operators mix with the $n = 6$ neutrino mass operator to linear order in the lepton Yukawa couplings. We derive the resulting bounds on the $g^V_{LR,RL}$ that follow from this mixing and find that they are comparable to expectations based on one-loop matching with the $n = 4$ mass operator for $\Lambda \gtrsim v$.

v) From the mixing with the $n = 6$ mass operator, we find that the bounds on the $|g^V_{LR,RL}|$ are two or more orders of magnitude stronger than those obtained in [68] and at least three orders of magnitude below the experimental limits given in [67].

vi) The neutrino mass implications for the couplings $g^{S,T}_{LR,RL}$ are more subtle. Of the twelve independent four-fermion operators that contribute to these couplings, only eight are directly constrained by the scale of neutrino mass and naturalness considerations. Based on one-loop matching, we expect that their contributions to the $g^{S,T}_{LR,RL}$ are generally $\sim 10^4$ times smaller than the present experimental bounds, and $\sim 10^3$ times smaller than obtained in the analysis of [68]. We show, however, that the flavor structure of the remaining four operators allows them to evade constraints implied by either one-loop matching or two-loop mixing. While from a theoretical perspective one might not expect their contributions to be substantially larger than those from the constrained operators, experimental efforts to determine the $g^{S,T}_{LR,RL}$ remain a worthwhile endeavor.

A summary of our results is given in Table 2.1. In the remainder of the paper we give the details of our analysis. In Section 3.3, we write down the complete set

Table 2.1: Constraints on μ-decay couplings $g^{\gamma}_{\epsilon\mu}$. The first eight rows give naturalness expectations in units of $(v/\Lambda)^2 \times (m_\nu/1\,\mathrm{eV})$ on contributions from $n = 6$ muon decay operators (defined in Section 3.3 below) based on one-loop matching with the $n = 4$ neutrino mass operators. For $\Lambda \sim v$, the bounds on $g^{V}_{LR,RL}$ obtained from one-loop mixing are similar to those listed. The ninth row gives upper bounds derived from a recent global analysis of [67], while the last row gives estimated bounds from [68] derived from two-loop mixing of $n = 6$ muon decay and mass operators. A "-" indicates that the operator does not contribute to the given $g^{\gamma}_{\epsilon\mu}$, while "None" indicates that the operator gives a contribution unconstrained by neutrino mass. The subscript D runs over the two generations of RH Dirac neutrinos.

Source	$\lvert g^{S}_{LR}\rvert$	$\lvert g^{T}_{LR}\rvert$	$\lvert g^{S}_{RL}\rvert$	$\lvert g^{T}_{RL}\rvert$	$\lvert g^{V}_{LR}\rvert$	$\lvert g^{V}_{RL}\rvert$
$\mathcal{O}^{(6)}_{F,122D}$	4×10^{-7}	2×10^{-7}	-	-	-	-
$\mathcal{O}^{(6)}_{F,212D}$	4×10^{-7}	-	-	-	-	-
$\mathcal{O}^{(6)}_{F,112D}$	None	None	-	-	-	-
$\mathcal{O}^{(6)}_{F,211D}$	-	-	8×10^{-5}	4×10^{-5}	-	-
$\mathcal{O}^{(6)}_{F,121D}$	-	-	8×10^{-5}	-	-	-
$\mathcal{O}^{(6)}_{F,221D}$	-	-	None	None	-	-
$\mathcal{O}^{(6)}_{\tilde{V},2D}$	-	-	-	-	8×10^{-7}	-
$\mathcal{O}^{(6)}_{\tilde{V},1D}$	-	-	-	-	-	2×10^{-4}
Global [67]	0.088	0.025	0.417	0.104	0.036	0.104
Two-loop [68]	10^{-4}	10^{-4}	10^{-2}	10^{-2}	10^{-4}	10^{-2}

of independent operators through $n = 6$ that contribute to m_ν^{AB} and/or μ-decay. Section 2.3 gives our analysis of operator mixing and matching considerations, while in Section 2.4 we discuss the resulting constraints on the $g^{\gamma}_{LR,RL}$ that follow from this analysis and the present upper bounds on the neutrino mass scale. We summarize in Section 3.6.

2.2 Operator Basis

To set notation, we follow [69] and consider the effective Lagrangian

$$\mathcal{L}_{\text{eff}} = \sum_{n,j} \frac{C^n_j(\mu)}{\Lambda^{n-4}} \mathcal{O}^{(n)}_j(\mu) \ + \text{h.c.} \tag{2.2}$$

where μ is the renormalization scale, $n \geq 4$ is the operator dimension, and j is an index running over all independent operators of a given dimension. The lowest dimension neutrino mass operator is

$$\mathcal{O}^{(4)}_{M,\,AD} = \bar{L}^A \tilde{\phi} \nu^D_R \tag{2.3}$$

where L^A is the left-handed (LH) lepton doublet for generation A, ν^D_R is a RH neutrino for generation D, and $\tilde{\phi} = i\tau_2 \phi^*$, with ϕ being the Higgs doublet field. After spontaneous symmetry breaking, one has

$$\phi \to \begin{pmatrix} 0 \\ v/\sqrt{2} \end{pmatrix} \tag{2.4}$$

so that

$$\begin{aligned} C^4_{M,\,AD} \mathcal{O}^{(4)}_{M,\,AD} &\to -m^{AD}_\nu \bar{\nu}^A_L \nu^D_R \\ m^{AD}_\nu &= -C^4_{M,\,AD}\, v/\sqrt{2} \quad . \end{aligned} \tag{2.5}$$

The other $n = 4$ operators are those of the SM and we do not write them down explicitly here.

For the case of Dirac neutrinos that we consider here, there exist no gauge-invariant $n = 5$ operators. In considering those with dimension six, it is useful to group them according to the number of fermion, Higgs, and gauge boson fields that enter:

Four fermion:

$$\bar{L}\gamma^\mu L\bar{L}\gamma_\mu L$$
$$\bar{\ell}_R\gamma^\mu \ell_R\bar{\ell}_R\gamma_\mu \ell_R$$
$$\bar{\ell}_R\gamma^\mu \ell_R\bar{\nu_R}\gamma_\mu \nu_R$$
$$\bar{\nu_R}\gamma^\mu \nu_R\bar{\nu_R}\gamma_\mu \nu_R$$
$$\bar{L}\ell_R\bar{\ell}_R L$$
$$\bar{L}\nu_R\bar{\nu_R} L$$
$$\epsilon^{ij}\bar{L}_i\ell_R\bar{L}_j\nu_R$$

Here ℓ_R is the right-handed charged lepton field. Several of the operators appearing in this list can contribute to μ-decay, but only the last one can also contribute to m_ν^{AD} through radiative corrections. Including flavor indices, we refer to this operator as

$$\mathcal{O}^{(6)}_{F,\,ABCD} = \epsilon^{ij}\bar{L}_i^A\ell_R^C\bar{L}_j^B\nu_R^D \tag{2.6}$$

where the indices i, j refer to the weak isospin components of the LH doublet fields and $\epsilon^{12} = -\epsilon^{21} = 1$.

Fermion-Higgs:

$$\begin{aligned} i(\bar{L}^A\gamma^\mu L^B)(\phi^+ D_\mu\phi) \\ i(\bar{L}^A\gamma^\mu\tau^a L^B)(\phi^+\tau^a D_\mu\phi) \\ i(\bar{\ell}_R^A\gamma^\mu\ell_R^B)(\phi^+ D_\mu\phi) \\ i(\bar{\nu}_R^A\gamma^\mu\nu_R^B)(\phi^+ D_\mu\phi) \\ i(\bar{\ell}_R^A\gamma^\mu\nu_R^B)(\phi^+ D_\mu\widetilde{\phi}) \end{aligned} \tag{2.7}$$

Neither of the first two operators in the list (2.7) can contribute significantly to

m_ν^{AD} since they contain no RH neutrino fields. Any loop graph through which they radiatively induce m_ν^{AD} would have to contain operators that contain both LH and RH fields, such as $\mathcal{O}^{(4)}_{M,\,AB}$ or other $n = 6$ operators. In either case, the resulting constraints on the operator coefficients will be weak. For similar reasons, the third and fourth operators cannot contribute substantially because they contain an even number of neutrino fields having the same chirality and since the neutrino mass operator contains one LH and one RH neutrino field. Only the last operator

$$\mathcal{O}^{(6)}_{\tilde{V},\,AD} \equiv i(\bar{\ell}^A_R \gamma^\mu \nu^D_R)(\phi^+ D_\mu \widetilde{\phi}) \tag{2.8}$$

can contribute signficantly to m_ν since it contains a single RH neutrino. It also contributes to the μ-decay amplitude after SSB via the graph of Fig. 2.1a since the covariant derivative D_μ contains charged W-boson fields. We also write down the $n = 6$ neutrino mass operators

$$\mathcal{O}^{(6)}_{M,\,AD} = (\bar{L}^A \widetilde{\phi} \nu^D_R)(\phi^+ \phi) \tag{2.9}$$

as well as the charged lepton mass operator $(\bar{L}\phi\ell_R)(\phi^+\phi)$ that we do not use in the present analysis.

Fermion-Higgs-Gauge:

$$\begin{aligned}
\bar{L}\tau^a \gamma^\mu D^\nu L W^a_{\mu\nu} \\
\bar{L}\gamma^\mu D^\nu L B_{\mu\nu} \\
\bar{\ell}_R \gamma^\mu D^\nu \ell_R B_{\mu\nu} \\
\bar{\nu}_R \gamma^\mu D^\nu \nu_R B_{\mu\nu} \\
g_2(\bar{L}\sigma^{\mu\nu}\tau^a\phi)\ell_R W^a_{\mu\nu} \\
g_1(\bar{L}\sigma^{\mu\nu}\phi)\ell_R B_{\mu\nu} \\
g_2(\bar{L}\sigma^{\mu\nu}\tau^a\widetilde{\phi})\nu_R W^a_{\mu\nu} \\
g_1(\bar{L}\sigma^{\mu\nu}\widetilde{\phi})\nu_R B_{\mu\nu}
\end{aligned} \tag{2.10}$$

As for the fermion-Higgs operators, the operators in (2.10) that contain an even number of ν_R fields will not contribute significantly to m_ν^{AB}, so only the last two in the list are relevant:

$$\mathcal{O}^{(6)}_{B,\,AD} = g_1(\bar{L}^A\sigma^{\mu\nu}\widetilde{\phi})\nu_R^D B_{\mu\nu} \tag{2.11}$$

$$\mathcal{O}^{(6)}_{W,\,AD} = g_2(\bar{L}^A\sigma^{\mu\nu}\tau^a\widetilde{\phi})\nu_R^D W^a_{\mu\nu} \tag{2.12}$$

In addition to these operators, there exist additional $n = 6$ operators that contain two derivatives. However, as discussed in [69], they can either be related to $\mathcal{O}^{(6)}_{B,\,AD}$ and $\mathcal{O}^{(6)}_{W,\,AD}$ through the equations of motion or contain derivatives acting on the ν_R fields so that they do not contribute to the neutrino mass operator. Consequently, we need not consider them here. We also observe that the operator $\mathcal{O}^{(6)}_{W,\,AD}$ will also contribute to the μ-decay amplitude via graphs as in Fig. 2.1b. We have computed its contributions to the Michel parameters and find that they are suppressed by $\sim (m_\mu/\Lambda)^2 \lesssim 1.7 \times 10^{-7}$ relative to the effects of the other $n = 6$ operators. This suppression arises from the presence of the derivative acting on the gauge field and the absence of an interference between the corresponding amplitude and that of the SM. Finally, we note that the operators whose chiral structure suppresses their contributions to the neutrino mass operator (as discussed above) may, in general, contribute to muon decay via the terms in Eq. (2.1) having $\epsilon = \mu$. We do not consider these terms in this study.

2.3 Operator Renormalization: Mixing and Matching Considerations

In analyzing the renormalization of operators that contribute to both μ-decay and m_ν^{AD} it is useful to consider separately two cases: (i) one-loop matching conditions at the scale Λ involving the $n = 6$ operators that enter μ-decay and the $n = 4$ mass operator, $\mathcal{O}^{(4)}_{M,\,AD}$, and (ii) mixing among the relevant $n = 6$ operators. In general,

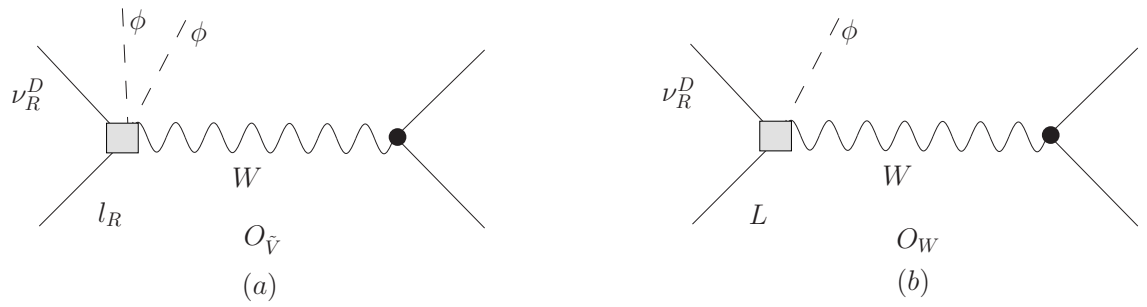

Figure 2.1: Contributions from the operators (a) $\mathcal{O}^{(6)}_{\tilde{V},\,AD}$ and (b) $\mathcal{O}^{(6)}_{W,\,AD}$ (denoted by the shaded box) to the amplitude for μ-decay. Solid, dashed, and wavy lines denote fermions, Higgs scalars, and gauge bosons, respectively. After SSB, the neutral Higgs field is replaced by its vev, yielding a four-fermion μ-decay amplitude.

contributions to m_ν^{AD} involving the second case will be smaller than those implied by matching with $\mathcal{O}^{(4)}_{M,\,AD}$ by $\sim (v/\Lambda)^2$, since $\mathcal{O}^{(6)}_{M,\,AD}$ contains an additional factor of $(\phi^\dagger\phi)/\Lambda^2$. We first consider this case and employ dimensional analysis to derive neutrino mass naturalness expectations for the $n = 6$ operator coefficients. For v not too different from Λ, the impact of the $n = 6$ mixing can also be important, and in this case we can employ a full renormalization group (RG) analysis to derive robust naturalness bounds.

2.3.1 Matching with $\mathcal{O}^{(4)}_{M,\,AD}$

The analysis of [68] employed dimensional regularization (DR) to regularize the one- and two-loop graphs through which four-fermion operators containing a single ν_R field contribute to the $n = 6$ mass operator. Mixing with lower-dimension operators does not arise in DR since the relevant graphs are quadratically divergent and must be proportional to the square of a mass scale. For $\mu > v$, all fields are massless, and μ itself appears only logarithmically. Since the mass operator exists for zero external momentum, all quadratically-divergent graphs vanish in this case.

The $n = 4$ mass operator will nevertheless receive contributions at the scale Λ associated with loop graphs containing the $n = 6$ operators. Simple power counting shows that these contributions go as $\sim \Lambda^2/(4\pi)^2$ times a product $n = 6$ operator coefficient C^6/Λ^2 and the gauge couplings $\sim g^2$ appearing in the loop. Thus, matching

of the effective theory with the full theory (unspecified) at the scale Λ implies the presence of a contribution to C_M^4 of order $\sim \alpha C^6/4\pi$. As emphasized in [77], the precise numerical coefficient that enters this matching contribution cannot be computed without knowing the theory above the scale Λ. One may, however, estimate the size of these contributions either using a gauge-invariant regulator, such as the generalized Pauli-Villars regulator of [78], or using naive dimensional analysis. Since we are interested in order-of-magnitude expectations, use of the latter is sufficient. We emphasize that these expectations can only be relaxed in specific models that suppress the matching conditions.

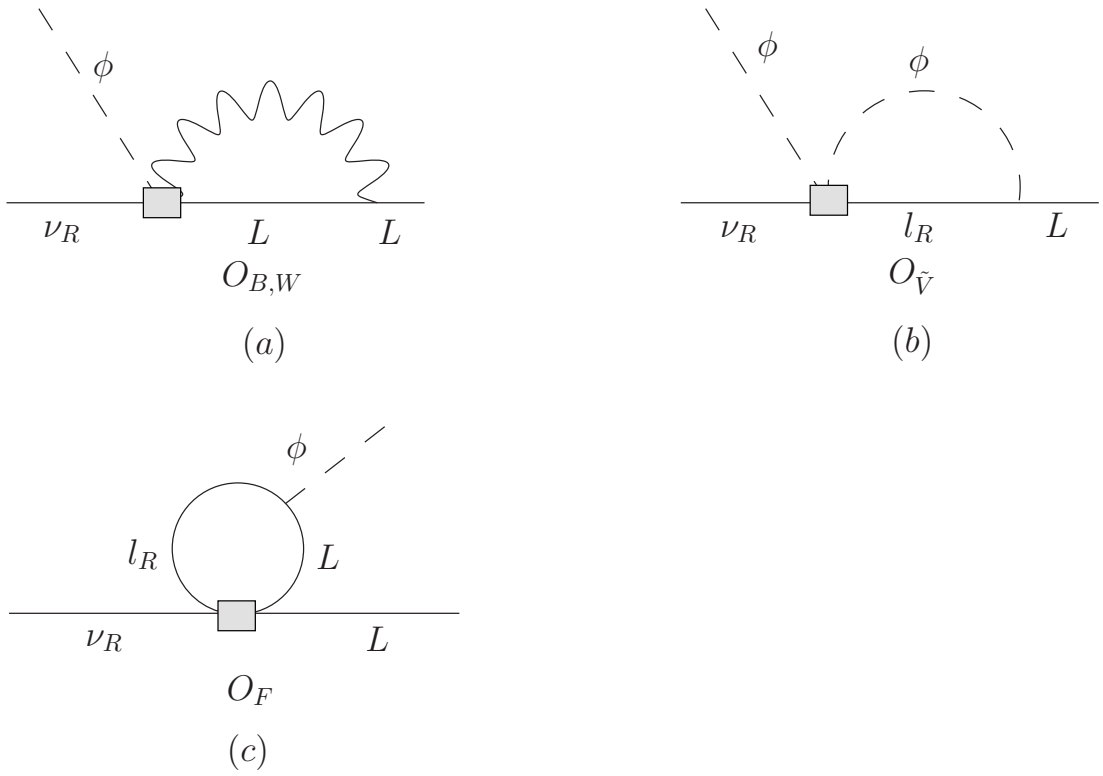

Figure 2.2: One-loop graphs for the matching contributions of the $n = 6$ operators (denoted by the shaded box) to the $n = 4$ mass operator $\mathcal{O}^{(4)}_{M,\ AD}$. Solid, dashed, and wavy lines denote fermions, Higgs scalars, and gauge bosons, respectively. Panels (a, b, c) illustrate contributions from $\mathcal{O}^{(6)}_{B,W}$, $\mathcal{O}^{(6)}_{\tilde{V}}$, and $\mathcal{O}^{(6)}_{F}$, respectively, to $\mathcal{O}^{(4)}_{M,\ AD}$.

The relevant one-loop graphs are shown in Fig. 2.2. For the matching of the four-fermion operators $\mathcal{O}^{(6)}_{F,\,ABCD}$ onto $\mathcal{O}^{(4)}_{M,\,AD}$, two topologies are possible, associated with either the fields $(\bar{L}^A,\, \nu_R^D)$ or $(\bar{L}^B,\, \nu_R^D)$ living on the external lines. For the matching

of $\mathcal{O}^{(6)}_{F,\,ABCD}$ as well as of $\mathcal{O}^{(6)}_{\tilde{V},\,AB}$ into $\mathcal{O}^{(4)}_{M,\,AD}$, one insertion of the Yukawa interaction $f^*_{AC}\,\bar{l}^C_R L^A$ is needed to convert the internal, RH lepton into a LH one. In contrast, no Yukawa insertion is required for the matching of $\mathcal{O}^{(6)}_{B,\,AD}$ and $\mathcal{O}^{(6)}_{W,\,AD}$ onto $\mathcal{O}^{(4)}_{M,\,AD}$.

To simplify the analysis of matching involving the $\mathcal{O}^{(6)}_{F,\,ABCD}$ we note that one may always redefine the fields L^A and ℓ^D_R so that the charged lepton Yukawa matrix f_{AD} is diagonal. Specifically, we take

$$\begin{aligned} L^A &\rightarrow L^{A\prime} = S_{AB} L^B \\ \ell^C_R &\rightarrow \ell^{C\prime} = T_{CD}\ell^D \end{aligned} \tag{2.13}$$

with S_{AB} and T_{CD} chosen so that

$$\bar{L}\,\tilde{f}\,\ell = \bar{L}'\,\tilde{f}_{\rm diag}\,\ell' \tag{2.14}$$

where L, L' denote vectors in flavor space, $\tilde{f}$ denotes the Yukawa matrix in the original basis, and $\tilde{f}_{\rm diag} = \tilde{S}^\dagger\,\tilde{f}\,\tilde{T}$. We note that the field redefinition (2.13) differs from the conventional flavor rotation used for quarks, since we have performed identical rotations on both isospin components of the left-handed doublet. Consequently, gauge interactions in the new basis entail no transitions between generations. We also note that Eqs. (2.13) also imply a redefinition of the operator coefficients $C^4_{M,\,AD}$, $C^6_{F,\,ABCD}$, etc.. For example, one has

$$\begin{aligned} C^{4,6}_{M,\,A'D} &= C^{4,6}_{M,\,AD}\,S_{M,\,A'A} \\ C^{6\prime}_{F,\,A'B'C'D} &= C^6_{F,\,ABCD}\,S_{A'A}\,S_{B'B}\,T^*_{C'C} \end{aligned} \tag{2.15}$$

where a sum over repeated indices is implied. Diagonalization of the neutrino mass matrix requires additional, independent rotations of the $\nu^D_{L,R}$ fields after inclusion of radiative contributions to the coefficients $C^{4,6}_{M,\,AD}$ generated by physics above the weak scale. Since we are concerned only with contributions generated above the scale of SSB, we will not perform the latter diagonalization and carry out computations using

the L', ℓ'_R basis[5].

In this case, the only four fermion operators $\mathcal{O}^{(6)}_{F,\,ABCD}$ that can contribute substantially to m_ν^{AD} are those having either $A = C$ or $B = C$. Thus, we obtain the following estimates of the contributions from the $n = 6$ operators to the coefficient of the $n = 4$ mass operator:

$$\begin{aligned}
\mathcal{O}^{(6)}_{B,\,AD} &\rightarrow C^4_{M,\,AD}(\Lambda) \sim \frac{\alpha}{4\pi\cos^2\theta_W} C^6_{B,\,AD}(\Lambda) \\
\mathcal{O}^{(6)}_{W,\,AD} &\rightarrow C^4_{M,\,AD}(\Lambda) \sim \frac{3\alpha}{4\pi\sin^2\theta_W} C^6_{W,\,AD}(\Lambda) \\
\mathcal{O}^{(6)}_{\tilde{V},\,AD} &\rightarrow C^4_{M,\,AD}(\Lambda) \sim \frac{f_{AA}}{16\pi^2} C^6_{\tilde{V},\,AD}(\Lambda) \\
\mathcal{O}^{(6)}_{F,\,ABAD} &\rightarrow C^4_{M,\,BD}(\Lambda) \sim \frac{f_{AA}}{8\pi^2} C^6_{F,\,ABAD}(\Lambda) \\
\mathcal{O}^{(6)}_{F,\,ABBD} &\rightarrow C^4_{M,\,AD}(\Lambda) \sim \frac{f_{BB}}{16\pi^2} C^6_{F,\,ABBD}(\Lambda)
\end{aligned} \tag{2.16}$$

where θ_W is the weak mixing angle and where we have made the dependence on the matching scale Λ explicit[6].

The relative factor of $3\cot^2\theta_W$ for the mixing of $\mathcal{O}^{(6)}_{W,\,AD}$ compared to the mixing of $\mathcal{O}^{(6)}_{B,\,AD}$ arises from the ratio of gauge couplings $(g/g')^2$ and the presence of a $\vec{\tau}\cdot\vec{\tau}$ appearing in Fig. 2.2a. The factor of two that enters the mixing of $\mathcal{O}^{(6)}_{F,\,ABAD}$ compared to that of $\mathcal{O}^{(6)}_{F,\,ABBD}$ arises from the trace associated with the closed chiral fermion loop that does not arise for $\mathcal{O}^{(6)}_{F,\,ABBD}$.

We observe that there exist two four-fermion operators that contribute to μ-decay that do not contribute to $C^4_{M,\,AD}$ in the basis giving a diagonal f_{AB}: $\mathcal{O}^{(6)}_{F,\,AABD}$ with either $A = 1, B = 2$ or $A = 2, B = 1$. It is similarly straightforward to see that these operators do not mix with $C^6_{M,\,AD}$, since in the basis of charged lepton mass eigenstates, there exist no Yukawa interactions that couple lepton doublet and charged lepton singlet fields of different generations. As we discuss in Section 2.4, the operators $\mathcal{O}^{(6)}_{F,\,AABD}$ with either $A = 1, B = 2$ or $A = 2, B = 1$ contribute to $g^{S,T}_{LR}$ and

[5]For notational simplicity, we henceforth omit the prime superscripts.

[6]In relating the coefficients $C(\Lambda)$ to those at the weak scale as needed for the analysis of both μ-decay and m_ν, we will neglect corrections to the relations in Eqs. (2.16) generated by running, as they are higher order in the gauge couplings and numerically insignificant for our purposes.

$g_{RL}^{S,T}$, respectively. Consequently, the magnitudes of these couplings are not directly bounded by m_ν and naturalness considerations, as indicated in Table 2.1.

These conclusions differ from those in [68], which did not take into account operators that contribute to μ-decay but do not mix with the neutrino mass operators. The corresponding bounds on $g_{LR}^{S,T}$ and $g_{RL}^{S,T}$ obtained in that work are, thus, not general and would apply only in scenarios for which $C^6_{F,\,112D}$ and $C^6_{F,\,221D}$ vanish. From a theoretical standpoint, one might expect the magnitudes of $C^6_{F,\,112D}$ and $C^6_{F,\,221D}$ to be comparable to those of the other four-fermion operator coefficients in models that are consistent with the scale of neutrino mass. Nevertheless, we cannot *a priori* rule out order of magnitude or more differences between operator coefficients.

2.3.2 Mixing among $n = 6$ operators

Because $\mathcal{O}^{(6)}_{M,\,AD}$ contains one power of $(\phi^\dagger\phi)/\Lambda^2$ compared to $\mathcal{O}^{(4)}_{M,\,AD}$, the constraints obtained from mixing with the former will generally be weaker than the one-loop $n = 4$ matching contributions by $\sim (v/\Lambda)^2$. However, for Λ not too different from the weak scale, the $n = 6$ mixing can be of comparable importance to the $n = 4$ matching. Here, we study the mixing among $n = 6$ operators by computing all one-loop graphs that contribute using DR and performing a renormalization group (RG) analysis. Doing so provides the exact result for contributions to the one-loop mixing from scales between Λ and v, summed to all orders in $f_{AA}\ln(v/\Lambda)$ and $\alpha\ln(v/\Lambda)$.

In carrying out this analysis, it is necessary to identify a basis of operators that close under renormalization. We find that the minimal set consists of seven operators that contribute to μ-decay and m_ν^{AD}:

$$\mathcal{O}^{(6)}_{B,\,AD},\ \mathcal{O}^{(6)}_{W,\,AD},\ \mathcal{O}^{(6)}_{M,\,AD},\ \mathcal{O}^{(6)}_{\tilde{V},\,AD},\ \mathcal{O}^{(6)}_{F,\,AAAD},\ \mathcal{O}^{(6)}_{F,\,ABBD},\ \mathcal{O}^{(6)}_{F,\,BABD} \quad . \tag{2.17}$$

For simplicity, we have included a single RH neutrino field ν_R^D in all seven operators. While one could, in principle, allow for different ν_R generation indices, the essential physics can be extracted from an analysis of this minimal basis.

The classes of graphs relevant to mixing among these operators are illustrated in

Fig. 2.3, where we show representative contributions to operator self-renormalization and mixing among the various operators. The latter include mixing of all operators into $\mathcal{O}^{(6)}_{M,\,AD}$ (a–c); mixing of $\mathcal{O}^{(6)}_{M,\,AD}$, $\mathcal{O}^{(6)}_{B,\,AD}$, and $\mathcal{O}^{(6)}_{W,\,AD}$ into $\mathcal{O}^{(6)}_{\tilde{V},\,AD}$ (d, e); and mixing between the four-fermion operators and the magnetic moment operators (f, g). Representative self-renormalization graphs are given in Fig. 2.3(h–j). As noted in [68], the mixing of the the four-fermion operators into $\mathcal{O}^{(6)}_{M,\,AD}$ contains three powers of the lepton Yukawa couplings and is highly suppressed. In contrast, all other mixing contains at most one Yukawa insertion.

Working to first order in the f_{AA} we find a total of 59 graphs that must be computed, not including wavefunction renormalization graphs that are not shown. Twenty-two of these graphs were computed by the authors of [69] in their analysis of the mixing between $\mathcal{O}^{(6)}_{M,\,AD}$ and the magnetic moment operators. Here, we compute the remaining 37. As in [69], we work with the background field gauge [79] in $d = 4 - 2\epsilon$ spacetime dimensions. We renormalize the operators using minimal subtraction, wherein counterterms simply remove the divergent $1/\epsilon$ terms from the one-loop amplitudes. The resulting renormalized operators $\mathcal{O}^{(6)}_{jR}$ are expressed in terms of the unrenormalized operators $\mathcal{O}^{(6)}_{j}$ as

$$\mathcal{O}^{(6)}_{jR} = \sum_k Z^{-1}_{jk} Z_L^{n_L/2} Z_\phi^{n_\phi/2} \mathcal{O}^{(6)}_k = \sum_k Z^{-1}_{jk} \mathcal{O}^{(6)}_{k0} \quad , \tag{2.18}$$

where

$$\mathcal{O}^{(6)}_{j0} = Z_L^{n_L/2} Z_\phi^{n_\phi/2} \mathcal{O}^{(6)}_j \tag{2.19}$$

are the μ-independent bare operators; $Z_L^{1/2}$ and $Z_\phi^{1/2}$ are the wavefunction renormalization constants for the fields L^A and ϕ, respectively; n_L and n_ϕ are the number of LH lepton and Higgs fields appearing in a given operator; and $Z^{-1}_{jk} Z_L^{n_L/2} Z_\phi^{n_\phi/2}$ are the counterterms that remove the $1/\epsilon$ divergences.

Since the bare operators $\mathcal{O}^{(6)}_{j0}$ do not depend on the renormalization scale, whereas the Z^{-1}_{jk} and the $\mathcal{O}^{(6)}_{jR}$ do, the operator coefficients C^6_j must carry a compensating μ-dependence to ensure that $\mathcal{L}_{\text{eff}}$ is independent of scale. This requirement leads to the

RG equation for the operator coefficients:

$$\mu\frac{d}{d\mu}C_j^6 + \sum_k C_k^6\ \gamma_{kj} = 0 \tag{2.20}$$

where

$$\gamma_{kj} = \sum_\ell \left(\mu\frac{d}{d\mu}Z_{k\ell}^{-1}\right) Z_{\ell j} \quad . \tag{2.21}$$

is the anomalous dimension matrix. We obtain[7] $\gamma_{jk} =$

$$\begin{pmatrix}
-\frac{3(\alpha_1-3\alpha_2)}{16\pi} & \frac{3\alpha_1}{8\pi} & -6\alpha_1(\alpha_1+\alpha_2) & -\frac{9\alpha_1 f_{AA}^*}{8\pi} & -\frac{9\alpha_1 f_{AA}}{4\pi} & -\frac{9\alpha_1 f_{BB}}{2\pi} & \frac{9\alpha_1 f_{BB}}{4\pi} \\
\frac{9\alpha_2}{8\pi} & \frac{3(\alpha_1-3\alpha_2)}{16\pi} & 6\alpha_2(\alpha_1+3\alpha_2) & \frac{27\alpha_2 f_{AA}^*}{8\pi} & -\frac{9\alpha_2 f_{AA}}{4\pi} & -\frac{9\alpha_2 f_{BB}}{2\pi} & \frac{9\alpha_2 f_{BB}}{4\pi} \\
0 & 0 & \frac{9(\alpha_1+3\alpha_2)}{16\pi} - \frac{3\lambda}{2\pi^2} & 0 & 0 & 0 & 0 \\
0 & 0 & \frac{9\alpha_2 f_{AA}}{8\pi} - \frac{3 f_{AA}\lambda}{8\pi^2} & \frac{3\alpha_1}{4\pi} & 0 & 0 & 0 \\
-\frac{3 f_{AA}^*}{128\pi^2} & -\frac{f_{AA}^*}{128\pi^2} & 0 & 0 & \frac{3(3\alpha_1-\alpha_2)}{8\pi} & 0 & 0 \\
-\frac{3 f_{BB}^*}{128\pi^2} & -\frac{f_{BB}^*}{128\pi^2} & 0 & 0 & 0 & \frac{3(\alpha_1+\alpha_2)}{8\pi} & \frac{3(\alpha_1-\alpha_2)}{4\pi} \\
0 & 0 & 0 & 0 & 0 & \frac{3(\alpha_1-\alpha_2)}{4\pi} & \frac{3(\alpha_1+\alpha_2)}{8\pi}
\end{pmatrix} \tag{2.22}$$

where the $\alpha_i = g_i^2/(4\pi)$ and λ is the Higgs self coupling defined by the potential $V(\phi) = \lambda[(\phi^\dagger\phi) - v^2/2]^2$.

Using this result for γ_{ij} and the one-loop β functions for α_1, α_2, and the lepton Yukawa couplings, we solve the RG equations to determine the operator coefficients $C_k^6(\mu)$ as a function of their values at the scale Λ. As in [69] we find that the the running of the gauge and Yukawa couplings has a negligible impact on the evolution of the $C_k^6(\mu)$. It is instructive to consider the results obtained by retaining only the leading logarithms $\ln(\mu/\Lambda)$ and terms at most first order in the Yukawa couplings.

[7] The term in γ_{33} proportional to λ differs from that of [69], which contains an error. However, this change does not affect the bounds on the neutrino magnetic moments obtained in that work.

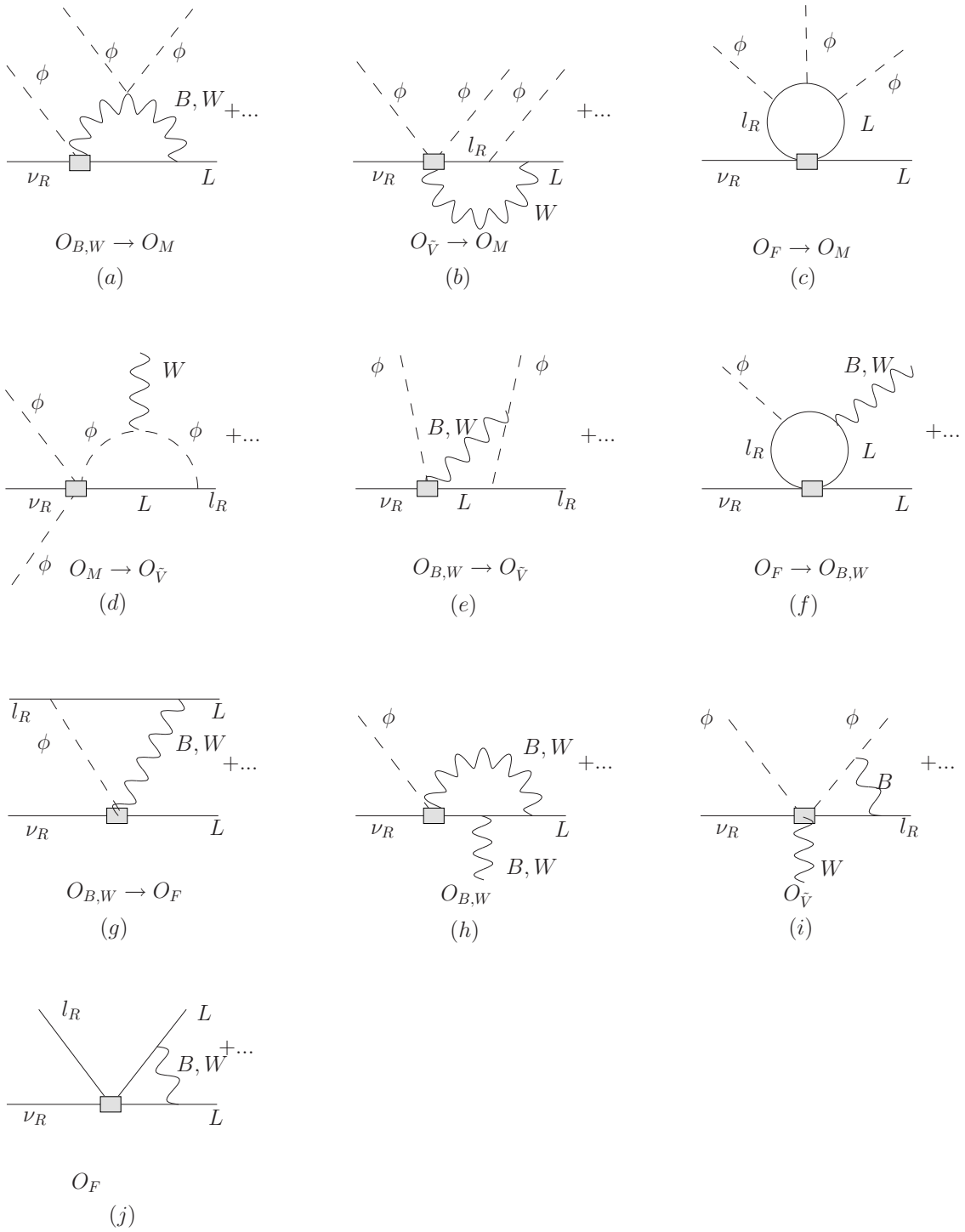

Figure 2.3: One-loop graphs for the mixing among $n = 6$ operators. Notation is as in previous figures. Various types of mixing (a–g) and self-renormalization (h–j) are as discussed in the text.

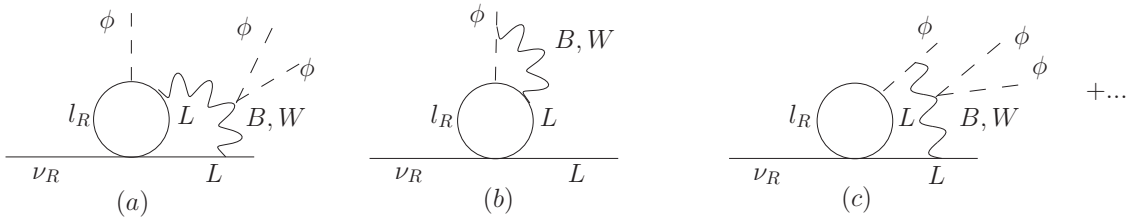

Figure 2.4: Two-loop graphs for the mixing of the $n = 6$ operators. Only representive graphs for the mixing of the four-fermion operators $\mathcal{O}^{(6)}_{F,\,ABCD}$ into $\mathcal{O}^{(6)}_{M,\,AD}$ are shown.

We find

$$
\begin{aligned}
C^6_{M,\,AD}(\mu) &= C^6_{M,\,AD}(\Lambda)\left[1-\gamma_{33}\ln\frac{\mu}{\Lambda}\right] \\
&\quad -\left[\gamma_- C^6_-(\Lambda)+\gamma_+ C^6_+(\Lambda)+\gamma_{43}C^6_{\tilde V,\,AD}(\Lambda)\right]\ln\frac{\mu}{\Lambda} \\
C^6_+(\mu) &= C^6_+(\Lambda)\left[1-\tilde\gamma\ln\frac{\mu}{\Lambda}\right] \\
&\quad +\left[\left(f^*_{AA}/32\pi^2\right)C^6_{F,\;AAAD}(\Lambda)+\left(f^*_{BB}/32\pi^2\right)C^6_{F,\;ABBD}(\Lambda)\right]\ln\frac{\mu}{\Lambda} \\
\tilde C^6(\mu) &= \tilde C^6(\Lambda)\left[1+\tilde\gamma\ln\frac{\mu}{\Lambda}\right] \\
&\quad +[\left(3f_{AA}/128\pi^2\right)(\alpha_1-\alpha_2)\,C^6_{F,\;AAAD}(\Lambda) \\
&\quad +\left(3f_{BB}/128\pi^2\right)(\alpha_1-\alpha_2)\,C^6_{F,\;ABBD}(\Lambda)]\ln\frac{\mu}{\Lambda} \\
C^6_{\tilde V,\,AD}(\mu) &= C^6_{\tilde V,\,AD}(\Lambda)\left[1-\gamma_{44}\ln\frac{\mu}{\Lambda}\right]+(9f_{AA}/8\pi)\tilde C^6(\Lambda)\ln\frac{\mu}{\Lambda} \qquad (2.23)\\
C^6_{F,\;AAAD}(\mu) &= C^6_{F,\;AAAD}(\Lambda)\left[1+\frac{3(\alpha_2-3\alpha_1)}{8\pi}\ln\frac{\mu}{\Lambda}\right] \\
&\quad +(9f_{AA}/4\pi)\left[C^6_{B,\,AD}(\Lambda)\alpha_1+C^6_{W,\,AD}(\Lambda)\alpha_2\right]\ln\frac{\mu}{\Lambda} \\
C^6_{F,\;ABBD}(\mu) &= C^6_{F,\;ABBD}(\Lambda)\left[1-\frac{3(\alpha_1+\alpha_2)}{8\pi}\ln\frac{\mu}{\Lambda}\right] \\
&\quad -\frac{3(\alpha_1-\alpha_2)}{4\pi}C^6_{F,\;BABD}(\Lambda)\ln\frac{\mu}{\Lambda} \\
&\quad +(9f_{BB}/2\pi)\left[C^6_{B,\,AD}(\Lambda)\alpha_1+C^6_{W,\,AD}(\Lambda)\alpha_2\right]\ln\frac{\mu}{\Lambda} \\
C^6_{F,\;BABD}(\mu) &= C^6_{F,\;BABD}(\Lambda)\left[1-\frac{3(\alpha_1+\alpha_2)}{8\pi}\ln\frac{\mu}{\Lambda}\right] \\
&\quad -\frac{3(\alpha_1-\alpha_2)}{4\pi}C^6_{F,\;ABBD}(\Lambda)\ln\frac{\mu}{\Lambda} \\
&\quad -(9f_{BB}/4\pi)\left[C^6_{B,\,AD}(\Lambda)\alpha_1+C^6_{W,\,AD}(\Lambda)\alpha_2\right]\ln\frac{\mu}{\Lambda}
\end{aligned}
$$

where

$$\begin{aligned} C^6_{\pm}(\mu) &\equiv C^6_{B,\,AD}(\mu) \pm C^6_{W,\,AD}(\mu) \\ \tilde{C}^6(\mu) &\equiv \alpha_1 C^6_{B,\;AD}(\mu) - 3\alpha_2 C^6_{W,\,AD}(\mu) \\ \gamma_{\pm} &\equiv (\gamma_{13} \pm \gamma_{23})/2 \\ \tilde{\gamma} &\equiv 3(\alpha_1 + 3\alpha_2)/16\pi \; . \end{aligned} \tag{2.24}$$

We note that the combination of coefficients $C^6_+(v)$ enters the neutrino magnetic moment. Its RG evolution was obtained in [69] to zeroth order in the Yukawa couplings; here we obtain the corrections that are linear in f_{AA} and f_{BB}. The corresponding contributions to the neutrino mass matrix δm_ν^{AD} and magnetic moment matrix μ_ν^{AD} are then given by

$$\delta m_\nu^{AD} = -\left(\frac{v^3}{2\sqrt{2}\Lambda^2}\right) C^6_{M,\,AD}(v) \tag{2.25}$$

$$\frac{\mu_\nu^{AD}}{\mu_B} = -4\sqrt{2}\left(\frac{m_e v}{\Lambda^2}\right) \mathrm{Re}\left\{C^6_+(v)\right\} \quad . \tag{2.26}$$

From Eqs. (2.23), (2.25), and (2.26) we observe that to linear order in the lepton Yukawa couplings, $C^6_{M,\,AD}(\mu)$ receives contributions from the two magnetic moment operators and $\mathcal{O}^{(6)}_{\tilde{V}}$ but not from the four fermion operators. This result is consistent with the result obtained by the authors of [68], who computed one-loop graphs containing the four-fermion operators of Eq. (2.1) using massive charged leptons and found that contributions to $m_\nu \propto m_\ell^3$. In the effective theory used here, the latter result corresponds to a one-loop computation with three insertions of the Yukawa interaction. However, mixing with $\mathcal{O}^{(6)}_{\tilde{V}}$ was not considered in [68], and our result that this operator mixes with $\mathcal{O}^{(6)}_{M,\,AD}$ to linear order in the Yukawa couplings represents an important difference with the former analysis.

We agree with the observation of [68] that the four fermion operators can mix with $\mathcal{O}^{(6)}_{M,\,AD}$ to linear order in the f_{AA} via two-loop graphs, such as those indicated in Fig. 2.4. These graphs were estimated in [68] by considering loops with massive $W^\pm$

and Z^0 bosons that correspond in our framework to the diagrams of Fig. 2.4a. We observe, however, that the two-loop constraints will be weaker than those obtained by one-loop matching with $\mathcal{O}^{(4)}_{M,\,AD}$ by $\sim (\alpha/4\pi)(v/\Lambda)^2$ (modulo logarithmic and model-dependent corrections), so we do not consider this two-loop mixing in detail here. Moreover, because we work at a scale $\mu > v$ for which the use of massless fields is appropriate, and because we adopt a basis in which the Yukawa matrix and gauge interactions are flavor diagonal (but m_ν^{AD} is not), the operators $\mathcal{O}^{(6)}_{F,\,112D}$ and $\mathcal{O}^{(6)}_{F,\,221D}$ will not mix with $\mathcal{O}^{(6)}_{M,\,AD}$ even at two-loop order.

2.4 Neutrino Mass Constraints

To arrive at neutrino mass naturalness expectations for the $g^\gamma_{\epsilon\mu}$ coefficients, it is useful to tabulate their relationships with the dimension-six operator coefficients. In some cases, one must perform a Fierz transformation in order to obtain the operator structures in Eq. (2.1). Letting

$$g^\gamma_{\epsilon\mu} = \kappa \left(\frac{v}{\Lambda}\right)^2 C^6_k(v) \tag{2.27}$$

we give in Table 2.2 the κs corresponding to the various dimension-six operators.

Using the entries in Table 2.2 and the estimates in Eqs. (2.16), we illustrate how the bounds in Table 2.1 were obtained. For the operator $\mathcal{O}^{(6)}_{F,\,122D}$, for example, we have from Eqs. (2.5) and (2.16)[8]

$$|C^6_{F,\,122D}| \lesssim 16\pi^2 \left(\frac{\delta m_\nu^{1D}}{m_\mu}\right) \tag{2.28}$$

leading to

$$|g^S_{LR}| \lesssim 4\pi^2 \left(\frac{\delta m_\nu^{1D}}{m_\mu}\right)\left(\frac{v}{\Lambda}\right)^2 \qquad |g^T_{LR}| \lesssim 2\pi^2 \left(\frac{\delta m_\nu^{1D}}{m_\mu}\right)\left(\frac{v}{\Lambda}\right)^2 \tag{2.29}$$

[8] In what follows, we suppress the scale dependence of the $C(\mu)$ and, as indicated earlier, neglect the effects of running in translating the one-loop matching bounds into constraints at the weak scale.

where δm_ν^{AD} denotes the radiative contribution to m_ν^{AD}. Choosing $\Lambda = v$ and $\delta m_\nu^{1D} =$ 1eV (corresponding to the scale of upper bounds derived from ^{3}H β-decay studies[31, 80]) leads to the bounds in the first row of Table 2.1. Similar arguments yield the other entries in the table. Note that the bounds become smaller as Λ is increased from v.

The constraints on the $g_{LR,RL}^V$ that follow from mixing among the $n = 6$ operators follows straightforwardly from Eqs. (2.23) and (2.25) and Table 2.2. We obtain

$$g_{LR}^V = \left(\frac{\delta m_\nu^{2D}}{m_\mu}\right)\left(\frac{8\pi \sin^2\theta_W}{9}\right)\left(\alpha - \frac{\lambda \sin^2\theta_W}{3\pi}\right)^{-1}\left(\ln\frac{\Lambda}{v}\right)^{-1} \quad . \tag{2.30}$$

A similar expression holds for g_{RL}^V but with $m_\mu \to m_e$ and $\delta m_\nu^{2D} \to \delta m_\nu^{1D}$. Note that in arriving at Eq. (2.30) we have ignored the running of the $C_{\tilde{V},\,AD}^6(\mu)$ between Λ and v, since the impact on the $g_{LR,RL}^V$ is higher order in the gauge and Yukawa couplings. To derive numerical bounds on the $g_{LR,RL}^V$ from Eq. (2.30) we use the running couplings in the $\overline{\rm MS}$ scheme $\alpha = \hat{\alpha}(M_Z) \approx 1/127.9$, $\sin^2\hat{\theta}_W(M_Z) \approx 0.2312$ and the tree-level relation between the Higgs quartic coupling λ, the Higgs mass m_H, and v: $2\lambda = (m_H/v)^2$. We quote two results, corresponding to the direct search lower bound on $m_H \gtrsim 114$ GeV and the one-sided 95 % C.L. upper bound from analysis of precision electroweak measurements, $m_H \lesssim 186$ GeV [81]. We obtain

$$\begin{aligned}
|g_{LR}^V| &= \left(\frac{\delta m_\nu^{2D}}{1\,\text{eV}}\right)\left(\ln\frac{\Lambda}{v}\right)^{-1}\begin{cases} 1.2\times10^{-6}, & m_H = 114\,\text{GeV} \\ 7.5\times10^{-6}, & m_H = 186\,\text{GeV} \end{cases} \\
|g_{RL}^V| &= \left(\frac{\delta m_\nu^{1D}}{1\,\text{eV}}\right)\left(\ln\frac{\Lambda}{v}\right)^{-1}\begin{cases} 2.5\times10^{-4}, & m_H = 114\,\text{GeV} \\ 1.5\times10^{-3}, & m_H = 186\,\text{GeV} \end{cases} .
\end{aligned} \tag{2.31}$$

For $\Lambda \sim 1$ TeV, the logarithms are $\mathcal{O}(1)$ so that for $\delta m_\nu \sim 1$ eV, the bounds on the $g_{LR,RL}^V$ derived from $n = 6$ mixing are comparable in magnitude to those estimated from one-loop matching with the $n = 4$ mass operators.

Although the four fermion operators do not mix with $\mathcal{O}_{M,\,AD}^{(6)}$ at linear order in the Yukawa couplings, they do contribute to the magnetic moment operators $\mathcal{O}_{B,\,AD}^{(6)}$

and $\mathcal{O}^{(6)}_{W,\,AD}$ at this order. From Eqs. (2.23) and (2.26) we have

$$\frac{\delta\mu_\nu^{AD}}{\mu_B} = \frac{\sqrt{2}}{8\pi^2}\left(\frac{m_e}{v}\right)\left(\frac{v}{\Lambda}\right)^2 \mathrm{Re}\left[f^*_{AA}C^6_{F,\,AAAD} + f^*_{BB}C^6_{F,\,ABBD}\right]\ln\frac{\Lambda}{v} \quad , \tag{2.32}$$

where $\delta\mu_\nu^{AD}$ denotes the contribution to the magnetic moment matrix and μ_B is a Bohr magneton. While $\mathcal{O}^{(6)}_{F,\,AAAD}$ does not contribute to μ-decay, the operator $\mathcal{O}^{(6)}_{F,\,ABBD}$ does, and its presence in Eq. (2.32) implies constraints on its coefficient from current bounds on neutrino magnetic moments. The most stringent constraints arise for $A = 1$, $B = 2$ for which we find

$$|C^6_{F,\,122D}|\left(\frac{v}{\Lambda}\right)^2 \lesssim 5\times 10^{10}\left(\ln\frac{\Lambda}{v}\right)^{-1}\left(\frac{\mu_\nu^{1D}}{\mu_B}\right) \quad . \tag{2.33}$$

Current experimental bounds on $|\mu_\nu^{\rm exp}/\mu_B|$ range from $\sim 10^{-10}$ from observations of solar and reactor neutrinos [82, 83, 84, 85] to $\sim 3\times 10^{-12}$ from the non-observation of plasmon decay into $\bar{\nu}\nu$ in astrophysical objects [87]. Assuming that the logarithm in Eq. (2.33) is of order unity, these limits translate into bounds on g^S_{LR} and g^T_{LR} ranging from $\sim 1 \to 0.03$ and $\sim 0.3 \to 0.01$, respectively. The solar and reactor neutrino limits on $|\mu_\nu^{\rm exp}/\mu_B|$ imply bounds on the $g^{S,T}_{LR}$ that are weaker than those obtained from the global analysis of μ-decay measurements, while those associated with the astrophysical magnetic moment limits are comparable to the global values. Nevertheless, the bounds derived from neutrino magnetic moments are several orders of magnitude weaker than those derived from the scale of neutrino mass.

The naturalness expectations for the C^6_k associated with the scale of m_ν have implications for the interpretation of μ-decay experiments. Because the coefficients $C^6_{F,\,112D}$ and $C^6_{F,\,221D}$ that contribute to $g^{S,T}_{LR,RL}$ are not directly constrained by m_ν, none of the eleven Michel parameters is directly constrained by neutrino mass alone. Instead, it is more relevant to compare the results of global analyses from which limits on the $g^\gamma_{e\mu}$ are obtained with the m_ν naturalness bounds, since the latter imply tiny values for the couplings $g^V_{LR,RL}$. Should future experiments yield a value for either of these couplings that is considerably larger than our expectations in Table 2.1, the

Table 2.2: Coefficients κ that relate $g^{\gamma}_{\epsilon\mu}$ to the dimension six operator coefficients C^6_k via Eq. (2.27)

Coefficient	g^S_{LR}	g^T_{LR}	g^S_{RL}	g^T_{RL}	g^V_{LR}	g^V_{RL}
$C^6_{F,122D}$	1/4	1/8	-	-	-	-
$C^6_{F,212D}$	1/2	-	-	-	-	-
$C^6_{F,112D}$	3/4	1/8	-	-	-	-
$C^6_{F,211D}$	-	-	1/4	1/8	-	-
$C^6_{F,121D}$	-	-	1/2	-	-	-
$C^6_{F,221D}$	-	-	3/4	1/8	-	-
$C^6_{\tilde{V},2D}$	-	-	-	-	$-1/2$	-
$C^6_{\tilde{V},1D}$	-	-	-	-	-	$-1/2$

new physics above Λ would have to exhibit either fine-tuning or a symmetry in order to evade unacceptably large contributions to m_ν. In addition, should future global analyses find evidence for non-zero $g^{S,T}_{LR,RL}$ with magnitudes considerably larger than given by the m_ν naturalness expectations listed in Table 2.1, then one would have evidence for a non-trivial flavor structure in the new physics that allows considerably larger effects from the operators $\mathcal{O}^{(6)}_{F,112D}$ and $\mathcal{O}^{(6)}_{F,221D}$ than from the other four fermion operators.

Finally, we note that one may use a combination of neutrino mass and direct studies of the Michel spectrum to derive bounds on a subset of the Michel parameters that are more stringent than one obtains from μ-decay experiments alone. To illustrate, we consider the parameters ρ and α, for which one has

$$\frac{3}{4} - \rho = \frac{3}{4}\left|g^V_{LR}\right|^2 + \frac{3}{2}\left|g^T_{LR}\right|^2 + \frac{3}{4}\mathrm{Re}\left(g^S_{LR}g^{T*}_{LR}\right) + (L \leftrightarrow R) \tag{2.34}$$

$$\alpha = 8\,\mathrm{Re}\left\{g^V_{RL}\left(g^{S*}_{LR} + 6g^{T*}_{LR}\right) + (L \leftrightarrow R)\right\} \quad . \tag{2.35}$$

From Table 2.1, we observe that the magnitudes of the $g^V_{LR,RL}$ contributions to ρ and α are expected to be several orders of magnitude below the current experimental sensitivities, based on neutrino mass naturalness considerations. In contrast, the contributions to $g^{S,T}_{LR,RL}$ that arise from $\mathcal{O}^{(6)}_{F,112D}$ and $\mathcal{O}^{(6)}_{F,221D}$ are only directly constrained

by μ-decay experiments and not neutrino mass. Thus, we may use the current experimental results for ρ to bound the operator coefficients $C^6_{F,\,112D}$ and $C^6_{F,\,221D}$ and subsequently employ the results—together with the m_ν bounds on the $g^V_{LR,RL}$—to derive expectations for the magnitude of α. For simplicity, we consider only the contributions from $C^6_{F,\,112D}$ to ρ, and using the current experimental uncertainty in this parameter, we find

$$\left|C^6_{F,\,112D}\right| \left(\frac{v}{\Lambda}\right)^2 \lesssim 0.1 \quad . \tag{2.36}$$

In the parameter α, this coefficient interferes with $C^6_{\tilde{V},\,1D}$:

$$\alpha = -6 \left(\frac{v}{\Lambda}\right)^4 \mathrm{Re}\left(C^6_{\tilde{V},\,1D} C^{6\,*}_{F,\,112D} + \cdots\right) \quad , \tag{2.37}$$

where the "$+\cdots$" indicates contributions from the other coefficients that we will assume to be zero for purposes of this discussion. From Eq. (2.36) and the m_ν limits on $C^6_{\tilde{V},\,1D}$ we obtain

$$|\alpha| \lesssim 2 \times 10^{-4} \left(\frac{v}{\Lambda}\right)^2 \left(\frac{m_\nu^{1D}}{1\,\mathrm{eV}}\right) \quad . \tag{2.38}$$

For $\Lambda = v$, this expectation for $|\alpha|$ is more than two orders of magnitude below the present experimental sensitivity and will fall rapidly as Λ increases from v. A similar line of reasoning can be used to obtain expectations for the parameter α' in terms of m_ν and the CP-violating phases that may enter the effective operator coefficients.

2.5 Conclusions

The existence of the small, non-zero masses of neutrinos have provided our first direct evidence for physics beyond the minimal Standard Model, and the incorporation of m_ν into SM extensions is a key element of beyond-the-SM model building. At the same time, the existence of non-vanishing neutrino mass—together with its scale—have important consequences for the properties of neutrinos and their interactions that can be delineated in a model-independent manner [69, 70, 68, 88]. In this paper, we have analyzed those implications for the decay of muons, using the effective

field theory approach of [69] and concentrating on the case of Dirac neutrinos. We have derived model-independent naturalness expectations for the contributions to the Michel parameters from various $n = 6$ operators that also contribute to the neutrino mass matrix via radiative corrections.

Our work has been motivated by the ideas in [68], but our conclusions differ in important respects. In particular, we find—after properly taking into account $\mathrm{SU}(2)_L \times \mathrm{U}(1)_Y$ gauge invariance and mixing between $n = 6$ μ-decay and neutrino mass operators —that the dominant constraints on the contributions from $g^V_{RL,LR}$ to the Michel parameters occur at one-loop order, rather than through two-loop effects as in [68]. Consequently, the naturalness bounds we derive on these contributions are two orders of magnitude stronger than those of [68]. Based on one-loop matching considerations that cannot be analyzed in the context of dimensional regularization, we also obtain expectations for contributions from various four-fermion operators to effective scalar and tensor interactions that are substantially smaller than the two-loop mixing constraints appearing in that earlier work. We emphasize that these expectations can only be relaxed in the presence of fine-tuning or model-dependent suppression of the matching conditions at the scale Λ.

In addition, we carefully study the flavor structure of the operators that can contribute to μ-decay and find that there exist four-fermion μ-decay operators that do not contribute to the neutrino mass matrix through radiative corrections. Since these operators contribute to the effective scalar and tensor couplings $g^{S,T}_{LR,RL}$ of Eq. (2.1), no model-independent neutrino mass naturalness bounds exist for these couplings, contrary to the conclusions of [68]. In contrast, all operators that generate the $g^V_{LR,RL}$ terms contribute to m^{AD}_ν, so these effective couplings do have neutrino-mass naturalness bounds. From a model-building perspective it might seem reasonable to expect the coefficients of the unconstrained four-fermion operator coefficients to have the same magnitude as those that are constrained by m_ν, but is important for precise muon-decay experiments to test this expectation.

While we have focused on the implications of Dirac mass terms, a similar analysis for the Majorana neutrinos is clearly called for. Indeed, in the case of neutrino

magnetic moments, the requirement of flavor non-diagonality for Majorana magnetic moments can lead to substantially weaker naturalness bounds than for Dirac moments [69, 70, 71]. While we do not anticipate similar differences between the Majorana and Dirac case for operators that contribute to μ-decay, a detailed comparison will be left to a separate work [39].

Chapter 3

Fermionic Effective Operators and Higgs Production at a Linear Collider

Having used the scale of neutrino mass to obtain interesting bounds on the chirality-changing terms in the muon decay Lagrangian in Chapter 2, we move on to the second of our two model-independent analyses: constraining the contributions of fermionic dimension-six operators to Higgs production at a future e^+e^- linear collider. As in the previous analysis, we include operators which contain right-handed Dirac neutrinos, ν_R; we find four such operators, three of which were relavant to the analysis of Chapter 2. However, for this analysis, we additionally consider all other linearly independent dimension-six operators which contain fermions and which could contribute to the Higgs production cross-section. We derive constraints on the contributions that each of these operators could make to Higgs production using the scale of neutrino mass, limits on neutrino magnetic moments, and electroweak precision observables (EWPO). We find three operators which, although constrained by EWPO, could still have observable effects on the Higgs production cross-section; operators which contain ν_Rs contribute negligibly to the cross-section. The content of this chapter is largely taken from [53].

3.1 Introduction

Uncovering the mechanism of electroweak symmetry-breaking (EWSB) will be a central goal of future experiments at the Large Hadron Collider (LHC) and the planned International Linear Collider (ILC) [44]. Although no direct evidence for the Standard Model Higgs boson exists and it is possible—as in many models of EWSB—that there exist additional scalar degrees of freedom, precision electroweak data favors at least one light scalar particle with properties akin to those of the SM Higgs boson. If it is discovered at the LHC, then measuring its properties will be an important part of the LHC and ILC program. If only a single Higgs scalar (H) is seen at the LHC, it is quite possible that its interactions will differ from those of the SM Higgs due to heavier degrees of freedom that are not directly accessible at the next generation of colliders. In this case, deviations of Higgs boson properties from SM expectations could provide indirect clues about the nature of physics above the TeV scale. This possibility has recently been analyzed in a model-independent way by the authors of [51], who considered the prospective effects of dimension (n) six, purely (scalar) bosonic operators on H production at the ILC, and in [52], where the the potential impact of $n = 6$ bosonic operators on H production at the LHC were analyzed. In both cases, substantial deviations from SM expectations appear to be possible. For recent related work, see [89].

Here, we consider the possible impact of $n = 6$ operators containing fermions on Higgs production at a 500 GeV or 1 TeV linear collider, following the spirit of [51] and [52]. Such operators can be generated when heavy degrees of freedom, associated with a scale Λ lying well above the EWSB scale (given by the Higgs vacuum expectation value, $v \approx 246$ GeV), are integrated out of the larger theory in which the SM is ultimately embedded. In this case, physics at low scales is described by an effective Lagrangian

$$\mathcal{L}_{\rm eff} = \sum_{n\geq 4,\, j} \frac{C_n^j}{\Lambda^{n-4}} \mathcal{O}_{n,j} \quad , \tag{3.1}$$

where the $\mathcal{O}_{n,j}$ are operators built entirely from SM fields (and possibly right-handed

neutrino fields) and where the index j runs over all independent operators of a given dimension. The operators with $n = 4$ are just those of the SM (including a Dirac neutrino mass term), while the coefficients C_n^j of the higher dimension operators are determined by the details of physics above the scale Λ. The effective theory described by Eq. (3.1) will be valid so long as $\Lambda >> \sqrt{s}$.

One may analyze the possible effects of $n > 4$ operators by making rather gentle assumptions about the magnitude of the operator coefficients. In the case of the $n = 6$ operators of interest here, we find it useful to consider the ratio of the C_6^j/Λ^2 to the Fermi constant, $G_F = 1/\sqrt{2}v^2$, that characterizes the strength of $n = 6$ effective operators in the SM. Assuming that the $n = 6$ operators arise from one-loop amplitudes containing particles of mass Λ, one would expect $|C_6^j/G_F\Lambda^2| \lesssim v^2/16\pi^2\Lambda^2$ or $|C_6^j v^2/\Lambda^2| \lesssim 10^{-2}$ for $v \sim \Lambda$. Taking $|C_6^j v^2/\Lambda^2| \sim 10^{-2}$, thus, gives a conservative benchmark for the magnitude of the operator coefficients[1]. In analyzing the general features $n = 6$ operator contributions to Higgs production in e^+e^- annihilation, we will generally adopt this benchmark, bearing in mind that if the new physics involves strong dynamics, the C_6^j could be considerably larger[2]. Doing so will allow us to determine which operators may have the largest possible effects.

After identifying the potentially most significant operators, we derive constraints on the $C_6^j v^2/\Lambda^2$ from electroweak precision observables (EWPO) and other considerations. It is well known that EWPO imply stringent bounds on operators that interfere with the SM amplitudes for $e^+e^- \to f\bar{f}$, and these bounds correspond to $\Lambda \gtrsim 10$ TeV or more for $C_6^j = 1$ [91, 92]. Below, we update the limits obtained in [91] and [92] on the operators with the largest prospective effects on Higgs production in e^+e^- annihilation. However, operators that contain right-handed neutrino fields do not interfere with the SM amplitudes for $e^+e^- \to f\bar{f}$, and their coefficients are not all constrained by EWPO. For such operators, we turn to other considerations, such as low-energy studies of weak decays and neutrino mass "naturalness" considerations.

From our study of the $n = 6$ operators containing both scalar and fermion fields,

[1]Since our effective theory is valid only when $\Lambda >> \sqrt{s} > v$, one would expect it to be applicable only when the $|C_6^j v^2/\Lambda^2|$ are much smaller than 10^{-2} unless the C_6^j are not loop suppressed.

[2]This possibility was considered more broadly in [51]. See also the discussion in [90]

we arrive the following highlights:

(i) In contrast to the situation with purely bosonic $n = 6$ operators, we show that the effects of $n = 6$ operators containing fermions are generally required to be smaller, due in large part to existing precision electroweak data that agrees with SM predictions and that constrains many of the relevant operators [91, 92]. As noted above, the latter constraints are particularly strong on operators that interfere with SM amplitudes for $e^+e^- \to Z^0 \to f\bar{f}$. However, we find that substantial deviations from SM Higgs production cross-sections are possible in some cases. In particular, $n = 6$ operators that contribute to the $e^+e^- \to HZ^0$ channel can generate large corrections to the SM Higgsstrahlung (HZ) cross-section at the energies considered here. The HZ cross-section can be separated from the gauge boson fusion process through appropriate choice of final states or study of the missing mass spectrum in $e^+e^- \to H\nu_e\bar{\nu}_e$. Thus, a dedicated study of HZ would provide the most sensitive probe of operators considered here.

(ii) Although operators containing right-handed neutrino fields have not been emphasized in earlier effective operator studies of collider physics [91, 92], the observation of neutrino oscillations and the implication of non-vanishing neutrino mass motivate us to include RH neutrinos[3]. Direct experimental limits on operators containing RH neutrino fields leave room for appreciable effects in Higgs production in the missing energy ($\not{E}$) channel, $e^+e^- \to H + \nu\bar{\nu}$. It is possible, however, to argue for more stringent limits on these effects by invoking neutrino mass "naturalness" considerations [69, 38]. Below, we argue that if the only particles lighter than the SM Higgs boson are other SM particles, then the observation of large deviations from SM expectations for Higgs production with missing energy without corresponding deviations in the $Hq\bar{q}$ and $H\ell\bar{\ell}$ channels would imply fine tuning in order to be consistent with the small scale of neutrino mass.

[3]In doing so, we consider only Dirac neutrinos, deferring the case of Majorana neutrinos to a future study.

(iii) With the possible exception of operators which would give magnetic moments to the quarks, operators containing both Higgs and quark fields, which contribute directly only to the $e^+e^- \to H\bar{q}q$ channel, yield small contributions since their contributions are kinematically suppressed relative to SM HZ for the energies of interest here and since their operator coefficients are strongly constrained by Z^0 pole precision observables (except for top quarks). While we do not directly constrain the coefficients of the quark magnetic moment operators, we find for reasonable values of these coefficients that their contributions to $e^+e^- \to H\bar{q}q$ would also be small.

(iv) The possible effects of $n = 6$ bosonic-fermionic operators are quite distinctive from those associated with purely bosonic operators. Effects of the latter are rather generic to a variety of Higgs production channels in e^+e^- annihilation, as they enter primarily through modifications of the Higgs self-couplings and Higgs coupling to gauge bosons [51] and do not change the topology or analytic properties of the Higgs production amplitudes. Moreover, these modified couplings can enter strongly in both the HZ and gauge boson fusion cross-sections and can, in principle, substantially modify the $e^+e^- \to H\bar{q}q$, $H+\not{E}$, and $H\ell^+\ell^-$ channels. In contrast, the impact of the $n = 6$ operators considered here is quite channel specific, with the largest effects arising in processes dominated by SM HZ. Moreover, the analytic structure and kinematic dependence of the amplitudes generated by the $n = 6$ Higgs-fermion operators is distinct from that of the SM HZ and gauge boson fusion amplitudes, a feature not associated with the purely scalar operators. Thus, a comprehensive program of Higgs production studies would provide an interesting way to disentangle the possible effects of purely bosonic and Higgs-fermion operators in Higgs production at a linear collider.

In the remainder of this chapter, we provide details of the analysis leading to these observations. In Section 3.2 we briefly review Higgs production in the SM. While the latter is well known, we include a short discussion here to provide a backdrop for

discussion of possible deviations from SM expectations, as the impact of the operators we consider depends strongly on both the production mechanism and energy as well as on the mass of the H. Section 3.3 contains a discussion of the $n = 6$ operator basis. The heart of our study lies in Sections 3.4 and 3.5 that contain, respectively, an analysis of prospective deviations from SM Higgs production due to the operators of Section 3.3 and an evaluation of bounds on the corresponding operator coefficients obtained from various phenomenological considerations. In arriving at the latter, we follow a somewhat different procedure than used by the authors of [91], though the numerical differences are small. Section 3.6 contains a discussion of our results and their implications.

Before proceeding, we make a few additional comments about our analysis.

(a) For simplicity we have considered the case of a linear collider with unpolarized beams, although the ILC will likely have one or both beams partially polarized (see [93] and references therein).

(b) We do not discuss changes in the Higgs production cross-section caused solely by modifications of the fermion-gauge boson vertices in the SM Higgs production amplitudes. Effects of this type do not entail any change in the analytic structure or kinematic-dependence of the SM amplitudes, and the constraints implied by precision electroweak data and neutrino mass preclude the introduction of any significant deviations from SM Higgs production cross-sections due to changes in these couplings.

(c) In principle, one should also consider modifications of the SM Higgs-gauge boson couplings due to contributions from $n = 6$ fermionic operators to the μ-decay amplitude. The HWW coupling depends on both the $\mathrm{SU}(2)_L$ gauge coupling, g_2, and M_W, while the HZZ coupling depends on g_2, M_Z, and $\cos\theta_W$, where θ_W is the weak mixing angle. The W boson mass, weak mixing angle, and g_2 are derived quantities that depend on the Fermi constant obtained from muon decay, corrected for μ-decay dependent radiative corrections and possible new physics contributions to the muon decay amplitude. Thus, any $n = 6$

operators that contribute to the μ-decay amplitude will affect the HWW and HZZ couplings. In practice, the constraints implied by precision electroweak data are too strong to allow for observable effects in Higgs production cross-sections due to changes in the Higgs-gauge boson couplings generated by $n = 6$ fermionic operator contributions to μ-decay.

(d) We concentrate on single Higgs production for simplicity, though the extension to HH production is straightforward.

(e) In this work, we do not consider operators that contain top quark fields. We direct the interested reader to [94].

3.2 Higgs Production in the Standard Model

In the Standard Model, the Higgs boson can be produced in e^+e^- collisions primarily by three mechanisms [95]. In the Higgsstrahlung process (HZ), the H is produced with an accompanying Z^0 boson, which then decays to a fermion-antifermion pair. In the WW-fusion (WWF) and ZZ-fusion (ZZF) processes, the H is produced with an accompanying $\nu_e\bar{\nu}_e$ and e^+e^- pair, respectively. The cross-sections for these three processes are shown in Fig. 3.1 for $\sqrt{s} = 500$ GeV and 1 TeV for a range of Higgs masses. At $\sqrt{s} = 1$ TeV, the WW-fusion diagram dominates, while at $\sqrt{s} = 500$ GeV, WW-fusion and Higgsstrahlung can be comparable. At lower energies (not shown here), Higgsstrahlung dominates. The ZZ-fusion cross-section is smaller than the WWF cross-section by about an order of magnitude at all energies. Thus, for $\sqrt{s} = 1$ TeV, the Higgs is primarily produced in conjunction with missing energy. At lower $\sqrt{s}$ where HZ is important, however, one must consider final states corresponding to all possible Z decay products: $q\bar{q}$ (70%), missing energy (20%), and charged leptons $\ell^+\ell^-$ (10%).

In general, consideration of specific final state topologies associated with Higgs production and decay, as well as Z^0-decay, can be used to select the production mechanism. For 114 GeV $\leq m_H \lesssim$ 130 GeV, the Standard Model Higgs decays

primarily to $b\bar{b}$; for higher Higgs masses, the main decay channel is W^+W^-. Thus, a final state with two b-jets and missing energy would arise either from WWF (high $\sqrt{s}$), HZ (low $\sqrt{s}$ with $Z^0 \to \nu\bar{\nu}$ and $H \to b\bar{b}$), or a combination (intermediate $\sqrt{s}$), and the corresponding event topologies at a linear collider have been studied [96] for light values of m_H. The analysis of [96] concluded that obtaining measurement of σ_{WWF} with $\sim 10\%$ precision or better would be feasible at a 500 GeV linear collider.

When H production is accompanied by a charged lepton-antilepton pair (e^+e^- or $\mu^+\mu^-$ in the case of HZ, and e^+e^- in the case of ZZF), the Higgs production cross-section and mass can be measured independently of its decay channel (including non-SM decays) [97]. The mass can be reconstructed from the recoil mass of the $\ell^+\ell^-$ system. The study of [97] considered the HZ process at $\sqrt{s} = 350$ and 500 GeV for 120 GeV $\leq m_H \leq$ 160 GeV and found that a measurement of the combined He^+e^- and $H\mu^+\mu^-$ HZ cross-section with $\sim 3\%$ precision could be achieved. Additionally, studies have also been performed for the case of HZ where $Z \to q\bar{q}$ [98, 99]. In what follows, we assume that each of these event topologies can be identified experimentally, and we study the corresponding impact of $n = 6$ operators assuming only SM decays of the H. We show that for some operators, deviations from the SM Higgs production cross-sections could be larger than the experimental error "benchmarks" indicated above.

3.3 Operator Basis

The basis of $n = 6$ operators containing the Standard Model fields has been enumerated in previous works [100, 101, 91, 92, 52, 69, 38]. Here, we include only those containing 1) the SM Higgs doublet ϕ with hypercharge $Y = 1$ and 2) SM fermion and/or RH neutrino fields. It is useful to distinguish three classes of such operators: (A) mass operators; (B) operators containing only fields that transform non-trivially under SM gauge symmetries (i.e., do not contain ν_R fields); and (C) operators containing right-handed neutrinos that are not mass operators.

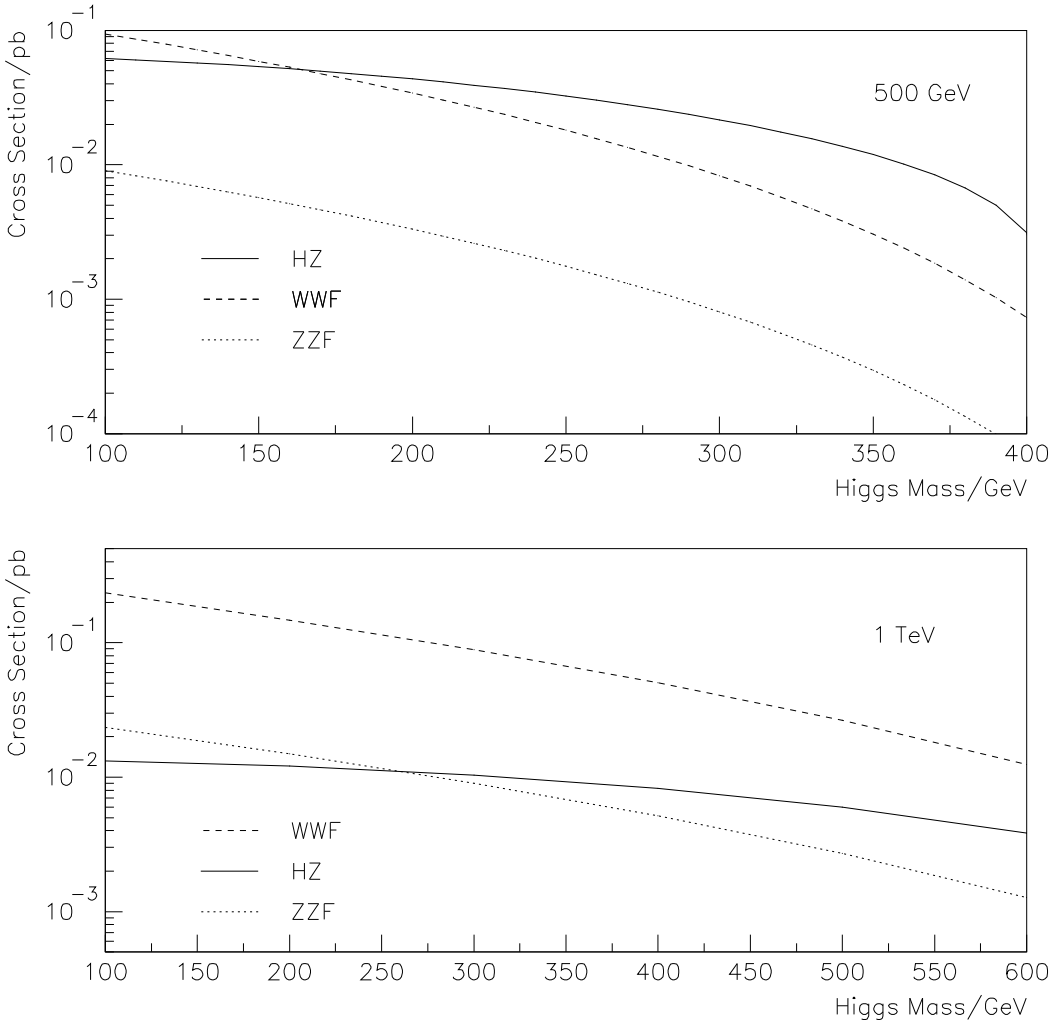

Figure 3.1: SM contributions to the Higgs production cross-section

Class A. We begin with the mass operators , of which there are two:

$$\begin{aligned} \mathcal{O}^{\ell}_{M,\,AB} &\equiv (\bar{L}^A \phi \ell^B_R)(\phi^+ \phi) + \text{h.c.} \\ \mathcal{O}^{\nu}_{M,\,AB} &\equiv (\bar{L}^A \widetilde{\phi} \nu^B_R)(\phi^+ \phi) + \text{h.c.} \quad , \end{aligned}$$

where L^A and ℓ^A are left-handed lepton doublet and singlet fields, respectively, and A, B are generation indices. (Mass operators for quark fields are analogous.) Operators containing a contracted pair of Pauli matrices, such as $\bar{L}\tau^a \phi \ell_R (\phi^\dagger \tau^a \phi)$ can be related to the two operators above via a Fierz transformation. The $\mathcal{O}^{\ell}_{M,\,AB}$ and $\mathcal{O}^{\nu}_{M,\,AB}$ can

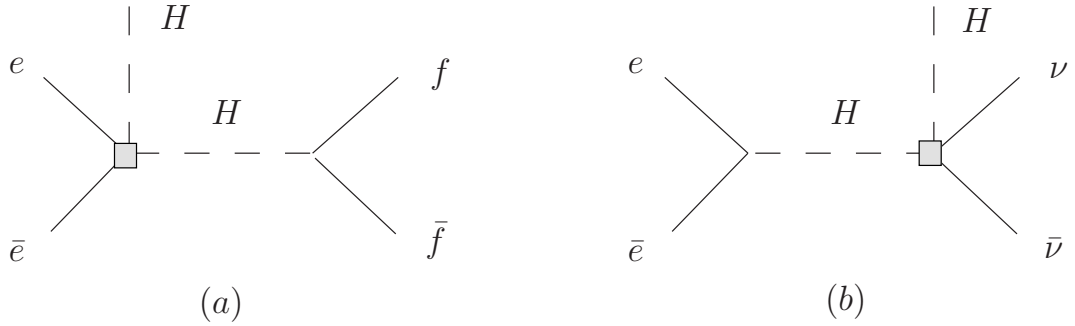

Figure 3.2: Contribution of Class A operators (*a*) $\mathcal{O}^{\ell}_{M,\,AB}$ and (*b*) $\mathcal{O}^{\nu}_{M,\,AB}$ to Higgs production

contribute to Higgs production via the diagrams shown in Fig. 3.2. In the absence of fine-tuning with the $n = 4$ Standard Model mass operators, their coefficients C^{ℓ}_M and C^{ν}_M are tightly constrained by the ℓ and ν mass, respectively:

$$\begin{aligned} \frac{\left|C^{\ell}_{M,ee}\right|}{\Lambda^2} &\lesssim \frac{2\sqrt{2} m_e}{v^2} \\ \frac{\left|C^{\nu}_{M,AB}\right|}{\Lambda^2} &\lesssim \frac{2\sqrt{2} m_{\nu,AB}}{v^2} \quad , \end{aligned}$$

where $m_{\nu,AB}$ is an element of the neutrino mass matrix before diagonalization. In addition to this (large) suppression, the interference of these diagrams with the SM Higgs production diagrams is additionally mass-suppressed due to the fermion chiralities. Thus, the contributions of these two operators to Higgs production are negligible,

and we will not consider them further.

Class B. These operators contain only fields that are not SM singlets (i.e., no ν_R):

$$\begin{aligned}
\mathcal{O}_{VR,AB} &\equiv i(\bar{f}_R^A \gamma^\mu f_R^B)(\phi^+ D_\mu \phi) + \text{h.c.} \\
\mathcal{O}_{VL,AB} &\equiv i(\bar{F}^A \gamma^\mu F^B)(\phi^+ D_\mu \phi) + \text{h.c.} \\
\mathcal{O}_{VL\tau,AB} &\equiv i(\bar{F}^A \gamma^\mu \tau^a F^B)(\phi^+ \tau^a D_\mu \phi) + \text{h.c.} \\
\mathcal{O}^q_{\tilde{V},\,AB} &\equiv i(\bar{d}_R^A \gamma^\mu u_R^B)(\phi^+ D_\mu \widetilde{\phi}) + \text{h.c.} \\
\mathcal{O}^f_{W,AB} &\equiv g_2(\bar{F}^A \sigma^{\mu\nu} \tau^a \phi) f_R^B W^a_{\mu\nu} + \text{h.c.} \\
\mathcal{O}^f_{B,AB} &\equiv g_1(\bar{F}^A \sigma^{\mu\nu} \phi) f_R^B B_{\mu\nu} + \text{h.c.} \quad ,
\end{aligned}$$

where F^A indicates either the left-handed lepton (L) or quark (Q) doublet for generation A and f^A indicates the RH fields for quarks or charged leptons of generation A. We have included the "R" subscript on the latter for clarity. The fields u_R^A and d_R^A denote the up- and down-type RH quarks of generation A. The operator $\mathcal{O}^q_{\tilde{V},\,AB}$ does not contribute to Higgs production in e^+e^- annihilation since it contains no neutral current component, so we will not discuss it further.

Class C. Lastly, we consider operators containing ν_R that are not mass-suppressed and that contribute only to the missing energy channel:

$$\begin{aligned}
\mathcal{O}_{V\nu,\,AB} &\equiv i(\bar{\nu}_R^A \gamma^\mu \nu_R^B)(\phi^+ D_\mu \phi) + \text{h.c.} \\
\mathcal{O}_{\tilde{V},\,AB} &\equiv i(\bar{\ell}_R^A \gamma^\mu \nu_R^B)(\phi^+ D_\mu \widetilde{\phi}) + \text{h.c.} \\
\mathcal{O}_{W,\,AB} &\equiv g_2(\bar{L}^A \sigma^{\mu\nu} \tau^a \widetilde{\phi}) \nu_R^B W^a_{\mu\nu} + \text{h.c.} \\
\mathcal{O}_{B,\,AB} &\equiv g_1(\bar{L}^A \sigma^{\mu\nu} \widetilde{\phi}) \nu_R^B B_{\mu\nu} + \text{h.c.}
\end{aligned}$$

For $\mathcal{O}_{\tilde{V},\,AB}$, $\mathcal{O}_{W,\,AB}$, and $\mathcal{O}_{B,\,AB}$, we follow the notation of [69] and [38]. Due to the presence of the ν_R field, interference of tree-level diagrams containing these operators

with the Standard Model Higgs production amplitudes is suppressed by the neutrino mass. Hence, we do not consider these interference effects here and compute only the contributions that are quadratic in their coefficients. As a result, their contributions can be appreciable only if the corresponding C_6^j are not loop suppressed.

3.4 Contributions to Higgs Production

3.4.1 General Considerations

Before considering in detail the corrections to various production channels, we make a few general observations regarding the operators and amplitudes that one may expect to be largest. To that end, we show in Figure 3.3 the H production amplitudes generated by the operators of Class B, and in Figure 3.4 those generated by Class C operators. The amplitudes in Figs. 3.3a, b and 3.4a correspond to taking the SM HZ amplitude and contracting one of the two Z^0 propagators to a point. In SM HZ, the initial Z^0 is far off shell for the energies considered here, while the final Z^0 propagator is resonant. Thus, we expect the contributions associated with Figs. 3.3b and 3.4a to be highly suppressed relative to the SM cross-section since they contain no resonating Z^0 propagator. In contrast, the amplitude of Fig. 3.3a contains a nearly on-shell Z^0 propagator but no off-shell Z^0 propagator. Consequently, it can be kinematically enhanced relative to the SM HZ amplitude and can generate an appreciable contribution to H production, even in the presence of strong constraints on the corresponding operator coefficient (see Section 3.5).

The corrections generated by the amplitudes of Figs. 3.3c, d and 3.4b, c contribute to the $Hl^A\bar{l}^B$ (where at least one of A and $B = e$) and missing energy channels. For large $\sqrt{s}$, the $H + \not{E}$ channel is dominated by WWF wherein both W bosons are off shell. Thus, the amplitudes of Figs. 3.3c, d and 3.4b, c experience no kinematic suppression relative to the SM cross-section[4]. Even in the intermediate energy regime,

[4]This situation contrasts with that of Fig. 3.3b, which corresponds to shrinking the resonating Z^0 propagator in HZ to a point, thus leading to a kinematic suppression relative to the SM HZ amplitude.

where WWF and HZ yield comparable contributions, the effects of Figs. 3.3c, d and 3.4b, c can, in principle, be appreciable. We reiterate, however, that for the operators containing ν_R fields, the amplitudes of Fig. 3.4 do not interfere appreciably with the SM amplitudes, and their contributions can only be large when the operator coefficients are not loop-suppressed.

We now turn to a detailed discussion of various operator effects.

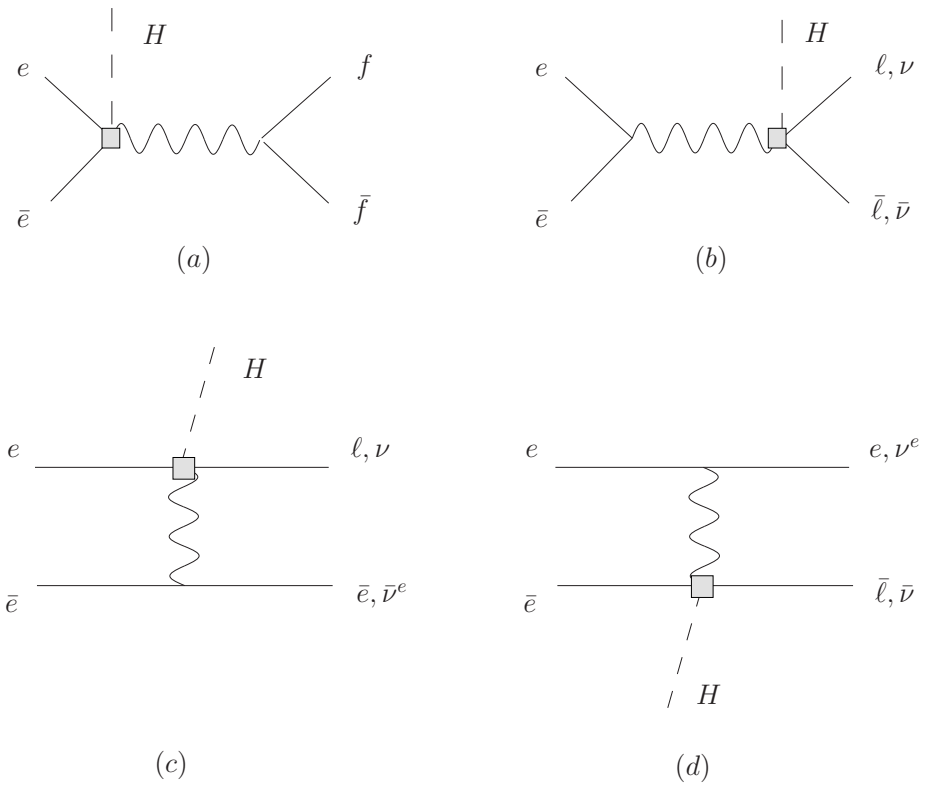

Figure 3.3: Contribution of Class B operators to Higgs production

3.4.2 Class B Operators

Here, we discuss in detail the possible effects of operators in Class B, which contain only fields that transform non-trivially under SM symmetries.

$\mathcal{O}_{VR,AB}$

The contributions from operator $\mathcal{O}_{VR,AB}$ depends on its flavor indices A, B. For $A = B = e$, $\mathcal{O}_{VR,ee}$ contributes to all Higgs production channels via the diagram in

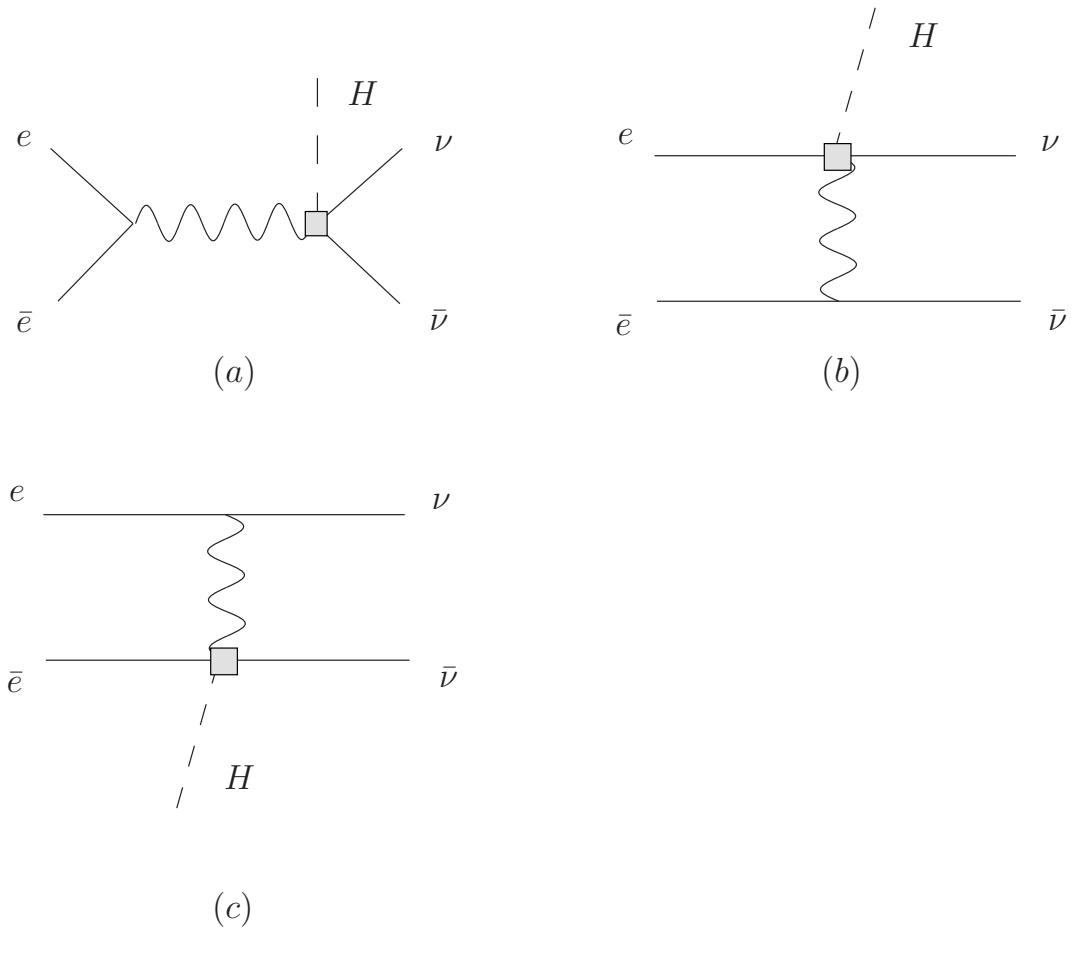

Figure 3.4: Contribution of Class C operators to Higgs production

Fig. 3.3a and additionally to the He^+e^- channel via the diagrams in 3.3b–d. In all cases, the exchanged gauge boson is a Z^0. As noted above, the analytic structure of the amplitude for Fig. 3.3a differs from that of the SM HZ amplitude only by the absence of the off-shell Z^0 propagator. The ratio of its interference with the SM HZ amplitude to the SM HZ cross-section is, thus, given by

$$\frac{\sigma_{3(a)-HZ\,\mathrm{int}}}{\sigma_{HZ}} = -\frac{Cv^2}{\Lambda^2}\frac{(s-M_Z^2)}{M_Z^2}\frac{\sin^2\theta_W}{2(\sin^4\theta_W - \frac{1}{2}\sin^2\theta_W + \frac{1}{8})} \quad , \tag{3.2}$$

where we have omitted the label on the operator coefficient for simplicity. For $Cv^2/\Lambda^2 = 10^{-2}$, this ratio is ~ -0.54 and ~ -2.2 for $\sqrt{s} = 500$ GeV and 1 TeV, respectively. The effect of $\sigma_{3(a)-HZ\,\mathrm{int}}$ relative to σ_{HZ} can be large for the values of $\sqrt{s}$ studied here since in the SM HZ amplitude the initial Z^0 is far off shell with $M_Z \ll \sqrt{s}$; thus, the SM HZ amplitude contains a kinematic suppression of roughly Λ^2/s that does not enter the amplitude of Fig. 3.3a.

For any of the final states of $Hf\bar{f}$ with $f = \mu$, τ, ν_μ, ν_τ, or q, Eq. (3.2) gives the ratio of the contribution of $\mathcal{O}_{VR,ee}$ to the SM cross-section. For the $H\nu_e\bar{\nu}_e$ final state, the SM also receives a contribution from the WWF process[5]. Interference between WWF—which involves only a LH (RH) initial state electron (positron)—-and diagram 3.3a containing $\mathcal{O}_{VR,ee}$ requires a Yukawa coupling on each of the initial-state fermion lines, and is thus strongly suppressed. For the He^+e^- production channel, we must include the interference of all of the diagrams shown in Fig. 3.3 with both SM HZ and ZZF.

We have computed the contribution of $\mathcal{O}_{VR,ee}$ arising from interference with the SM amplitudes[6] to the total H production cross-section using the calchep package [102, 103]. Results are shown in Fig. 3.5, where we give the ratio $\sigma_{\mathrm{int}}/\sigma_{\mathrm{SM}}$ as a function of the Higgs mass for different final state topologies, where σ_{int} is the contribution to the cross-section of the interference between all of the diagrams in Fig. 3.3 and

[5]Since the neutrinos in the missing energy channel are not detected, one may discuss the relative magnitudes of non-SM contributions using the neutrino flavor basis.

[6]Here, we neglect the contributions that are not due to interference with the SM; we will defer discussion of the non-interference terms to Section 3.6.

all of the relevant SM diagrams. We observe that for the $Hf\bar{f}$ channels with $f = \mu$, τ, ν_μ, ν_τ, or q, the ratio is independent of m_H, as implied by Eq. (3.2). In contrast, for the He^+e^- and $H + \not{E}$ channels, the ratio varies with m_H due to the additional contributions from the SM WWF and ZZF processes, as well as other diagrams in Fig 3.3. We also note that the effect of $\mathcal{O}_{VR,ee}$ can be large compared with the SM HZ cross-section. Thus, one could in principle discern the effects of this operator by analyzing events that cannot be produced by the WWF process, such as a dilepton pair and two b-jets, or two b-jets and two other jets. In contrast, the relative effect of $\mathcal{O}_{VR,ee}$ on the He^+e^- and $H + \not{E}$ channels is considerably smaller, due to the much larger SM ZZF and WWF contributions in these cases.

In contrast to the situation with $\mathcal{O}_{VR,ee}$, the operator $\mathcal{O}_{VR,AA}$, $A = \mu, \tau, q$ contributes only through diagram 3.3b. This diagram interferes only with the HZ amplitude and contributes only to the $H\mu^+\mu^-$, $H\tau^+\tau^-$, and $Hq\bar{q}$ channels. The contribution of $\mathcal{O}_{VR,\mu\mu}$ to the $H\mu^+\mu^-$ channel—relative to the SM cross-section—is shown in Fig. 3.6 as a function of m_H. The results for $\mathcal{O}_{VR,\tau\tau}$ are identical; those for $\mathcal{O}_{VR,qq}(q \neq t)$ differ from Fig. 3.6 only due to the difference between the Zqq and $Z\ell^+\ell^-$ SM couplings. As indicated in Fig. 3.6, the contribution from $\mathcal{O}_{VR,\mu\mu}$ to the $H\mu^+\mu^-$ channel is $\lesssim 10^{-3}$ of the SM cross-section, and we do not show the correspondingly small correction from $\mathcal{O}_{VR,qq}$ to the $Hq\bar{q}$ channel.

Comparing the contributions of $\mathcal{O}_{VR,ee}$ and $\mathcal{O}_{VR,\mu\mu}$ to the $H\mu^+\mu^-$ channel in Figs. 3.5 and 3.6, we can see that the effects of diagram 3.3b are strongly suppressed relative to those of diagram 3.3a. As noted above, this suppression is to be expected, since in the amplitude of Fig. 3.3b the Z^0 is always off-shell ($M_Z \ll \sqrt{s}$), whereas for the values of $\sqrt{s}$ of interest here, on-shell production of both the H and Z^0 can occur for the amplitude of Fig. 3.3a. As the same arguments will hold for $\mathcal{O}_{VL,AB}$ and $\mathcal{O}_{VL\tau}$, we will not consider the case of $A = B = \mu, \tau$ for those operators below.

$\mathcal{O}_{VL,ee}$

As with $\mathcal{O}_{VR,ee}$, the operator $\mathcal{O}_{VL,ee}$ contributes to Higgs production via the di-

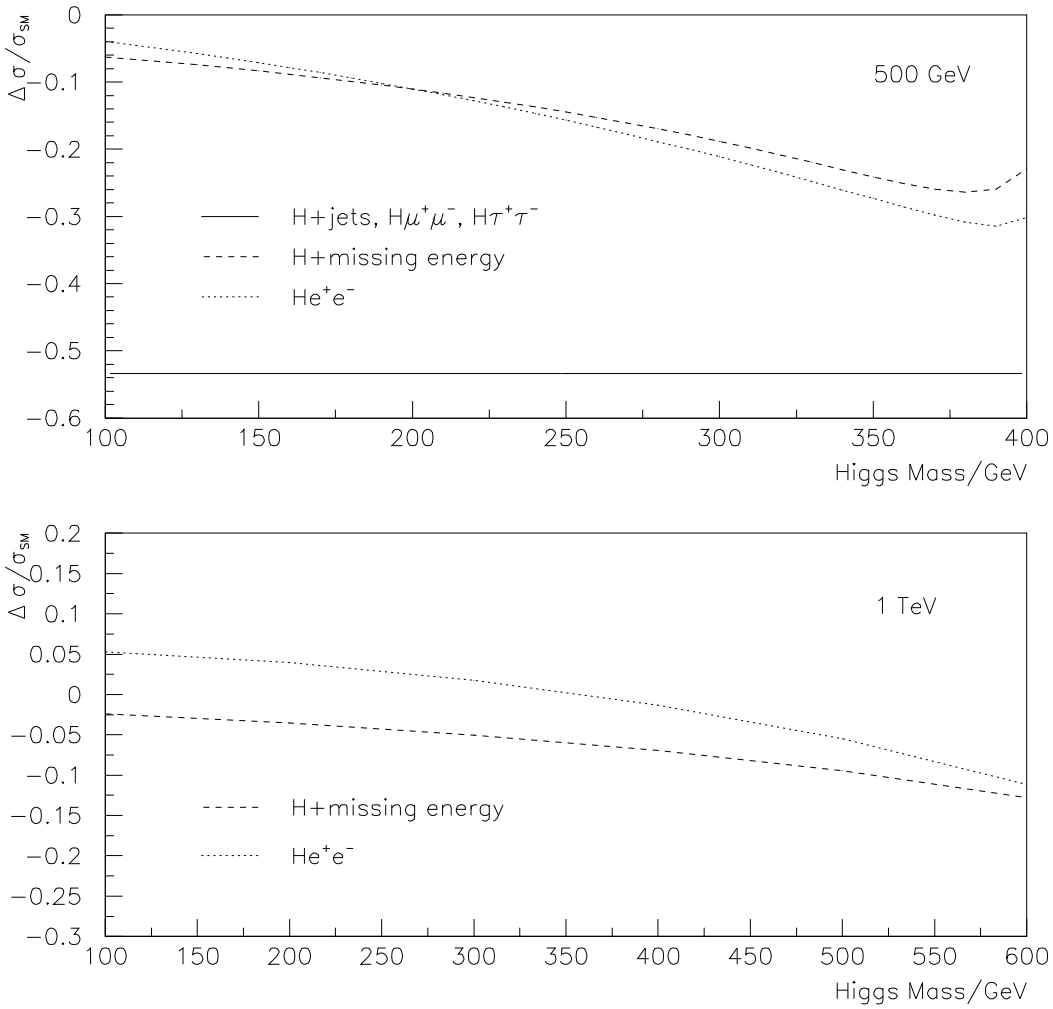

Figure 3.5: Ratio of contribution of $\mathcal{O}_{VR,ee}$ to SM Higgs production cross-section for (*top*) $\sqrt{s} = 500$ GeV and (*bottom*) 1 TeV for $C_{VR,ee}v^2/\Lambda^2 = 10^{-2}$. For $\sqrt{s} = 1$ TeV, the line for the $Hq\bar{q}$, $H\mu^+\mu-$, and $H\tau^+\tau^-$ channels is not shown; it has the value of -2.2, independent of Higgs mass.

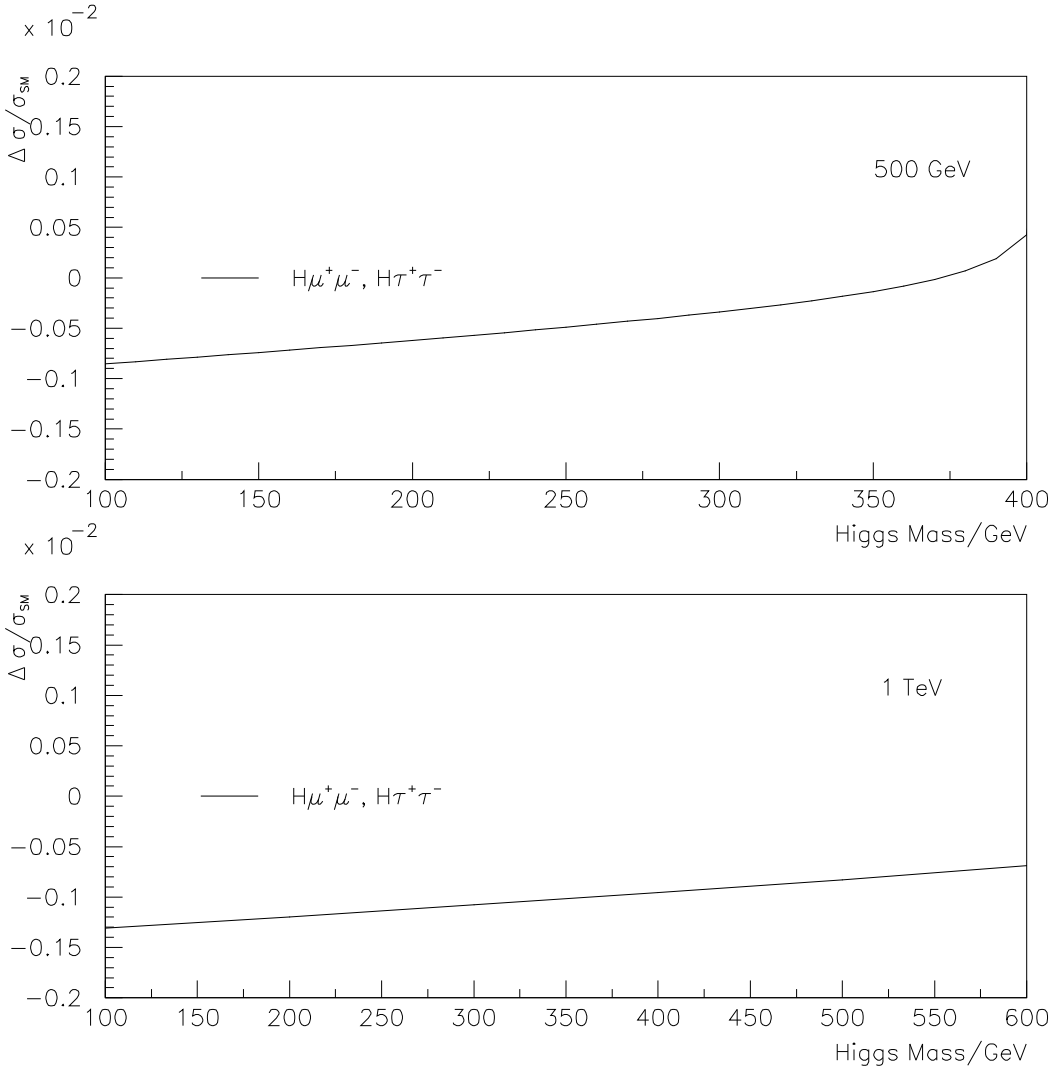

Figure 3.6: Ratio of contribution of $\mathcal{O}_{VR,\mu\mu}$ to SM Higgs production cross-section for (*top*) $\sqrt{s} = 500$ GeV and (*bottom*) 1 TeV for $C_{VR,\mu\mu}v^2/\Lambda^2 = 10^{-2}$. Curves for $\mathcal{O}_{VR,\tau\tau}$ are identical.

agrams in Fig. 3.3a–d. In all four diagrams, the gauge boson exchanged is always a Z^0. Diagram 3.3a contributes to all channels, in analogy with $\mathcal{O}_{VR,ee}$ above. This contribution of the interference of this diagram with HZ obeys

$$\frac{\sigma_{3(a)-HZint}}{\sigma_{HZ}} = \frac{Cv^2}{\Lambda^2}\frac{(s-M_Z^2)}{M_Z^2}\frac{(\frac{1}{2}-\sin^2\theta_W)}{2(\sin^4\theta_W-\frac{1}{2}\sin^2\theta_W+\frac{1}{8})} \ . \tag{3.3}$$

This expression gives the ratio of the contribution of $\mathcal{O}_{VL,ee}$-SM HZ interference to the SM cross-section for the final states of $Hf\bar{f}$ for $f = \mu$, τ, $\nu_{\mu,\tau}$, and q. However, in contrast to the situation with $\mathcal{O}_{VR,ee}$, the insertion of this operator diagram 3.3a will also interfere with WWF without electron mass insertions (as well as with HZ and ZZF). Additionally, $\mathcal{O}_{VL,ee}$ contributes to the He^+e^- channel through diagrams 3.3b–d, all of which interfere with HZ and ZZF, and to the $H\nu_e\bar{\nu}_e$ through diagram 3.3b (although this latter contribution is strongly kinematically suppressed for the reasons discussed above). These contributions are summarized in Fig. 3.7 for $Cv^2/\Lambda^2 = 10^{-2}$ as a function of m_H. As before, the relative effect on the $Hf\bar{f}$ cross-section is m_H-independent for $f = \mu$, τ, $\nu_{\mu,\tau}$, and q, whereas for the He^+e^- and $H+\not{E}$ channels, the relative importance decreases with m_H, owing to the increasing ZZF and WWF contributions.

As in the case of $\mathcal{O}_{VR,AA}$, the contribution from $\mathcal{O}_{VL,AA}$ for $A = \mu$, τ, or q arises only from Fig. 3.3b. Since the corresponding effects are highly suppressed, we do not discuss this case further.

$\mathcal{O}_{VL\tau,ee}$

As in the previous cases, $\mathcal{O}_{VL\tau,ee}$ contributes to the Higgs production cross-section through all of the diagrams in Fig. 3.3. However, unlike the operators $\mathcal{O}_{VR,ee}$ and $\mathcal{O}_{VL,ee}$, $\mathcal{O}_{VL\tau,ee}$ also contains a charge-changing component. Thus, the gauge boson in diagrams 3.3c and d can be either a Z^0 or a $W^\pm$, so the insertion of $\mathcal{O}_{VL\tau,ee}$ in these diagrams contributes to both the He^+e^- and $H+\not{E}$ channels.

Inserting $\mathcal{O}_{VL\tau,ee}$ in diagram 3.3a generates the same contribution to all decay channels in the same manner as $O_{VL,ee}$, yielding the same contribution to the HZ

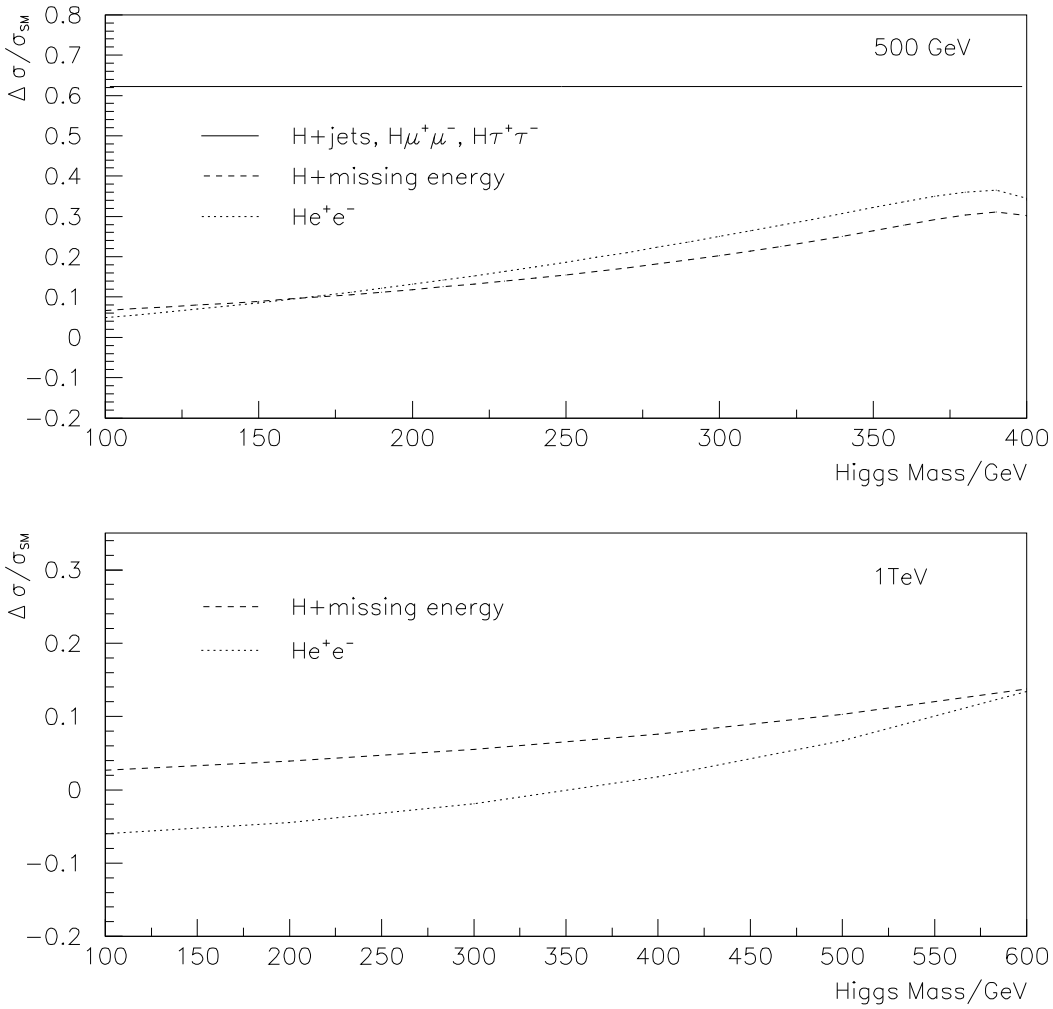

Figure 3.7: Ratio of contribution of $\mathcal{O}_{VL,ee}$ to SM Higgs production cross-section for (top) $\sqrt{s} = 500$ GeV and (bottom) $\sqrt{s} = 1$ TeV for $C_{VL,ee}v^2/\Lambda^2 = 10^{-2}$. For $\sqrt{s} = 1$ TeV, the line for the $Hq\bar{q}$, $H\mu^+\mu-$, and $H\tau^+\tau^-$ channels is not shown; it has the value of 2.6, independent of Higgs mass.

cross-section as for $\mathcal{O}_{VL\tau,ee}$ (see, e.g., Eq. (3.3)). The insertion of $\mathcal{O}_{VL\tau,ee}$ in diagram 3.3a also interferes with ZZF and WWF in the He^+e^- and $H\nu_e\bar{\nu}_e$ channels, respectively. Additionally, $\mathcal{O}_{VL\tau,ee}$ contributes to these channels via diagrams 3.3b–d. The contributions of $\mathcal{O}_{VL\tau,ee}$ to the Higgs production cross-section are are shown in Fig. 3.8 for $Cv^2/\Lambda^2 = 10^{-2}$.

As in the case of $\mathcal{O}_{VR,AA}$, the contribution from $\mathcal{O}_{VL\tau,AA}$ for $A = \mu$, τ, or q arises only from Fig. 3.3b. Since the corresponding effects are highly suppressed, we do not discuss this case further.

$\mathcal{O}^f_{W,AB}$ and $\mathcal{O}^f_{B,AB}$

The operators $\mathcal{O}^f_W$ and $\mathcal{O}^f_B$ contribute to the magnetic and electric dipole moments of the charged leptons. Stringent limits on the electric dipole moments and non-SM contributions to the magnetic moments exist for the cases $A = B = e$ and $A = B = \mu$ [1]. Limits on the branching fractions $\mu \to e\gamma$, $\tau \to e\gamma$, and $\tau \to \mu\gamma$ tightly constrain the cases where A and B are lepton fields and $A \neq B$ [1]. Thus, here we will only consider the possibilities $A = B = \tau$ and $A, B = q^A q^B$.

$\mathcal{O}^f_{W,\tau\tau}$ and $\mathcal{O}^f_{B,\tau\tau}$ will contribute only to the $H\tau^+\tau^-$ final state; production occurs only through diagram 3.3b. Due to the derivative on the gauge boson field in each of these operators, the kinematic suppression of this diagram is not as severe as in the previous cases of $\mathcal{O}_{VR,AB}$, $\mathcal{O}_{VL,AB}$, and $\mathcal{O}_{VL\tau,AB}$.

We have calculated the contributions of $\mathcal{O}^f_{W,\tau\tau}$ and $\mathcal{O}^s_{B,\tau\tau}$ to the $H\tau^+\tau^-$ cross-section for $C^j v^2/\Lambda^2 = 10^{-2}$, neglecting the Yukawa-suppressed contribution to the cross-section due to the interference of diagram 3.3b with the SM HZ process. We find that the contribution to the cross-section is generally less than 0.1% for $\sqrt{s} = 500$ GeV, and less than 2% for $\sqrt{s} = 1$ TeV. We also find that the interference of diagram 3.3b with other (tiny) SM processes which contain a Higgs insertion on one of the τ lines could give comparable contributions to the $H\tau^+\tau^-$ cross-section.

For the case where A and B are light quark fields (u, d, and s), interference with the SM diagrams can be neglected as these contributions are Yukawa-suppressed. There is a contribution to the $Hq^A\bar{q}^B$ cross-section that is $N_C = 3$ times larger

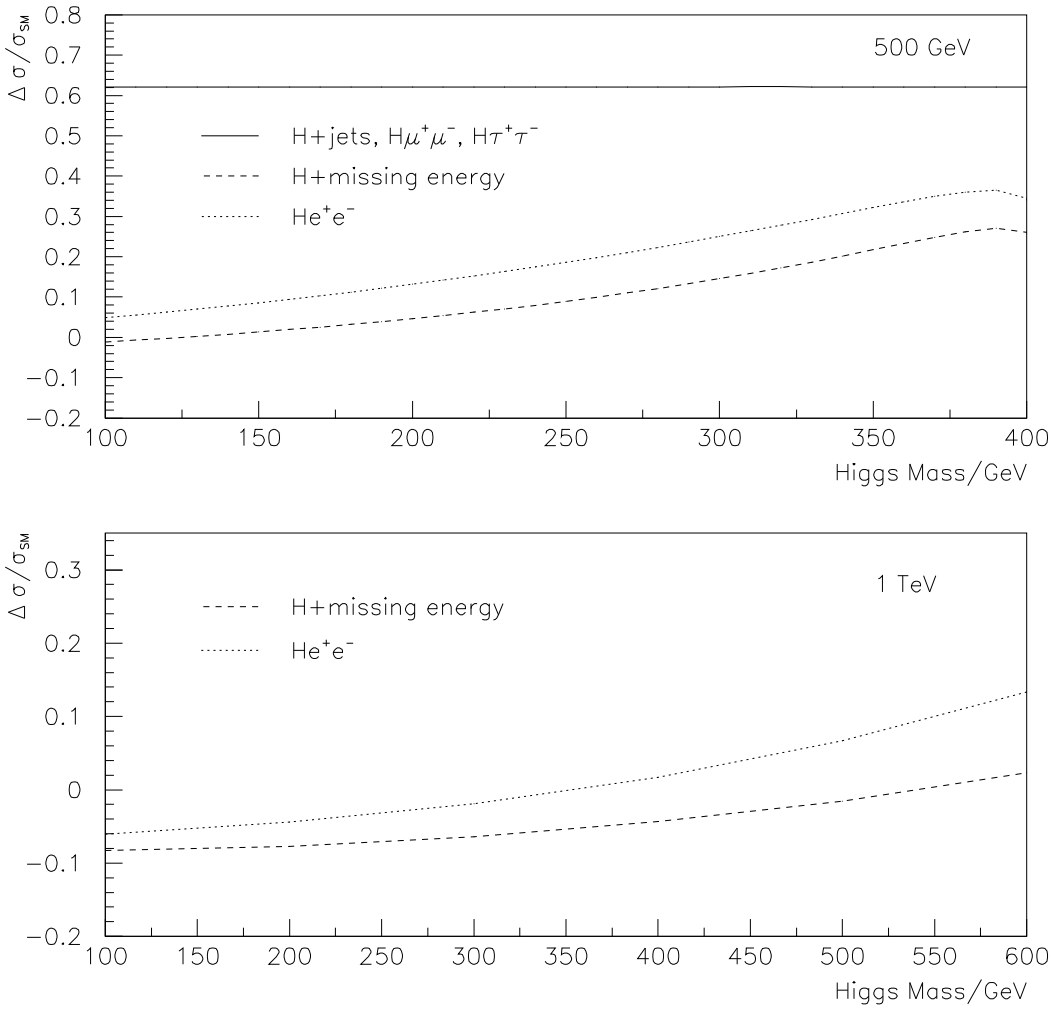

Figure 3.8: Ratio of contribution of $\mathcal{O}_{VL\tau,ee}$ to SM Higgs production cross-section for (top) $\sqrt{s} = 500$ GeV and (bottom) 1 TeV for $C_{VL\tau,ee}v^2/\Lambda^2 = 10^{-2}$. For $\sqrt{s} = 1$ TeV, the line for the $Hq\bar{q}$, $H\mu^+\mu-$, and $H\tau^+\tau^-$ channels is not shown; it has the value of 2.6, independent of Higgs mass.

than the $A = B = \tau$ noninterference cross section discussed above and is, thus, negligible. In the case where $A = B = b$ or c, interference with the SM diagrams can give additional contributions with magnitude comparable to the non-intereference contributions.

Current limits [1] on the τ magnetic moment allow values for $C^f_{B,\tau\tau}v^2/\Lambda^2$ and $C^f_{W,\tau\tau}v^2/\Lambda^2$ of order unity. Somewhat improved limits, but still significantly weaker than $C^f_{B,W,\tau\tau}v^2/\Lambda^2 = 10^{-2}$ can be obtained from $\Gamma(Z \to \tau^+\tau^-)$. Similarly weak limits on the quark magnetic moment operators can be obtained from $\Gamma(Z \to q^A\bar{q}^B)$. However, we will take 10^{-2} as an estimate of the upper bound for $C^f_{B,W}v^2/\Lambda^2$. Nevertheless, we do not rule out the possibility that the coefficients of these operators could be considerably larger due to strong dynamics above the scale Λ.

3.4.3 Class C Operators

All of the Class C operators contribute only to the missing energy channel since they contain ν_R fields. The Higgs production diagrams for these operators are shown in Fig. 3.4. For each operator, the interference of any amplitude in Fig. 3.4 with relevant SM amplitude is m_ν-suppressed, so we do not include the interference contributions here. The resulting corrections to the SM Higgs production cross-sections are, thus, quadratic in the operator coefficients.

Since the final state neutrino-antineutrino pair is not observed, we do not require their flavors to be the same. As discussed above, the contribution from diagram 3.4a is kinematically suppressed due to the off-shell Z^0 boson, so we expect that only those operators contributing through diagrams 3.4b and c will be able to generate substantial contributions. The comparison between the contribution from these operators to the $H + \not{E}$ channel is given in Fig. 3.9 for $Cv^2/\Lambda^2 = 10^{-2}$.

For $Cv^2/\Lambda^2 = 10^{-2}$ as assumed above, the correction induced by the Class C operators is generally less than 10^{-3} of the SM cross-section. However, if these operators are generated by strong dynamics or tree-level gauge interactions, their relative effects could be substantially larger. In this respect, the operator $\mathcal{O}_{\tilde{V},AB}$ is particularly

interesting, as an operator of this type could arise in models with mixing between LH and RH gauge bosons. Moreover, it is not as strongly constrained by precision electroweak data as the Class B operators, since it does not interfere with the SM amplitudes that contain only LH neutrino fields. In Section 3.5 we discuss the various phenomenological and theoretical constraints on $\mathcal{O}_{\tilde{V},AB}$, including those implied by the scale of neutrino mass and naturalness considerations.

$\mathcal{O}_{V\nu,AB}$

The operator $\mathcal{O}_{V\nu,AB}$ contributes to the missing energy channel only via the diagram in Fig. 3.4a where the exchanged gauge boson is a Z^0 and the final state contains a right-handed neutrino and a left-handed antineutrino. Thus, the contribution of this operator is strongly kinematically suppressed, as reflected in Fig. 3.9.

$\mathcal{O}_{\tilde{V},AB}$

The gauge boson in $\mathcal{O}_{\tilde{V},AB}$ is always a $W^{\pm}$, and this operator contributes to the missing energy channel via the diagrams in Figs. 3.4b and c. The final state contains one right-handed neutrino and one right-handed antineutrino, in the case of 3.4b, or a left-handed neutrino and antineutrino in the case of 3.4c. As this operator contributes through diagrams 3.4b and c whose effect on the production cross-section is not kinematically suppressed relative to WWF, the relative importance of its contribution is larger than that of $\mathcal{O}_{V\nu,AB}$.

$\mathcal{O}_{W,AB}$ and $\mathcal{O}_{B,AB}$

The neutrino dipole operators $\mathcal{O}_{W,AB}$ and $\mathcal{O}_{B,AB}$ contribute to Higgs production via diagram 3.4a wherein the exchanged gauge boson is either a Z^0 or a γ and the final state contains a neutrino and an antineutrino that are either both right-handed or both left-handed. The insertion of $\mathcal{O}_{W,AB}$ in diagrams 3.4b and c only contain the $W^{\pm}$ boson; they contribute to the same final states does $\mathcal{O}_{\tilde{V},AB}$. Note that since $\mathcal{O}_{B,AB}$ contributes only through 3.4a, its contribution will be suppressed relative to that of $\mathcal{O}_{W,AB}$. Again, this feature can be seen from Fig. 3.9.

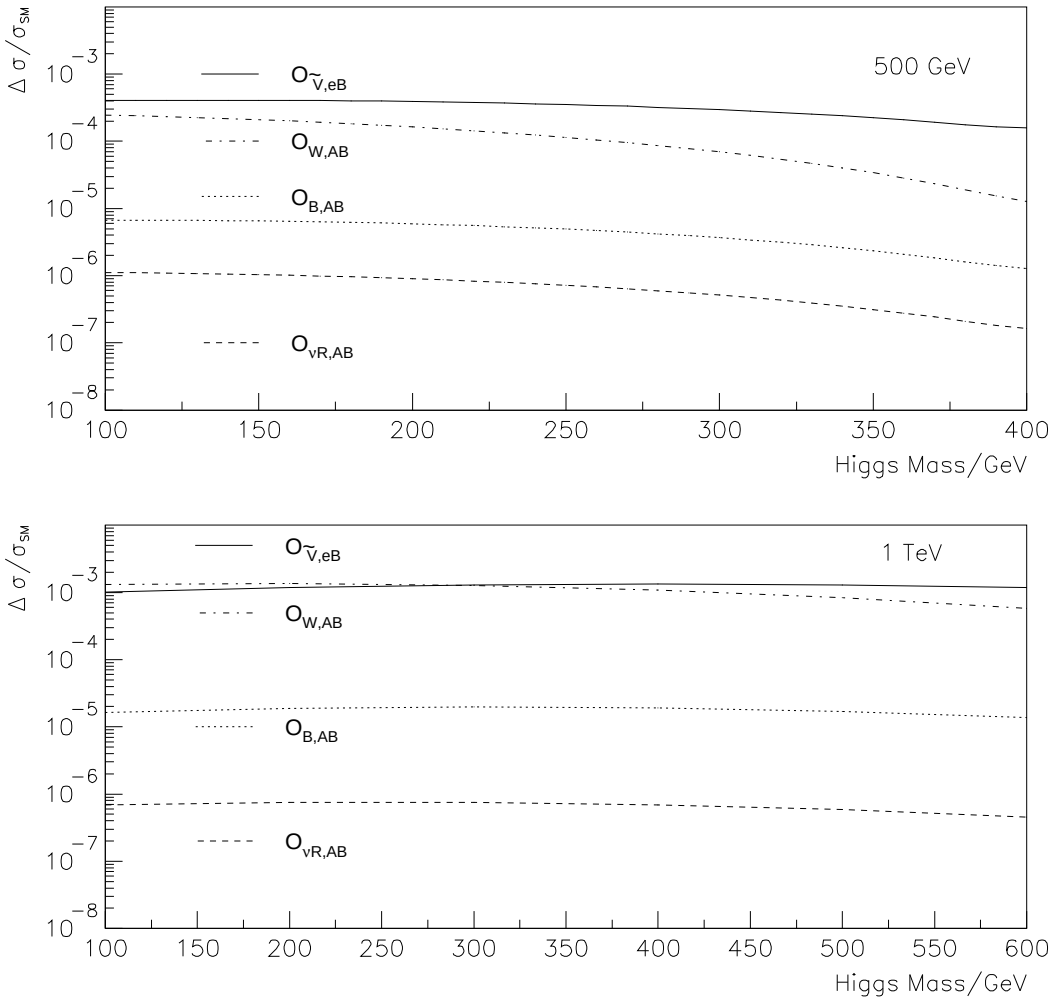

Figure 3.9: Contributions of operators containing ν_R to Higgs missing energy final state for $\sqrt{s} = 500$ GeV. Results are as a fraction of the total Standard Model $H\nu\bar{\nu}$ cross-section, summed over the three flavors. Curves are drawn for the case $C^j v^2/\Lambda^2 = 10^{-2}$.

Table 3.1: Cross-sections for flavor-nonconserving processes $e^+e^- \to He^\pm l^\mp$, $l = \mu, \tau$ for $Cv^2/\Lambda^2 = 10^{-2}$. Both charge combinations are included. Results are in units of 10^{-6} pb.

	$\sqrt{s} = 500$ GeV			$\sqrt{s} = 1$ TeV		
m_H/GeV	100	250	400	100	300	500
$\mathcal{O}_{VR,e\ell}$	3.4	0.72	0.024	28.	14.	4.2
$\mathcal{O}_{VL,e\ell}$, $\mathcal{O}_{VL\tau,e\ell}$	3.2	0.67	0.023	27.	13.	4.1

3.4.4 Flavor Nonconserving Operators

Now, we consider the case $A \neq B$ for those operators having the potentially largest effects in the flavor conserving channels: $\mathcal{O}_{VR,AB}$, $\mathcal{O}_{VL,AB}$, and $\mathcal{O}_{VL\tau,AB}$. Here, we have two distinct cases, A or $B = e$, and both A, $B \neq e$. The latter case can only contribute through diagram 3.3b, whose effect is kinematically suppressed. Hence, we ignore this case. For all three of these flavor nonconserving operators, Higgs production can occur through diagrams 3.3b, and c or d, giving a final state containing $e^\pm\mu^\mp$ or $e^\pm\tau^\mp$. Although diagrams 3.3b (in the case of $\mathcal{O}_{VL,AB}$ or $\mathcal{O}_{VL\tau,AB}$) and c, and d (for $\mathcal{O}_{VL\tau,AB}$ only) could also contribute to the missing energy final state, given the small number of events involved (to be seen in Section 3.5), we consider only the final states with charged leptons, due to their unique flavor-nonconserving signature. Results for the case $Cv^2/\Lambda^2 = 10^{-2}$ are shown in Table 3.1 in units of ab^{-1}. For a linear collider with $1\,\text{ab}^{-1}$ of data, these numbers can be interpreted as numbers of events.

3.5 Limits on Operator Coefficients

Precision electroweak data constrains the magnitude of many of the $C_6^j v^2/\Lambda^2$ to be considerably smaller than the 10^{-2} reference value used in Section 3.4. Constraints on a subset of the Class B operator coefficients have been obtained using data from LEP Z^0-pole data [91] and from a wider array of precision electroweak observables that includes studies at LEP2 and low-energy experiments [92]. Both analyses relied on the assumption of $\text{U}(3)^5$ symmetry and [92] performed fits to EWPO including the effects of more than one operator simultaneously.

Here, we update these earlier analyses in a way that focuses on the Class B and Class C operators with the potentially largest effects in Higgs production. For the Class B case, these operators are $\mathcal{O}_{VR,\,ee}$, $\mathcal{O}_{VL,\,ee}$, and $\mathcal{O}_{VL\tau,\,ee}$. For the Class C operators, the direct experimental limits on the coefficient of $\mathcal{O}_{\tilde{V},\,AB}$ are weaker than our reference value of 10^{-2}. Since the effect of this operator is quadratic in the corresponding coefficient, any significant increase in its value could lead to a several percent effect in the missing energy channel. We discuss the direct experimental and indirect constraints on these operators below.

In order to obtain constraints on $\mathcal{O}_{VR,\,ee}$, $\mathcal{O}_{VL,\,ee}$, and $\mathcal{O}_{VL\tau,\,ee}$, we have performed a fit to EWPO using the GAPP routine [104]. The precision observables included in this fit include the data collected from Z^0 pole studies at LEP and SLD and a variety of low-energy precision observables, including cesium atomic parity violation [105], parity-violating Møller scattering [106], elastic neutrino-electron scattering [107], and deep inelastic neutrino-nucleus scattering [108] (for a complete list of EWPO used, see [1]). We have used the value 171.4 ± 2.1 GeV given in [109] for M_t.

For each operator, we derive bounds on the corresponding $C_6^j v^2/\Lambda^2$ by including both the direct contributions to a given observable as well as indirect effects that enter through modifications of the SM input parameters. The $\mathcal{O}_{VL\tau,\,ee}$, for example, contains both neutral and charged current components. The neutral current component modifies the coupling of LH electrons to the Z^0 and enters all e^+e^- annihilation observables, as well as those involving low-energy parity violating processes. The charged-current component contributes to the amplitude for muon decay. Inclusion of the latter contribution modifies the value of the Fermi constant, G_μ, extracted from the experimental muon lifetime and used to normalize all electroweak amplitudes in the SM. It also indirectly affects the value of $\sin^2\hat{\theta}_W(M_Z)$ that is a derived quantity in the SM given G_μ, α, and M_Z as inputs.

Our procedure differs from that followed by [91] and [92] in a few respects. First, we do not assume a $\mathrm{U}(3)^5$ symmetry that relates operators involving different fermion generations. For example, $\mathcal{O}_{VR,\,ee}$ and $\mathcal{O}_{VR,\,\mu\mu}$ are treated as distinct. Although it is quite reasonable to assume that flavor-dependent effects from physics above the scale

Table 3.2: Bounds on coefficents C_6^j of the $n = 6$ leptonic operators obtained from a fit to the electroweak precision observables (EWPO). The first column lists the operator. The second column gives the result for $C_6^j v^2/\Lambda^2$ obtained from the fit to all EWPO using the GAPP routine [104]. The third column gives the 95% C.L. range on $C_6^j v^2/\Lambda^2$, while the last column gives the corresponding fit values for the Higgs mass, m_H.

Operator	$C_6^j v^2/\Lambda^2$	95% C.L. range	m_H
$O_{VR,ee}$	-0.00037 ± 0.00041	$-0.0012, \rightarrow 0.00044$	72^{+35}_{-24} GeV
$O_{VL,ee}$	0.00053 ± 0.00035	$-0.00015 \rightarrow 0.0012$	95^{+38}_{-28} GeV
$O_{VL\tau,ee}$	0.00039 ± 0.00039	$-0.00036 \rightarrow 0.0011$	90^{+36}_{-26} GeV

Λ are determined by Yukawa interactions (as in models with minimal flavor violation) and are, thus, suppressed, we will not make that assumption here. Second, the fits performed in [91] and [92] allowed for the simultaneous contribution from multiple effective operators and were correspondingly performed for a fixed value of m_H. Here, we instead include the effect of only one operator and allow the value of m_H to remain a fit parameter.

The results for the three most important Class B operators are given in Table 3.2, where we show the 1σ results and 95% C.L. ranges for the $C_6^j v^2/\Lambda^2$ in the second and third columns, respectively. In the last column, we give the fit results for m_H; for comparison, an SM fit, with the C_6^j set to 0, gives $m_H = 84 + 33 - 24$ GeV. We find that inclusion of the operator containing e_R fields tends to lower the best fit value for m_H, although it still falls within 2σ of the direct search lower bound, $m_H = 114.4$ GeV. In contrast, the two operators containing first generation lepton doublet fields increases the best fit value for m_H. We also observe that the constraints given in Table 3.2 are somewhat weaker than those obtained in [92], presumably because we have not invoked a $U(3)^5$ symmetry and have allowed the value of m_H to vary[7]. The results of our fit—together with the analysis of Section 3.4—thus indicate the largest possible effects that one might anticipate for Class B operators.

We have also checked that EWPO do not allow the $|C_6^j v^2/\Lambda^2|$ to be larger than 10^{-2} for the other flavor-conserving Class B operators by considering the Z^0 pole

[7]In the notation of [92], the operators $\mathcal{O}_{VR,\,ee}$, $\mathcal{O}_{VL,\,ee}$, and $\mathcal{O}_{VL\tau,\,ee}$ correspond to $\mathcal{O}_{he}$, $\mathcal{O}^s_{h\ell}$, and $\mathcal{O}^t_{h\ell}$ when a $U(3)^5$ symmetry is assumed.

observables alone and comparing SM predictions for a range of m_H with the results obtained from LEP and SLD. To this end, we obtain the SM predictions using ZFITTER [110], [111], which requires input values for M_Z, M_t, m_H, $\alpha_s(M_Z)$, and $\Delta\alpha^{(5)}_{had}$. We take the following for our ZFITTER inputs:

$$\begin{aligned} M_Z &= 91.1876 \pm 0.0021\,\text{GeV}\,[1] \\ M_t &= 171.4 \pm 2.1\,\text{GeV}\,[109] \\ m_H &= 200 \pm 100\,\text{GeV} \\ \alpha_s(M_Z) &= 0.1176 \pm 0.002\,[1] \\ \Delta\alpha^{(5)}_{had}(\alpha_s(M_Z) = 0.1176) &= 0.02772 \pm 0.0002 \end{aligned} \tag{3.4}$$

where the value for $\Delta\alpha^{(5)}_{had}$ is a linear interpolation of points given in [112]. The range on m_H is chosen to be (possibly artificially) large to accomodate any possibility that the current upper bounds on m_H could be evaded with the addition of the operators $\mathcal{O}_{6,j}$. The authors of [91] find, for a particular Higgs mass, ranges of the operator coefficients for which $\chi^2 - \chi^2_{min} < 3.85$, where χ^2_{min} is the χ^2 of the SM fit with the operator coefficients set to zero. They find values of the coefficients of $\mathcal{O}_{VR}$ and $\mathcal{O}_{VL\tau}$ which satisfy this criterion for values of m_H as high as 300 GeV. Even when we include the error for this broad range of Higgs mass, we still find limits on the operator coefficients that are tighter than our reference value of 10^{-2}.

These yield the following predictions for the SM observables:

$$\begin{aligned} \Gamma(Z \to \text{inv}) &= 501.399 + 0.216 - 0.201\,\text{MeV} \\ \Gamma(Z \to e^+e^-) &= 83.932 + 0.053 - 0.044\,\text{MeV} \\ \Gamma(Z \to \mu^+\mu^-) &= 83.932 + 0.053 - 0.044\,\text{MeV} \\ \Gamma(Z \to \tau^+\tau^-) &= 83.742 + 0.053 - 0.044\,\text{MeV}. \end{aligned}$$

The errors on these values were obtained by separately computing the errors due to the uncertainties on the input parameters given in Eqs. (3.4) and adding them in

quadrature. The asymmetry in the errors is due to the dependence of the results on $\ln m_H$.

These predictions are to be compared with the experimental values for the Z widths and branching fractions [1]:

$$\begin{aligned}
\Gamma(Z \to \text{inv}) &= 499.0 \pm 1.5\,\text{MeV} \\
\Gamma(Z \to e^+e^-) &= 83.91 \pm 0.12\,\text{MeV} \\
\Gamma(Z \to \mu^+\mu^-) &= 83.99 \pm 0.18\,\text{MeV} \\
\Gamma(Z \to \tau^+\tau^-) &= 84.08 \pm 0.22\,\text{MeV} \\
BR(Z \to e^\pm\mu^\mp) &= < 1.7 \times 10^{-6}\,\text{at}\,95\%\,\text{CL} \\
BR(Z \to e^\pm\tau^\mp) &= < 9.8 \times 10^{-6}\,\text{at}\,95\%\,\text{CL}.
\end{aligned}$$

The largest source of theoretical error in the SM predictions, as well as the asymmetry in the theoretical error, arises from the range taken for m_H. However, the experimental error dominates over the theoretical error for all of the above observables. The resulting bounds on the Cv^2/Λ^2 for the Class B operators are given in Table 3.3. We do not include bounds on the $\mathcal{O}_{VR,ee}$, $\mathcal{O}_{VL,ee}$, and $\mathcal{O}_{VL\tau,ee}$ operators in this table because the GAPP fit provides significantly tighter limits than using the Z partial widths alone.

From the limits on the branching fractions of the Z to $e^\pm\mu^\mp$ and $e^\pm\tau^\mp$, we can deduce limits on the coefficients for $\mathcal{O}_{VR,AB}$, $\mathcal{O}_{VL,AB}$, and $\mathcal{O}_{VL\tau,AB}$, where $A \neq B$ and A or $B = e$. We obtain

$$\begin{aligned}
\left|\frac{C_{e\mu}v^2}{\Lambda^2}\right| &< 0.0071 \\
\left|\frac{C_{e\tau}v^2}{\Lambda^2}\right| &< 0.017
\end{aligned} \tag{3.5}$$

at 95% CL for all three operators. As these coefficients enter into the cross-sections for these processes quadratically, we can see from Table 3.1 that these limits allow, for example, as many as ~ 80 $He^\pm\tau^\mp$ events for a Higgs in the low-mass region at

Table 3.3: 95% CL intervals on the coefficents C_6^j of the 6D leptonic operators, multiplied by v^2/Λ^2. In the case of $\mathcal{O}_{\nu_R,AB}$, the limit is instead on $\sum_{A,B}\left|C_{\nu_R}^{AB}\right|^2 v^4/\Lambda^4$.

Operator	$Min(\frac{C^j v^2}{\Lambda^2})$	$Max(\frac{C^j v^2}{\Lambda^2})$
$\mathcal{O}_{VR,\mu\mu}$	-0.0027	0.0020
$\mathcal{O}_{VR,\tau\tau}$	-0.0050	0.0007
$\mathcal{O}_{VR,e\mu}$	-0.0071	0.0071
$\mathcal{O}_{VR,e\tau}$	-0.017	0.017
$\mathcal{O}_{VL,\mu\mu}$	-0.0017	0.0023
$\mathcal{O}_{VL,\tau\tau}$	-0.0006	0.0043
$\mathcal{O}_{VL,e\mu}$	-0.0071	0.0071
$\mathcal{O}_{VL,e\tau}$	-0.017	0.017
$\mathcal{O}_{VL\tau,\mu\mu}$	-0.0039	0.0054
$\mathcal{O}_{VL\tau,\tau\tau}$	-0.0006	0.0043
$\mathcal{O}_{VL\tau,e\mu}$	-0.0071	0.0071
$\mathcal{O}_{VL\tau,e\tau}$	-0.017	0.017
$\mathcal{O}_{\nu_R,AB}$		$< .0068$

a linear collider with $\sqrt{s} = 1$ TeV. It will be interesting to explore the feasibility of observing these events at a linear collider.

Some, but not all, of the Class C operators are also constrained by EWPO. To constrain $C_{V\nu,AB}$, we consider the contribution of $\mathcal{O}_{V\nu,AB}$ to the invisible width of the Z boson, Γ_{inv}. Although the measured value of Γ_{inv} disagrees slightly with the SM prediction (the experimental value is 1.6σ below the SM expectation), $\mathcal{O}_{V\nu,AB}$ cannot explain this small discrepancy, as it does not interfere with the SM process and can only increase the cross-section for $Z \to \nu\bar{\nu}$. We calculate the limit on this operator using the procedure for obtaining one-sided confidence level intervals given in [113].

For the remaining operators, all of which contain ν_R, we consider first direct experimental constraints. For example, the operator $\mathcal{O}_{\tilde{V},eB}$ also contributes to the Michel spectrum for the decay of polarized muons. From the recent global analysis of muon decay measurements reported in [67] we obtain

$$\left|C_{\tilde{V},eB} v^2/\Lambda^2\right| \leq 0.208 \tag{3.6}$$

at 90 % C.L. In contrast to the situation with the Class B operators and $\mathcal{O}_{V\nu,AB}$, the

direct constraints on $\mathcal{O}_{\tilde{V},eB}$ are considerably weaker than our benchmark 10^{-2} value for $C_6^j v^2/\Lambda^2$. Considerably more stringent expectations can be obtained by observing that $\mathcal{O}_{\tilde{V},eB}$ contributes to the $n = 6$ neutrino mass operator $\mathcal{O}^{\nu}_{M,\,AB}$ through radiative corrections. A complete renormalization group analysis of the mixing between these operators was carried out in [38]. In order to avoid "unnatural" fine tuning, the radiative contributions to the neutrino mass matrix element m_ν^{AB} due to $\mathcal{O}_{V\nu,AB}$ cannot be substantially larger than the scale of neutrino mass itself. Using an upper bound of 1 eV for this scale we obtain the following naturalness bound on $C_{\tilde{V},eB}v^2/\Lambda^2$

$$\left|\frac{C_{\tilde{V},eB}v^2}{\Lambda^2}\ln\frac{v}{\Lambda}\right| < (0.5-3)\times 10^{-3} \tag{3.7}$$

where the range on $C_{\tilde{V},eB}$ corresponds to $114\,\mathrm{GeV} < m_H < 185\,\mathrm{GeV}$. The latter affects the renormalization group analysis since the entries in the anomalous dimension matrix depend on the Higgs boson quartic self coupling, $\lambda = m_H^2/2v^2$.

The coefficients of the magnetic moment operators are bounded by upper limits on neutrino magnetic moments that range from 10^{-10} to 10^{-12} Bohr magnetons [82, 83, 84, 85, 86, 87]. Taking the upper limit of these bounds implies that $|C_{W,AB}v^2/\Lambda^2|$ and $|C_{B,AB}v^2/\Lambda^2|$ are no larger than $\sim 10^{-5}$. Neutrino mass naturalness considerations imply bounds that are roughly four orders of magnitude more stringent than those obtained directly from magnetic moment limits. Either way, the effects of these operators on Higgs production will be unobservable.

3.6 Discussion and Conclusions

The bounds we obtain on the operator coefficients generally satisfy $|Cv^2/\Lambda^2| < 10^{-2}$, implying smaller corrections to the Higgs production cross-sections than those given in Figs. 3.5-3.9, for which we have used $Cv^2/\Lambda^2 = 10^{-2}$. Nevertheless, comparing the bounds on $|Cv^2/\Lambda^2|$ for $\mathcal{O}_{VR,ee}$, $\mathcal{O}_{VL,ee}$, and $\mathcal{O}_{VL\tau,ee}$ with the results in Figs. 3.5, 3.7, and 3.8, we see that the interference with the SM HZ process can be substantial in the $Hf\bar{f}$ channel with $f = \mu$, τ, or q, with corrections of more than 5% (20%) allowed

for $\sqrt{s} = 500$ GeV (1 TeV). The relative impact of these operators on the He^+e^- and $H + \not{E}$ channels is considerably smaller, since the SM cross-section receives large WWF and ZZF contributions. Additionally, we have checked the non-interference contributions of these operators and find that, for $|Cv^2/\Lambda^2| = 10^{-3}$ (toward the upper end of the 95% CL range) the non-interference terms can contribute an additional 3% to the $Hf\bar{f}$ cross-section for $\sqrt{s} = 1$ TeV. The contributions of the non-interference terms to the $Hf\bar{f}$ channel at $\sqrt{s} = 500$ GeV and to the $H + \not{E}$ and He^+e^- channels at either $\sqrt{s}$ are all $< 1\%$.

Conversely, despite the less stringent limits on their coefficients, the operators $\mathcal{O}_{VR,AA}$, $\mathcal{O}_{VL,AA}$, and $\mathcal{O}_{VL\tau,AA}$ for $A = \mu$, τ, or q cannot generate significant corrections to the $HA\bar{A}$ production cross-section, due to the kinematic suppression of the corresponding interference amplitude relative to SM HZ.

In the case of the Class C operators, which contribute only to the $H + \not{E}$ channel, the magnitude of possible corrections is generally smaller than 10^{-3} of the SM cross-section, assuming $Cv^2/\Lambda^2 = 10^{-2}$. Amplitudes containing these operators do not interfere with SM amplitudes as they contain RH neutrino states, so the quadratic dependence of their contribution to the cross-section on the operator coefficients can lead to considerable suppression. From our analysis of the limits in Section 3.5, we conclude that for $\mathcal{O}_{V\nu_R,AB}$, whose coefficient is constrained by the invisible width of the Z^0, the possible effect is negligible. A similar conclusion applies to $\mathcal{O}_W$ and $\mathcal{O}_B$, which are constrained by limits on neutrino magnetic moments. For the operator $\mathcal{O}_{\tilde{V},eB}$, the constraint on the coefficient implied from the μ-decay Michel spectrum is more than an order of magnitude weaker than assumed in obtaining Fig. 3.9, and would allow the corresponding correction to the missing energy channel to be of order 10% or more (recall that the dependence on the coefficient is quadratic). On the other hand, the bound obtained from neutrino mass naturalness considerations is substantially smaller than $|Cv^2/\Lambda^2| = 10^{-2}$, suggesting an unobservable contribution from this operator to the $H + \not{E}$ cross-section. Thus, the observation of a deviation in this channel without similar deviations in the $Hq\bar{q}$ and $H\ell\bar{\ell}$ channels—though unlikely—would imply the presence of fine tuning in order to avoid unacceptably

large radiative contributions to neutrino mass.

Summarizing the situation more broadly, we find that there exists considerably less room for effects on Higgs production from higher dimension operators containing fermions than from purely bosonic operators. Constraints from EWPO generally imply $|Cv^2/\Lambda^2| << 10^{-2}$. The impact of this suppression can be overcome only in channels that are dominated by SM HZ due to the absence of an off-shell Z^0-boson propagator in amplitudes containing any of the operators $\mathcal{O}_{VR,ee}$, $\mathcal{O}_{VL,ee}$, and $\mathcal{O}_{VL\tau,ee}$. In contrast, purely bosonic operators, such as $\partial^\mu(\phi^\dagger\phi)\partial_\mu(\phi^\dagger\phi)$, can lead to potentially significant deviations in a variety of channels simultaneously, since (a) they affect the couplings of the Higgs to gauge bosons and (b) the constraints from EWPO are weak [51]. A comprehensive study of Higgs production in a variety of channels at a linear collider would allow one to disentangle possible effects from different classes of effective operators, thereby providing new clues about physics at high scales[8].

[8]Studies of polarization observables or angular distributions may also allow one to distinguish the effects of different effective operators, along the lines suggested in [114]. We thank V. Barger for bringing this possibility to our attention.

Chapter 4

Gravitational Perturbations of a Six-Dimensional Self-Tuning Model

In this chapter, we switch gears from model-independent analyses to studying a specific model of extra dimensions, originally proposed in [54], which is an interesting approach to understanding the cosmological constant problem. This model has two extra dimensions, compactified into a sphere, as well as a bulk magnetic field F_{ij} and a bulk cosmological constant Λ, which must be fine-tuned against each other in order that a four-dimensional observer would see a cosmological constant of zero. When two branes, each with tension f^4, are added to the model (one at each pole), a new flat-space solution can be found where the 2-sphere has a deficit angle which depends on f^4; however, the relation between F_{ij} and Λ is unchanged. This led to the hope that this model could be self-tuning: that, once F_{ij} and Λ were fine-tuned against one another, the cosmological constant seen by a four-dimensional observer would be zero, regardless of any changes that might occur in the brane tension.

This possibility raises an interesting question, however; it might be expected that the model's ability to self-tune by adjusting the deficit angle would correspond to a massless scalar mode in the perturbed Einstein's Equations. As lunar laser-ranging measurements [115, 60] and measurements of the frequency shift of radio signals to and from the Cassini spacecraft [61] very tightly constrain scalar-tensor theories of gravity, the existence of a scalar mode would make this model very strongly disfavored.

Our analysis, described in this chapter, was to look for such modes. Surprisingly,

as will be shown below, no such scalar modes were found. While we were thus unable to rule out this model, we concluded that perhaps the hoped-for self-tuning property of this model did not, in fact, exist.

The content of this chapter, with small modifications, is taken from [62].

4.1 Introduction

There has been much speculation on the possibility that the Standard Model fields are confined on a four-dimensional brane in a higher-dimensional universe [55, 56, 57, 58, 59]. The usual cosmological constant problem is reformulated in these theories, since in general the cosmological constant in the four dimensional effective theory receives contributions from both bulk physics and from brane physics. The cosmological problem in these models is balancing the bulk terms against the vacuum energy on the brane to produce the very small value seen in nature.

A general class of five-dimensional models [116, 117] were introduced to partially resolve this problem. Instead of canceling bulk terms against brane terms, these models have the interesting feature that flat space solutions always exist for arbitrary values of the tension on the brane. This is a big improvement, since for these class of models there is a hope that the cosmological constant problem could be immune to phase transitions on the brane, although this has not been demonstrated.

It has been recognized that six-dimensional brane world models might be more promising for the cosmological constant problem, due to the co-dimension-two nature of the geometry [118, 119, 120, 121, 122, 123]. As might be expected by locality, a three brane with arbitrary tension in six-dimensional flat space does not cause the space to inflate, but just introduces a conical singularity. But as such a model does not lead to four-dimensional Einstein gravity, one must compactify the transverse space.

An interesting co-dimension-two spherical compactification was originally considered by Sundrum [121, 122], and modified by Carroll and Guica [54] and also by Navarro [124]. In their model, a fine-tuning of bulk parameters is required to obtain

a small four-dimensional cosmological constant. What is intriguing though, is that this fine tuning is independent of the tension on the brane. With non-vanishing brane tension the bulk geometry is still locally a sphere, but globally it has a conical deficit angle. Pictorially, a "banana peel" has been removed.

A generic difficulty with the five-dimensional models was that self-tuning required a curvature singularity in the bulk [125, 126]. Resolving the singularity by introducing another brane in the bulk reintroduces a fine-tuning of the brane tensions [127]. Naively the six–dimensional model may be an improvement on the five-dimensional self-tuning models, since here the curvature singularities are conical and perhaps less severe. Still, this may be too much. [128] finds that in geometries with conical singularities it is inconsistent to add anything other than tension to the brane. Since we would like to also have stars and dogs on the brane, this is clearly problematic. It is unclear though whether this is an artifact of treating the brane as infinitely thin[1], and it would be interesting to see whether higher dimension operators on the brane could overcome this obstacle[2].

In this chapter we will not dispel this concern. Rather, we address an independent issue, which is whether this six-dimensional model leads to a scalar-tensor theory of gravity at low energies. Given the presupposition of a self-tuning mechanism, one might expect such a mode is necessary, for example, to self-tune a change in the brane tension that is much smaller than the compactification scale.

As is well known, gravitational couplings of a scalar admixture to gravity are strongly constrained by measurements [115, 60] of the Nordtvedt effect [131, 132, 133]. Other phenomenological constraints could be obtained from cosmology, for here parameters in the four-dimensional effective theory depend on the brane tension, which probably had a cosmological history [134].

Our main result is that while we do find massless scalars allowed by the bulk equations of motion, these are all eliminated by the boundary conditions. Our analysis can also be extended to exclude light scalars whose mass vanishes in the limit that

[1] Finite thickness co-dimension–2 models have been discussed in [129, 130].

[2] [128] did find that adding the Gauss-Bonnet operator in the bulk could lead to Einstein gravity with arbitrary sources.

the tension goes to zero. To linear order in perturbation theory then, this model does not have any phenomenological difficulties of this sort. Our results support the conclusions of [135], but we improve on their work since here we are able to obtain all of our results analytically, without having to resort to a numerical analysis.

If this model does have a self-tuning mechanism, then the absence of any massless scalars does raise a puzzle though, for there is no light scalar to adjust a change in the brane tension. If this model does in fact have a self-tuning mechanism, then our results surprisingly suggest that by default, it is the collective motion of many massive Kaluza-Klein states that is responsible for canceling a change in the tension.

But there is another reason to doubt whether their model has a self-tuning mechanism. For here the deficit angle is an integration parameter that may be chosen to satisfy the boundary conditions after assuming a four-dimensional flat space ansatz. However, one might be worried that this feature may not be sufficient in order realize the self-tuning. We elaborate on this in Section 4.

The content of this chapter is as follows. In Section 2, we briefly review the key features of the model. In Section 3.1, we determine Einstein's equations to linear order and discuss the appropriate gauge fixing. Here there is a subtlety due to a brane bending mode, and we discuss how we gauge fix this mode. Then we present our solutions for the most general massless scalar modes that could couple to matter on the brane. In Section 3.2 we discuss the boundary conditions. After imposing these conditions, none of our zero modes survive. Section 4 reconsiders the self-tuning feature of this model. Section 5 contains some concluding remarks.

A few notes on notation are in order. We will use G_{AB} to denote the full 6D metric, Greek indices for the non-compact four dimensions, and Roman letters for components of tensors in the internal directions.

4.2 The Unperturbed Model

The authors of [54] and [124] consider a six-dimensional model with two dimensions compact. The bulk geometry has the topology of a sphere with metric

$$ds^2 = r^2 g_{ij} dx^i dx^j = r^2[d\theta^2 + \beta^2 \sin^2\theta d\alpha^2] \tag{4.1}$$

and α has period 2π.

The field content in the bulk is six-dimensional gravity together with a $U(1)$ gauge field. The field strength for the gauge field is non-vanishing on the sphere,

$$F_{ij} = \sqrt{G^{(2)}}\epsilon_{ij} B \ , \tag{4.2}$$

with $\epsilon_{\theta\phi} \equiv 1$. The corresponding flux

$$\Phi = \int d^2x \sqrt{G^{(2)}} \epsilon^{ij} F_{ij} \tag{4.3}$$

is conserved.

There is also a bulk cosmological constant Λ. Obtaining a static solution requires

$$\Lambda = B^2/2 \tag{4.4}$$

which is the usual cosmological constant problem. The radius of the sphere is

$$r = (\kappa B)^{-1} \tag{4.5}$$

where κ^2 is the six-dimensional Newton's constant. What is intriguing about this model is that if we add a brane at the north and south poles ($\theta = \theta^i$), each with tension f^4, corresponding to a stress tensor

$$T_{\mu\nu} = -g_{\mu\nu} \frac{f^4}{2\pi} \frac{\sqrt{g^{(4)}}}{\sqrt{G^{(6)}}} \sum_i \delta(\theta - \theta^i) \ , \tag{4.6}$$

a new static solution is obtained without any additional fine tuning. The new geometry is still locally a sphere, but now there is a deficit angle

$$\gamma = \kappa^2 f^4 \tag{4.7}$$

corresponding to a local change in curvature at the locations of the branes,

$$R_{ij} = g_{ij} + g_{ij}\frac{\gamma}{\beta}\sum_i \frac{\delta(\theta - \theta^i)}{2\pi \sin\theta} \ . \tag{4.8}$$

In terms of the parameters above,

$$\beta = 1 - \frac{\gamma}{2\pi} \ . \tag{4.9}$$

It is transparent that the geometry is locally still a sphere, since we may rescale α so that

$$ds^2 = r^2[d\theta^2 + \sin^2\theta d\phi^2] \tag{4.10}$$

but now $0 \leq \phi \leq 2\pi\beta$. This coordinate system is a physically convenient choice for the linear perturbation analysis, since all the effect of the tension and deficit angle is put into the boundary.

With a non-vanishing tension, the area of the sphere is smaller due to the deficit angle. As a result, the magnetic flux depends on the tension. If a quantization condition is imposed on the flux, then the self-tuning feature of this model would no longer work, for then the cancellation of bulk parameters needed to obtain a static solution would depend on the tension [136, 137, 138].

To avoid this conclusion we will assume that there is no quantization condition. This requires us to assume that there are no electric sources for the bulk $U(1)$ gauge field[3]. Since the Standard Model fields are not charged under this gauge group, this is not necessarily a phenomenological problem.

[3]This assumption does not affect the stability analysis.

4.3 Linear Analysis

4.3.1 Gauge Fixing and Perturbed Equations

A general perturbation of the background metric (4.10) is given by

$$\begin{aligned} ds^2 &= (\eta_{\mu\nu} + h_{\mu\nu})dx^\mu dx^\nu + 2h_{\mu\theta}dx^\mu d\theta + 2h_{\mu\phi}dx^\mu d\phi \\ &\quad +(1 + h_{\theta\theta})d\theta^2 + 2h_{\theta\phi}d\theta d\phi + \sin^2\theta(1 + \tilde{h}_{\phi\phi})d\phi^2 \ . \end{aligned} \tag{4.11}$$

Here we work in units with $r = 1$. For non-zero tension there are curvature singularities at $\theta = 0$ and π. Then $0 \leq \phi \leq 2\pi\beta$. When the tension vanishes, there are coordinate singularities at these points.

A convenient gauge choice would be Gaussian Normal-like gauge conditions in the bulk. These are

$$h_{\theta\mu} = h_{\theta\theta} = \partial^\mu h_{\mu\phi} = 0 \ , \tag{4.12}$$

providing six conditions.

There is an important subtlety in choosing this gauge though, which we now discuss. In the end we will choose a gauge that is very similar to this one.

To set $h^{new}_{\theta\theta} = 0$ one chooses a gauge parameter

$$\epsilon_\theta(x, \theta) = -\frac{1}{2}\int_0^\theta d\theta' h^{old}_{\theta\theta}(x, \theta') \ . \tag{4.13}$$

The problem with this gauge transformation is with the location of the boundaries. In the gauge with $h_{\theta\theta} = 0$, the brane at the north pole is located at $\theta = 0$, but the brane at the south pole is now located at $\overline{\theta} = \pi + \epsilon_\theta(x, \pi)$, or

$$\overline{\theta} = \pi - F(x)\pi/2 \tag{4.14}$$

in general (F is defined by these two equations). Imposing boundary conditions at the location of the south pole brane is technically too subtle in this gauge.

Since F represents a perturbation that cannot be gauged away, it is more conve-

nient to put it in the metric rather than the location of the boundary. This is done by choosing a slightly different gauge parameter,

$$\epsilon_\theta(x,\theta) = -\frac{1}{2}\int_0^\theta d\theta' h^{old}_{\theta\theta}(x,\theta') + \theta F(x)/2 \tag{4.15}$$

which keeps the branes located at 0 and π. The price we pay is that we cannot completely gauge $h_{\theta\theta}$ away, for in this gauge $h^{new}_{\theta\theta} = F(x)$.

We use the $U(1)$ gauge invariance to set

$$\partial^\mu a_\mu = 0 \ . \tag{4.16}$$

This together with

$$h_{\theta\mu} = \partial^\mu h_{\mu\phi} = 0 \tag{4.17}$$

and

$$h_{\theta\theta}(\theta, x) = F(x) \tag{4.18}$$

represent our gauge conditions.

We search for massless scalar perturbations only, since only these lead to possibly dangerous long-distance deviations from Einstein gravity.

In addition, we focus on scalar perturbations that are independent of the angular coordinate ϕ. The reason is that only ϕ-independent scalar perturbations couple to matter on the brane, either through kinetic mixing with the graviton or because of a non-vanishing wavefunction at the brane locations. Perturbations with non-trivial ϕ dependence only "see" the brane tension through a change in their periodicity, and will therefore still vanish at the location of the branes.

All this gauge fixing leaves seven scalar perturbations,

$$\begin{aligned} ds^2 &= \left(\eta_{\mu\nu} + \partial_\mu\partial_\nu\lambda + \frac{1}{4}\eta_{\mu\nu}h_{(4)}\right) dx^\mu dx^\nu \\ &\quad + (1+F)d\theta^2 + 2h_{\theta\phi}d\theta d\phi + \sin^2\theta(1+\tilde{h}_{\phi\phi})d\phi^2 \end{aligned} \tag{4.19}$$

and $A = a_\theta d\theta + a_\phi d\phi$ with field strengths $f_{AB} = \partial_A a_B - \partial_B a_A$.

Next, Einstein's equations

$$E_{AB} = \kappa^2 T_{AB} \tag{4.20}$$

in units with $r_0 = 1$ are obtained. Focusing on ϕ-independent perturbations, the linearized Einstein equations in the bulk and in the gauges (4.16)–(4.18) are given by

$$\begin{aligned}(\mu\nu): \quad 0 \;=\; & -\frac{1}{2}(\Box + \partial_\theta^2 + \cot\theta\partial_\theta)\left(h_{\mu\nu} - \eta_{\mu\nu}h_{(4)}\right) - \frac{1}{2}\eta_{\mu\nu}\partial^\rho\partial^\sigma h_{\rho\sigma} \\ & + \frac{1}{2}\eta_{\mu\nu}(\Box\tilde{h}_{\phi\phi} + \Box F + F - \tilde{h}_{\phi\phi}) + \frac{1}{2}\left(\partial_\mu\partial_\rho h^\rho_\nu + (\nu \leftrightarrow \mu)\right) \\ & + \frac{1}{2}\eta_{\mu\nu}\left(\partial_\theta^2\tilde{h}_{\phi\phi} + 2\cot\theta\partial_\theta\tilde{h}_{\phi\phi}\right) \\ & - \frac{1}{2}\partial_\mu\partial_\nu h_{(4)} - \frac{1}{2}\partial_\mu\partial_\nu\tilde{h}_{\phi\phi} - \frac{1}{2}\partial_\mu\partial_\nu F + \eta_{\mu\nu}\frac{\kappa^2 B}{\sin\theta}\partial_\theta a_\phi\end{aligned} \tag{4.21}$$

$$\begin{aligned}(\theta\mu): \quad 0 \;=\; & \partial_\theta\partial^\rho h_{\rho\mu} \\ & + \partial_\mu\left(\cot\theta(F - \tilde{h}_{\phi\phi}) - \partial_\theta h_{(4)} - \partial_\theta\tilde{h}_{\phi\phi} - 2\kappa^2 B\frac{a_\phi}{\sin\theta}\right)\end{aligned} \tag{4.22}$$

$$\begin{aligned}(\phi\mu): \quad 0 \;=\; & -\left(\Box + \partial_\theta^2 - \cot\theta\partial_\theta\right)h_{\phi\mu} \\ & + \partial_\mu\left(\partial_\theta h_{\theta\phi} + \cot\theta h_{\theta\phi} + 2\kappa^2 B\sin\theta a_\theta\right) \\ & - 2\kappa^2 B\sin\theta\partial_\theta a_\mu\end{aligned} \tag{4.23}$$

$$\begin{aligned}(\theta\theta): \quad 0 \;=\; & \Box h_{(4)} - \partial^\mu\partial^\nu h_{\mu\nu} + \Box\tilde{h}_{\phi\phi} + \cot\theta\partial_\theta h_{(4)} + F + \tilde{h}_{\phi\phi} \\ & - 2\kappa^2 B\frac{\partial_\theta a_\phi}{\sin\theta}\end{aligned} \tag{4.24}$$

$$(\theta\theta - \phi\phi): \quad 0 \;=\; \partial_\theta^2 h_{(4)} - \cot\theta\partial_\theta h_{(4)} + \Box F - \Box\tilde{h}_{\phi\phi} \tag{4.25}$$

$$(\theta\phi): \quad 0 \;=\; -\Box h_{\theta\phi}\ . \tag{4.26}$$

The linearized $U(1)$ gauge equations in these gauges are

$$(\mu): \quad 0 \;=\; \left(\Box_{(4)} + \frac{\partial^2}{\partial\theta^2} + \cot\theta\frac{\partial}{\partial\theta}\right)a_\mu - \partial_\mu(\nabla\cdot a) - \frac{B}{\sin\theta}\partial_\theta h_{\mu\phi} \tag{4.27}$$

$$(\theta): \quad 0 \;=\; \Box_{(4)}a_\theta \tag{4.28}$$

$$(\phi): \quad 0 \;=\; \sin\theta\partial_\theta\left(\frac{1}{\sin\theta}\partial_\theta a_\phi\right) + \Box a_\phi - \frac{B}{2}\sin\theta(\partial_\theta\tilde{h}_{\phi\phi} - \partial_\theta h_{(4)}) \tag{4.29}$$

with $\nabla\cdot a = \partial_\theta a_\theta + \cot\theta a_\theta$ in the Lorentz gauge and acting on ϕ independent perturba-

tions, and $\Box = \partial^\mu \partial_\mu$. For massive states, (4.27) together with the gauge choices (4.16) and (4.17) imply $\nabla \cdot a = 0$. These equations in the bulk must be supplemented with boundary conditions imposed at the locations of the conical singularities. Boundary conditions are discussed in the next section.

We emphasize that the equations obtained above are valid for arbitrary brane tension. Due to the choice of parameterization of the background given by (4.10), the effect of the brane tension appears only in the boundary conditions, and for solutions with non-trivial ϕ dependence (which we are not looking at here), in $2\pi\beta$ periodicity conditions.

As may be anticipated by considering the four-dimensional effective potential [121, 122, 139], the radion in this model is massive. It is given by the mode

$$h_{\theta\theta} = \tilde{h}_{\phi\phi} = -\frac{h_{(4)}}{4} = F(x) \ , \tag{4.30}$$

with all other fields vanishing. It has a mass $m^2 = 1/r_0^2$. This result agrees with previous computations [135].

In the remainder of this chapter we focus on massless modes only.

For the zero modes there is, in addition, the usual residual gauge invariances Ω where $\Box\Omega = 0$. Here we have a residual $U(1)$ gauge invariance Λ, and residual diffeomorphism invariances ϵ_ϕ and ϵ_μ only, since ϵ_θ is fixed by our gauge choice. We use Λ and ϵ_ϕ to set the zero modes of of a_μ and $h_{\phi\mu}$ to be purely transverse, and ϵ_μ to set the vector components of the four-dimensional zero mode graviton to zero.

In total there are naively 10 equations for 7 variables. But fortunately not all of these equations are independent. Eq. (4.29) and the trace of (4.22) are derivable from other equations. Eqs. (4.26) and (4.28) are trivial acting on the zero modes we are focusing on. This leaves six non-trivial equations for seven scalar perturbations (but recall that F is pure gauge in the bulk).

Inspecting the equations further, a_θ and $h_{\theta\phi}$ decouple from the other perturba-

tions. Their wavefunctions are fixed by (4.23) and (4.27) to be

$$a_\theta = \frac{c_0(x)}{\sin\theta} \quad , \quad h_{\theta\phi} = 2\kappa^2 B c_0(x)\cot\theta \ . \tag{4.31}$$

Next we proceed to solving the other equations. Eq. (4.25) can be solved immediately to give

$$h_{(4)} = c_1(x) - c_2(x)\cos\theta \ . \tag{4.32}$$

Next use (4.24) to solve for $\tilde{h}_{\phi\phi}$ and substitute this into (4.22) to obtain

$$\frac{\partial^2 a_\phi}{\partial\theta^2} + a_\phi = -\frac{c_2(x)}{8\kappa^2 B}\left(7 - 11\cos^2\theta\right) + \frac{F(x)}{\kappa^2 B}\cos\theta \ . \tag{4.33}$$

This will have two homogeneous solutions and one inhomogeneous solution. Since the sources are independent, we may think of this as four solutions in total. Finally, (4.22) with $\mu \neq \nu$ determines λ in terms of the previous solutions.

The most general solutions to these equations are given by

$$\begin{aligned}
\tilde{h}_{\phi\phi} &= c_3(x) + \frac{5}{6}c_2(x)\cos\theta + 2\kappa^2 B c_4(x)\cot\theta + \theta\cot\theta F(x) \\
a_\phi &= -\frac{c_3(x)}{2\kappa^2 B}\cos\theta + \frac{c_2(x)}{24\kappa^2 B}(1 - 11\cos^2\theta) + c_4(x)\sin\theta \\
&\quad + \frac{F(x)}{2\kappa^2 B}\theta\sin\theta \\
h_{\theta\theta} &= F(x)
\end{aligned} \tag{4.34}$$

together with (4.32).

To summarize, for an arbitrary tension we have found the the most general $\phi-$independent massless scalar perturbation solution to the $U(1)$ and Einstein field equations. Imposing boundary conditions on these solutions is discussed in the next section.

4.3.2 Boundary Conditions

For non-zero tension the locations of the branes are special points on the sphere with curvature singularities. To obtain the boundary conditions for the perturbations at these points we need to inspect the field equations and match the singularities.

It is useful to rewrite the internal metric, including perturbations, as

$$ds^2_{int} = r_0^2\,(1+h_{\theta\theta})\left[d\theta^2 + \beta^2 \sin^2\theta(1+\tilde{h}_{\phi\phi}-h_{\theta\theta})d\alpha^2\right]\ , \tag{4.35}$$

where in a change of notation, $r_0 = (\kappa B)^{-1}$ denotes the unperturbed radius. To linear order in the perturbations this is equivalent to our previous parameterization. Here we are also only focusing on $h_{\theta\theta}$ and $\tilde{h}_{\phi\phi}$, since $h_{\theta\phi}$ decouples and does not couple to brane matter. For long-wavelength perturbations this describes a new background with effective radius

$$r^2 \;=\; r_0^2(1+h_{\theta\theta}) \tag{4.36}$$

and effective deficit angle

$$\tilde{\beta}^2 \;=\; \beta^2(1+\tilde{h}_{\phi\phi}-h_{\theta\theta})\ . \tag{4.37}$$

To obtain first-order terms in the equations of motion with explicit delta-function singularities, which correspond to perturbations without derivatives, we may use (4.8), using (4.9) and substituting for the effective radius (4.36) and effective deficit angle (4.37).

This implies that to linear order there are no singular contributions to the (i,j) Einstein equations. There is however, a singular contribution to the (μ,ν) equation,

given by

$$\begin{aligned} E_{\mu\nu}|_{sing.} &= \sum_i g_{\mu\nu} \frac{1}{\tilde{\beta} r^2} \left[\tilde{\beta} - 1\right] \frac{\delta(\theta - \theta^i)}{\sin\theta} \\ &= \kappa^2 T_{\mu\nu}|_{sing.} \\ &= -\kappa^2 f^4 \sum_i g_{\mu\nu} \frac{\sqrt{g^{(4)}}}{2\pi\sqrt{G^{(6)}}} \delta(\theta - \theta^i) \\ &= -\kappa^2 f^4 \sum_i g_{\mu\nu} \frac{1}{\tilde{\beta} r^2} \frac{\delta(\theta - \theta^i)}{2\pi \sin\theta} \ . \end{aligned} \tag{4.38}$$

Before concluding that these singularities must match, we must check that perturbations involving derivatives cannot contribute additional singularities. To see that they cannot, use the $(\mu\theta)$ equation to solve for $\tilde{h}_{\phi\phi}$ and substitute it into the $(\mu = \nu)$ equation. One finds all the terms cancel identically, except for the singularities appearing in (4.38). Inspecting (4.38), we see that to satisfy the equations of motion requires

$$[\tilde{\beta} - 1]| = -\frac{\kappa^2}{2\pi} f^4 \tag{4.39}$$

or

$$[\tilde{h}_{\phi\phi} - h_{\theta\theta}]| = 0 \tag{4.40}$$

at the location of either brane. This is just the statement that without a change in the tension, a perturbation in the metric cannot change the deficit angle.

To obtain other boundary conditions we must inspect the other field equations.

The $(\theta\theta - \phi\phi)$ metric equation does not contain any curvature singularities. Requiring that the solution is finite gives the boundary condition

$$\partial_\theta h_{(4)}| = 0 \ . \tag{4.41}$$

Finally, to obtain the boundary condition for a_θ, consider spreading the brane out into a ring located at $\theta \sim \epsilon$. Later we will send $\epsilon \to 0$. Inside the ring we have no deficit angle, so all fields are regular at the pole, and therefore $a_\theta \to 0$. The ring does not affect the a_μ gauge equation of motion, so $\nabla \cdot a = 0$ is the a_θ equation both inside

and outside the ring. The only solution inside the ring, consistent with this equation and the boundary condition at the pole, is $a_\theta = 0$. By continuity at the location of the ring, the boundary condition outside the ring is then

$$a_\theta| = 0 \ . \tag{4.42}$$

Eqs. (4.40), (4.41) and (4.42) are our boundary conditions when the tension is non-vanishing.

For vanishing tension, there are stronger constraints than these from requiring that the north and south poles not be special points. This means that our solutions in polar coordinates should have sensible (C) values when expressed in a Cartesian basis local to the poles. This implies that near a pole,

$$h_{\mu\phi} \sim f_{\mu\phi} \sim \tilde{h}_{\phi\phi} - h_{\theta\theta} \sim \theta^2 \ . \tag{4.43}$$

Inspecting the four solutions above, we first note that the normal mode $c_0(x)$ and $c_4(x)$ are too singular to satisfy the boundary conditions. However the linear combination

$$c_3(x) = -\frac{5}{6}c_2(x) \tag{4.44}$$

and the normal mode $F(x)$ both independently satisfy the boundary conditions at $\theta = 0$. Thus there are two independent solutions that satisfy the boundary conditions at $\theta = 0$.

But neither solution satisfies the boundary conditions at $\theta = \pi$. As $\theta \to \pi$, a general combination of these two solutions behaves as

$$\tilde{h}_{\phi\phi} - h_{\theta\theta} \ \ \to \ \ -\frac{5}{3}c_2(x) - F(x) - \frac{\pi}{\sin\theta}F(x) \ . \tag{4.45}$$

The boundary condition implies that the left side should vanish at the boundary, so both $c_2 = F$=0. Thus there are no solutions that satisfy the boundary conditions at both $\theta = 0$ and $\theta = \pi$.

This conclusion is true for arbitrary tension. It is straightforward to repeat the analysis for vanishing tension. The only difference is that the boundary conditions are *stronger*, because of the constraint of regularity. No zero modes therefore exist in this limit either. Thus any light mode with mass that vanishes as the tension is sent to zero is also excluded by our analysis.

4.4 Fine-tuning or Self-tuning?

We return to an issue briefly issue raised in the introduction of this chapter. One might think that the relation (4.7) between the deficit angle and the brane tension does not represent a fine-tuning, since the deficit angle is an integration parameter, not a parameter of the Lagrangian. But a simple four-dimensional counter-example illustrates that the issue is not as straightforward [140].

Consider a four-dimensional theory with a bare cosmological constant Λ_0 and a four-form field strength with value

$$F_{\mu\nu\rho\sigma} = c\epsilon_{\mu\nu\rho\sigma} \tag{4.46}$$

which satisfies the field equations of motion and where c is an integration parameter [141, 142]. The source for gravity in this theory is

$$\Lambda = \Lambda_0 + c^2 \ . \tag{4.47}$$

The integration parameter may be chosen to be $c^2 = -\Lambda_0$, giving a flat space solution. But obviously this is not the only solution, as there is a family of de-Sitter and anti-de-Sitter solutions.

In analogy with this four-form example, does setting the deficit angle—an integration parameter— of the six-dimensional model to be equal to the tension involve a fine-tuning? For recall that it has not been demonstrated that the deficit angle is forced by the equations of motion to be equal to the tension—that only followed from the equations of motion after assuming a flat-space ansatz. For maximally symmetric

space-times, [135] has found that once the bulk cosmological constant is finetuned against the magnetic flux, then de-Sitter or anti-de Sitter solutions along the brane directions are forbidden, and the deficit angle is equal to the tension.

But that still does not completely address the issue. In other words, it isn't clear that a change in the tension is canceled by a change in the deficit angle. If other cosmological solutions exist, for the same tension but other values of the deficit angle, then (4.7) is a fine-tuning, and this model would then be less appealing.

What might these solutions look like?[4] A dynamical change in the tension could lead to a solution that is not maximally symmetric, but instead interpolates between an inflating or generally time-dependent solution near the brane, to a static geometry far from the brane. Far from the brane, the deficit angle would be (approximately) equal to its unperturbed value.

4.5 Conclusions

We have performed a linear perturbation analysis of the model presented in [54] and [124] to search for phenomenologically dangerous massless or approximately massless scalars. After imposing the boundary conditions, we have found that there are no such modes.

If this model does have a self-tuning mechanism, then our results do raise a puzzle. Namely, below the compactification scale the only light modes are the four dimensional graviton, the Standard Model fields, a gravi-vector boson from the residual isometry of the bulk, and a $U(1)$ gauge boson. The latter two do not couple to the tension on the brane and so we can forget about them. The puzzle is that one might have expected that the self-tuning of a small enough change in the brane tension could be understood in the four-dimensional effective theory—but this does not seem likely, since our results show that this model lacks any additional light degree of freedom.

If this is the case here, then in order for this model to be compatible with the observed size or bound on the cosmological constant, we would need $1/r \sim 10^{-3}$ eV

[4]The authors thank Maxim Perelstein for discussions on this point.

[123]. There is an additional puzzle here, if the model does self-tune: from the higher dimensional perspective, it appears that it is the full quantum mechanical tension on the brane that is canceled, not just the high-energy contribution. If this were true, then there would not be a constraint on the size of the internal space arising from vacuum fluctuations of brane localised matter.

Our results suggest that if there is self-tuning, then it must be due to modes no lighter than the compactification scale. A consistent story would then be that the massive states only partially cancel a dynamical change in the tension, down to an amount set by the compactification scale.

Finally, demonstrating that these models do or do not self-tune might be difficult: one would need to find or demonstrate the absence of non-maximally symmetric solutions with an approximately static deficit angle and geometry far from the brane, but with a cosmological geometry near the brane. That is, to follow the cosmological evolution of this system through a phase transition.

Bibliography

[1] W. M. Yao et al. [Particle Data Group], *J. Phys.* **G 33**, 1 (2006).

[2] [ALEPH Collaboration], *Phys. Rept.* **427**, 257 (2006) [arXiv:hep-ex/0509008].

[3] S. P. Martin [arXiv:hep-ph/9709356].

[4] C. Csaki [arXiv:hep-ph/0404096].

[5] F. Feruglio, *Eur. Phys. J.* **C 33**, S114 (2004) [arXiv:hep-ph/0401033].

[6] J. Hewett and M. Spiropulu, *Ann. Rev. Nucl. Part. Sci.* **52**, 397 (2002) [arXiv:hep-ph/0205106].

[7] A. Leike, *Phys. Rept.* **317**, 143 (1999) [arXiv:hep-ph/9805494].

[8] K. Lane [arXiv:hep-ph/0202255].

[9] M. Gell-Mann, P. Ramond, and R. Slansky, In *Supergravity: Proceedings of the supergravity workshop at Stony Brook, September 27-29, 1979.*

[10] T. Yanagida, In *Proceedings of the Workshop on the Baryon Number of the Universe and Unified Theories, Tsukuba, Japan, 13-14 Feb 1979.*

[11] R. N. Mohapatra and G. Senjanovic, *Phys. Rev. Lett.* **44**, 912 (1980).

[12] S. Weinberg, *Phys. Rev. Lett.* **43**, 1566 (1979).

[13] E. J. Copeland, M. Sami, and S. Tsujikawa, *Int. J. Mod. Phys.* **D 15**, 1753 (2006) [arXiv:hep-th/0603057].

[14] N. Straumann, *Mod. Phys. Lett.* **A 21**, 1083 (2006) [arXiv:hep-ph/0604231].

[15] T. Padmanabhan, *Phys. Rept.* **380**, 235 (2003) [arXiv:hep-th/0212290].

[16] R. J. Davis, D. S. Harmer, and K. C. Hoffman, *Phys. Rev. Lett.* **20**, 1205 (1968).

[17] R. D. McKeown and P. Vogel, *Phys. Rept.* **394**, 315 (2004) [arXiv:hep-ph/0402025].

[18] A. Strumia and F. Vissani [arXiv:hep-ph/0606054].

[19] J. Hosaka et al. [Super-Kamkiokande Collaboration], *Phys. Rev.* **D 73**, 112001 (2006) [arXiv:hep-ex/0508053].

[20] B. Aharmim et al. [SNO Collaboration], *Phys. Rev.* **C 72**, 055502 (2005) [arXiv:nucl-ex/0502021].

[21] T. Araki et al. [KamLAND Collaboration], *Phys. Rev. Lett.* **94**, 081801 (2005) [arXiv:hep-ex/0406035].

[22] Q. R. Ahmad et al. [SNO Collaboration], *Phys. Rev. Lett.* **89**, 011301 (2002) [arXiv:nucl-ex/0204008].

[23] Y. Ashie et al. [Super-Kamiokande Collaboration], *Phys. Rev.* **D 71**, 112005 (2005) [arXiv:hep-ex/0501064].

[24] Y. Ashie et al. [Super-Kamiokande Collaboration], *Phys. Rev. Lett.* **93**, 101801 (2004) [arXiv:hep-ex/0404034].

[25] K. Abe et al. [Super-Kamiokande Collaboration], *Phys. Rev. Lett.* **97**, 171801 (2006) [arXiv:hep-ex/0607059].

[26] C. Athanassopoulos et al. [LSND Collaboration], *Phys. Rev. Lett.* **75**, 2650 (1995) [arXiv:nucl-ex/9504002].

[27] C. Athanassopoulos et al. [LSND Collaboration], *Phys. Rev. Lett.* **77**, 3082 (1996) [arXiv:nucl-ex/9605003].

[28] C. Athanassopoulos et al. [LSND Collaboration], *Phys. Rev. Lett.* **81**, 1774 (1998) [arXiv:nucl-ex/9709006].

[29] A. Aguilar et al. [LSND Collaboration], *Phys. Rev.* **D 64**, 112007 (2001) [arXiv:hep-ex/0104049].

[30] A. A. Aguilar-Arevalo et al. [The MiniBooNE Collaboration] [arXiv:0704.1500] [hep-ex].

[31] V. M. Lobashev et al., *Phys. Lett.* **B 460**, 227 (1999).

[32] C. Kraus et al., *Eur. Phys. J.* **C 40**, 447 (2005) [arXiv:hep-ex/0412056].

[33] U. Seljak et al. [SDSS Collaboration], *Phys. Rev.* **D 71**, 103515 (2005) [arXiv:astro-ph/0407372].

[34] L. Michel, *Proc. Roy. Soc. Lond.* **A 63**, 514 (1950)

[35] C. Bouchiat and L. Michel, *Phys. Rev.* **106**, 170 (1957).

[36] J. R. Musser [TWIST Collaboration], *Phys. Rev. Lett.* **94**, 101805 (2005) [arXiv:hep-ex/0409063]

[37] A. Gaponenko et al. [TWIST Collaboration], *Phys. Rev.* **D 71**, 071101 (2005) [arXiv:hep-ex/0410045]

[38] R. J. Erwin, J. Kile, M. J. Ramsey-Musolf, and P. Wang [arXiv:hep-ph/0602240].

[39] R. J. Erwin, M. J. Ramsey-Musolf (in preparation).

[40] P. Herczeg, *Phys. Rev.* **D 34**, 3449 (1986).

[41] R. Barate et al. [LEP Working Group for Higgs boson searches], *Phys. Lett.* **B 565**, 61 (2003) [arXiv:hep-ex/0306033].

[42] [ALEPH Collaboration] [arXiv:hep-ex/0511027].

[43] M. Battaglia and K. Desch [arXiv:hep-ph/0101165].

[44] S. Heinemeyer et al., [arXiv:hep-ph/0511332].

[45] M. D. Hildreth, T. L. Barklow, and D. L. Burke, *Phys. Rev.* **D 49**, 3441 (1994).

[46] S. Heinemeyer, W. Hollik, J. Rosiek, and G. Weiglein, *Eur. Phys. J.* **C 19**, 535 (2001) [arXiv:hep-ph/0102081].

[47] M. Carena, H. E. Haber, H. E. Logan, and S. Mrenna, *Phys. Rev.* **D 65**, 055005 (2002) [Erratum-ibid. D **65**, 099902 (2002)] [arXiv:hep-ph/0106116].

[48] P. K. Das, S. K. Rai, and S. Raychaudhuri, *Phys. Lett.* **B 618**, 221 (2005) [arXiv:hep-ph/0410244].

[49] J. L. Hewett and T. G. Rizzo, *JHEP* **0308**, 028 (2003) [arXiv:hep-ph/0202155].

[50] D. Dominici, B. Grzadkowski, J. F. Gunion, and M. Toharia, *Nucl. Phys.* **B 671**, 243 (2003) [arXiv:hep-ph/0206192].

[51] V. Barger, T. Han, P. Langacker, B. McElrath, and P. Zerwas, *Phys. Rev.* **D 67**, 115001 (2003) [arXiv:hep-ph/0301097].

[52] A. V. Manohar and M. B. Wise, *Phys. Lett.* **B 636**, 107 (2006) [arXiv:hep-ph/0601212].

[53] J. Kile and M. J. Ramsey-Musolf [arXiv:0705.0554] [hep-ph].

[54] S. M. Carroll and M. M. Guica [hep-th/0302067].

[55] N. Arkani-Hamed, S. Dimopoulos, and G. R. Dvali, *Phys. Lett.* **B 429**:263–272 (1998) [hep-ph/9803315].

[56] I. Antoniadis, N. Arkani-Hamed, S. Dimopoulos, and G. R. Dvali, *Phys. Lett.* **B 436**:257–263 (1998) [hep-ph/9804398].

[57] N. Arkani-Hamed, S. Dimopoulos, and G. R. Dvali,*Phys. Rev.* **D 59**:086004 (1999) [hep-ph/9807344].

[58] L. Randall and R. Sundrum, *Phys. Rev. Lett.* **83**:3370–3373 (1999) [hep-ph/9905221].

[59] L. Randall and R. Sundrum, *Phys. Rev. Lett.* **83**:4690–4693 (1999) [hep-th/9906064].

[60] J. G. Williams, S. G. Turyshev, and D. H. Boggs [arXiv:gr-qc/0507083].

[61] B. Bertotti, L. Iess, and P. Tortora, *Nature* **425** (2003) 374.

[62] M. L. Graesser, J. E. Kile, and P. Wang, *Phys. Rev.* **D 70**, 024008 (2004) [arXiv:hep-th/0403074].

[63] T. Kinoshita and A. Sirlin, *Phys. Rev.* **108**, 844 (1957).

[64] N. Danneberg et al., *Phys. Rev. Lett.* **94**, 021802 (2005).

[65] R. Tribble and G. Marshall, *private communication*. See also J. Hu, to appear in *The proceedings of the PANIC05 conference*, Santa Fe, N.M., 2005.

[66] F. Scheck, *Electroweak and Strong Interactions: An Introduction to Theoretical Particle Physics*, Springer Verlag, 1996, p. 282.

[67] C. A. Gagliardi, R. E. Tribble, and N. J. Williams [arXiv:hep-ph/0509069].

[68] G. Prezeau and A. Kurylov, *Phys. Rev. Lett.* **95**, 101802 (2005) [arXiv:hep-ph/0409193].

[69] N. F. Bell, V. Cirigliano, M. J. Ramsey-Musolf, P. Vogel, and M. B. Wise, *Phys. Rev. Lett.* **95**, 151802 (2005) [arXiv:hep-ph/0504134].

[70] S. Davidson, M. Gorbahn, and A. Santamaria, *Phys. Lett.* **B 626**, 151 (2005) [arXiv:hep-ph/0506085].

[71] N. F. Bell, M. Gorchtein, M. J. Ramsey-Musolf, P. Vogel, and P. Wang [arXiv:hep-ph/0606248].

[72] J. Giedt, G. L. Kane, P. Langacker, and B. D. Nelson, *Phys. Rev.* **D 71**, 115013 (2005) [arXiv:hep-th/0502032].

[73] P. Langacker and B. D. Nelson, "String-inspired triplet see-saw from diagonal embedding of SU(2)L in SU(2)A x SU(2)B," *Phys. Rev.* **D 72**, 053013 (2005) [arXiv:hep-ph/0507063].

[74] C. Aalseth et al., [arXiv:hep-ph/0412300].

[75] S. R. Elliott and P. Vogel, *Ann. Rev. Nucl. Part. Sci.* **52**, 115 (2002) [arXiv:hep-ph/0202264].

[76] M. Doi, T. Kotani, and H. Nishiura, *Prog. Theor. Phys.* **114**, 845 (2005) [arXiv:hep-ph/0502136].

[77] C. P. Burgess and D. London, *Phys. Rev.* **D 48**, 4337 (1993) [arXiv:hep-ph/9203216].

[78] S. A. Frolov and A. A. Slavnov, *Phys. Lett.* **B 309**, 344 (1993).

[79] L. F. Abbott, *Nucl. Phys.* **B 185**, 189 (1981).

[80] C. Weinheimer et al., *Phys. Lett.* **B 460**, 219 (1999).

[81] LEP Electroweak Working Group [http: //lepewwg.web.cern.ch/LEPEWWG/].

[82] J. F. Beacom and P. Vogel, *Phys. Rev. Lett.* **83**, 5222 (1999) [arXiv:hep-ph/9907383].

[83] D. W. Liu et al. [Super-Kamiokande Collaboration], *Phys. Rev. Lett.* **93**, 021802 (2004) [arXiv:hep-ex/0402015].

[84] Z. Daraktchieva et al. [MUNU Collaboration], *Phys. Lett.* **B 615**, 153 (2005) [arXiv:hep-ex/0502037].

[85] B. Xin et al. [TEXONO Collaboration], *Phys. Rev.* **D 72**, 012006 (2005) [arXiv:hep-ex/0502001].

[86] P. Sutherland, J. N. Ng, E. Flowers, M. Ruderman, and C. Inman, *Phys. Rev.* **D 13**, 2700 (1976).

[87] G. G. Raffelt, *Phys. Rept.* **320**, 319 (1999).

[88] T. M. Ito and G. Prezeau, *Phys. Rev. Lett.* **94**, 161802 (2005) [arXiv:hep-ph/0410254].

[89] B. Grinstein and M. Trott [arXiv:0704.1505] [hep-ph].

[90] D. Black, T. Han, H. J. He, and M. Sher, *Phys. Rev.* **D 66**, 053002 (2002) [arXiv:hep-ph/0206056].

[91] R. Barbieri and A. Strumia, *Phys. Lett.* **B 462**, 144 (1999) [arXiv:hep-ph/9905281].

[92] Z. Han and W. Skiba, *Phys. Rev.* **D 71**, 075009 (2005) [arXiv:hep-ph/0412166].

[93] G. A. Moortgat-Pick et al. [arXiv:hep-ph/0507011].

[94] T. Han, T. Huang, Z. H. Lin, J. X. Wang, and X. Zhang, *Phys. Rev.* **D 61**, 015006 (2000) [arXiv:hep-ph/9908236].

[95] J. F. Gunion, H. E. Haber, G. L. Kane and S. Dawson, *The Higgs Hunter's Guide*, Westview Press, 2001.

[96] K. Desch and N. Meyer, LC-PHSM-2001-025, In **2nd ECFA/DESY Study 1998-2001* 1694-1704.*

[97] P. Garcia-Abia and W. Lohmann, *Eur. Phys. J. Direct* **C 2**, 2 (2000) [arXiv:hep-ex/9908065].

[98] P. Garcia-Abia, W. Lohmann, and A. Raspereza [arXiv:hep-ex/0505096].

[99] N. Meyer and K. Desch, *Eur. Phys. J.* **C 35**, 171 (2004).

[100] C. N. Leung, S. T. Love, and S. Rao, *Z. Phys.* **C 31**, 433 (1986).

[101] W. Buchmuller and D. Wyler, *Nucl. Phys.* **B 268**, 621 (1986).

[102] A. Pukhov et al. [arXiv:hep-ph/9908288].

[103] A. Pukhov [arXiv:hep-ph/0412191].

[104] J. Erler [arXiv:hep-ph/0005084].

[105] C. S. Wood, S. C. Bennett, D. Cho, B. P. Masterson, J. L. Roberts, C. E. Tanner, and C. E. Wieman, *Science* **275**, 1759 (1997).

[106] P. L. Anthony et al. [SLAC E158 Collaboration], *Phys. Rev. Lett.* **92**, 181602 (2004) [arXiv:hep-ex/0312035].

[107] P. Vilain et al. [CHARM-II Collaboration], *Phys. Lett.* **B 335**, 246 (1994).

[108] G. P. Zeller et al. [NuTeV Collaboration], *Phys. Rev. Lett.* **88**, 091802 (2002) [Erratum-ibid. **90**, 239902 (2003)] [arXiv:hep-ex/0110059].

[109] E. Brubaker et al. [Tevatron Electroweak Working Group] [arXiv:hep-ex/0608032].

[110] D. Y. Bardin, P. Christova, M. Jack, L. Kalinovskaya, A. Olchevski, S. Riemann, and T. Riemann, *Comput. Phys. Commun.* **133**, 229 (2001) [arXiv:hep-ph/9908433].

[111] A. B. Arbuzov et al., *Comput. Phys. Commun.* **174**, 728 (2006) [arXiv:hep-ph/0507146].

[112] J. Erler, *Phys. Rev.* **D 59**, 054008 (1999) [arXiv:hep-ph/9803453].

[113] G. J. Feldman and R. D. Cousins, *Phys. Rev.* **D 57**, 3873 (1998) [arXiv:physics/9711021].

[114] V. D. Barger, K. M. Cheung, A. Djouadi, B. A. Kniehl, and P. M. Zerwas, *Phys. Rev.* **D 49**, 79 (1994) [arXiv:hep-ph/9306270].

[115] K. Hagiwara et al., *Phys. Rev.* **D 66**, 010001–1 (2002)

[116] N. Arkani-Hamed, S. Dimopoulos, N. Kaloper, and R. Sundrum, *Phys. Lett.* **B 480**:193–199 (2000) [hep-th/0001197].

[117] S. Kachru, E. Silverstein, and M. Schulz, *Phys. Rev.* **D 62**:045021 (2000) [hep-th/0001206].

[118] K. Akama, "Pregeometry" in *Lecture Notes in Physics, 176, Gauge Theory and Gravitation, Proceedings, Nara, 1982*, edited by K. Kikkawa, N. Nakanishi, and H. Nariai, Springer-Verlag, 1983, 267–271 [hep-th/0001113].

[119] V.A. Rubakov and M.E. Shaposhnikov, *Phys. Lett.* **B 125**:139,1983

[120] V.A. Rubakov and M.E. Shaposhnikov, *Phys. Lett.* **B 125** :136-138,1983.

[121] R. Sundrum, *Phys. Rev.* **D 59**:085009 (1999) [hep-ph/9805471].

[122] R. Sundrum, *Phys. Rev.* **D 59**:085010 (1999) [hep-ph/9807348].

[123] J-W. Chen, M. A. Luty, and E. Ponton, *JHEP* 0009:012 (2000) [hep-th/0003067].

[124] I. Navarro, *JCAP* **0309**:004 (2003) [hep-th/0302129].

[125] C. Csaki, J. Erlich, C. Grojean, and T. J. Hollowood, *Nucl. Phys.* **B 584**:359–386 (2000) [hep-th/0004133].

[126] P. Binetruy, J.M. Cline and C. Grojean, *Phys. Lett.* **B 489**:403–410 (2000) [hep-th/0007029].

[127] S. Forste, Z. Lalak, S. Lavignac, and H. P. Nilles, *Phys. Lett.* **B 481**:360–364 (2000) [hep-th/0002164].

[128] P. Bostock, R. Gregory, I. Navarro, and J. Santiago, [hep-th/0311074].

[129] M. Giovannini, *Phys. Rev.* **D 66**:044016 (2002).

[130] M. Giovannini, J.-V. Le Be, and S. Riederer *Class. Quant. Grav.* **19**:3357 (2002).

[131] K. Nordtvedt, *Phys. Rev.* **169**, 1014 (1968).

[132] K. Nordtvedt, *Phys. Rev.* **169**, 1017 (1968).

[133] K. Nordtvedt, *Phys. Rev.* **170**, 1186 (1968).

[134] H-P. Nilles, A. Papazoglou, and G. Tasinato, *Nucl. Phys.* **B** 677:405–429 (2004) [hep-th/0309042].

[135] J.M.Cline, J.Descheneau, M.Giovannini and J.Vinet, *JHEP* **0306**:048 (2003) [hep-th/0304147].

[136] Y. Aghababaie, C. P. Burgess, S. L. Parameswaran, F. Quevedo, *Nucl.Phys.* **B 680**:389–414 (2004) [hep-th/0304256].

[137] I. Navarro, *Class. Quant. Grav.* **20**:3603–3612 (2003) [hep-th/0305014].

[138] Hyun Min Lee [hep-th/0309050].

[139] S. M. Carroll, J. Geddes, M. B. Hoffman, and R. M. Wald, *Phys. Rev.* **D66**:024036 (2002) [hep-th/0110149].

[140] S. Weinberg, *Rev. Mod. Phys.* **61**:1–23 (1989).

[141] E. Witten, in *Proceedings of the 1983 Shelter Island Conference on Quantum Field Theory and the Fundamental Problems of Physics*, R. Jackiw, N.N. Khuri, S. Weinberg, and E. Witten, Eds. MIT, Cambridge, MA (1983).

[142] M. Henneaux and C. Teitelboim, *Phys. Lett.* **B 143**:415 (1984).